AFFDL-TR-77-114

THE DEVELOPMENT OF A THEORY FOR THE DESIGN OF LIGHTWEIGHT ARMOR

AERONAUTICAL RESEARCH ASSOCIATES OF PRINCETON, INC.
50 WASHINGTON ROAD
PRINCETON, NEW JERSEY 08540

NOVEMBER 1977

TECHNICAL REPORT AFFDL-TR-77-114
Final Report for Period October 1976 -- October 1977

AIR FORCE FLIGHT DYNAMICS LABORATORY
AIR FORCE WRIGHT AERONAUTICAL LABORATORIES
AIR FORCE SYSTEMS COMMAND
WRIGHT-PATTERSON AIR FORCE BASE, OHIO 45433

NOTICE

When Government drawings, specifications, or other data are used for any purpose other than in connection with a definitely related Government procurement operation, the United States Government thereby incurs no responsibility nor any obligation whatsoever; and the fact that the Government may have formulated, furnished, or in any way supplied the said drawings, specifications, or other data, is not to be regarded by implication or otherwise as in any manner licensing the holder or any other person or corporation, or conveying any rights or permission to manufacture, use, or sell any patented invention that may in any way be related thereto.

This report has been reviewed by the Information Office (IO) and is releasable to the National Technical Information Service (NTIS). At NTIS, it will be available to the general public, including foreign nations.

This technical report has been reviewed and is approved for publication.

Andre J. Holten
Project Engineer

Ambrose B. Nutt
Director,
Vehicle Equipment Division

Copies of this report should not be returned unless return is required by security considerations, contractual obligations, or notice on a specific document.

AIR FORCE/56780/7 March 1978 — 150

UNCLASSIFIED

SECURITY CLASSIFICATION OF THIS PAGE (When Data Entered)

14 ARAP-313

19 REPORT DOCUMENTATION PAGE

READ INSTRUCTIONS BEFORE COMPLETING FORM

1. REPORT NUMBER: 18 AFFDL-TR-77-114	2. GOVT ACCESSION NO.
3. RECIPIENT'S CATALOG NUMBER	
4. TITLE (and Subtitle): 1 THE DEVELOPMENT OF A THEORY FOR THE DESIGN OF LIGHTWEIGHT ARMOR	5. TYPE OF REPORT & PERIOD COVERED: 9 Final Report 16 Oct 1976-17 Oct 1977
	6. PERFORMING ORG. REPORT NUMBER: A.R.A.P. Report No. 313
7. AUTHOR(s): 4 Ross Contiliano and Coleman duP. Donaldson	8. CONTRACT OR GRANT NUMBER(s): 15 F33615-76-C-3156
9. PERFORMING ORGANIZATION NAME AND ADDRESS: Aeronautical Research Associates of Princeton, Inc., 50 Washington Road, P.O. Box 2229, Princeton, NJ 08540	10. PROGRAM ELEMENT, PROJECT, TASK AREA & WORK UNIT NUMBERS: Program Element 61101F Project 680100 Work Unit #43630403
11. CONTROLLING OFFICE NAME AND ADDRESS: Air Force Flight Dynamics Laboratory Wright-Patterson AFB, Ohio 45433	11 12. REPORT DATE: November 1977
	13. NUMBER OF PAGES: 84 (12) 84
14. MONITORING AGENCY NAME & ADDRESS (if different from Controlling Office)	15. SECURITY CLASS. (of this report): UNCLASSIFIED
	15a. DECLASSIFICATION/DOWNGRADING SCHEDULE

16. DISTRIBUTION STATEMENT (of this Report)

Approved for public release; distribution unlimited.

17. DISTRIBUTION STATEMENT (of the abstract entered in Block 20, if different from Report)

18. SUPPLEMENTARY NOTES

19. KEY WORDS (Continue on reverse side if necessary and identify by block number)

Integral Theory of Impact
Impact
Armor
Lightweight Armor
Penetrator
Ceramic Armor
Material Properties

20. ABSTRACT (Continue on reverse side if necessary and identify by block number)

An Analytical and experimental program was conducted, the purpose of which was the development and application of the Integral Theory of Impact to the design of lightweight armor. The experimental program consisted of deforming and nondeforming spherical projectiles impacting monolithic and layered targets. Crater depth data were obtained for thick targets; residual velocity data for thin targets. The program verified two key aspects of the theory: (1) a simple, deforming particle model can be used to predict the gross response

(cont.)

DD FORM 1 JAN 73 1473 EDITION OF 1 NOV 65 IS OBSOLETE

UNCLASSIFIED

SECURITY CLASSIFICATION OF THIS PAGE (When Data Entered)

ØØ8 4ØØ JOB

20. ABSTRACT (cont.)

of a target; (2) the theory can be used to predict layered target response.

Materials have been identified which have the potential to reduce armor weight and/or cost. In general, these materials are ceramics which must be used in combination with more ductile materials. An optimization study is presented which demonstrates the method by which the tradeoffs between these materials can be estimated and suggests the potential payoff. The optimization is based on a typical high velocity fragment threat.

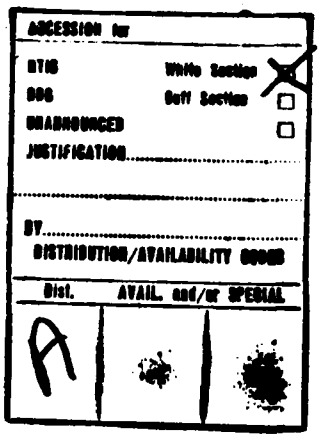

PREFACE

This report was prepared by the Aeronautical Research Associates of Princeton, Inc., 50 Washington Road (P.O. Box 2229), Princeton, New Jersey 08520 under USAF Contract F33615-76-C-3156, "Design of Lightweight Armor Systems." The report summarizes the results of a research program conducted at A.R.A.P. during the period 16 September 1976 - 7 September 1977.

The program was administered under the direction of the Air Force Flight Dynamics Laboratory, Air Force Systems Command, Wright-Patterson Air Force Base, Ohio. Mr. R. H. Adams was Contracting Officer and Mr. Andre J. Holten of AFFDL/FES was Project Engineer. The Principal Investigator for A.R.A.P. was Dr. Coleman duP. Donaldson, assisted by Mr. Ross M. Contiliano.

TABLE OF CONTENTS

LIST OF ILLUSTRATIONS

LIST OF ILLUSTRATIONS (continued)

1. INTRODUCTION

The purpose of this report is to present the results of the research program carried out by A.R.A.P. under Contract No. F33615-76-C-3156. The objectives of the program were to prove the value of A.R.A.P.'s Integral Theory of Impact for armor design and to apply the theory to the design of lightweight armor systems. The validation consisted of specifying and analyzing certain key experiments designed to isolate particular aspects of the theory.

During the past several years, A.R.A.P. has been engaged in the development of a simple, yet rational, approach to the problem of projectile impact that relates the physical properties of target and projectile materials to the character of the projectile-target interaction. This approach contains the essential physics of the impact process, satisfies all of the global conservation equations, and is contained in a computer code which is simple and inexpensive. The theory avoids the gross empiricism of some models and the high cost and complexity of multielement codes. Most importantly, the theory can be used as an inexpensive tool to guide experimental programs, suggest directions to be taken for new armor systems and to identify those designs which warrant further study using the large codes.

As a result of our early studies, it was determined that, for the purpose of calculating target response during impact, it was necessary to determine at least two characteristic quantities for any target material. One of these quantities, E_{*p}, represents the energy per unit mass absorbed during plastic deformation of the target. The other quantity, E_{*e}, represents the elastic energy per unit mass absorbed by the target during impact. Under a DARPA-sponsored program,* these characteristic quantities have been experimentally obtained for a variety of materials including metals, plastics, and ceramics. In addition, a theory has been developed which relates these quantities to more fundamental material properties.

*Contract No. DAAD05-76-C-0757.

Under the present contract, A.R.A.P. has placed special emphasis on the development and application of the integral theory to the design of lightweight armor systems. An experimental program was conducted using materials which had been previously qualified in the DARPA program to verify certain key aspects of the theory. The object was to show that the simple model for the penetration of a layered target by a deforming projectile accurately predicted the data.

In addition to the experimental program, the integral theory was used for a number of analytical studies. The comparative ability of several present-day armor materials to defeat a typical threat was investigated. Materials were identified which offer potential improvements; i.e., lighter and/or cheaper, relative to present-day armor. An optimization study was completed which demonstrates the design tradeoffs which are required and suggests the possible payoff when these materials are used in various combinations to defeat a typical threat.

In what follows, we will review the Integral Theory of Impact in Section 2 and the experimental program in Section 3. The analytical studies comparing present and potential armor materials and the armor optimization procedure are described in Section 4. Finally, conclusions and recommendations are given in Sections 5 and 6.

2. INTEGRAL THEORY OF IMPACT

2.1 Particle Characterization

In the Integral Theory of Impact, an impacting particle is characterized by a single cell representation,* but straining of the particle is permitted consistent with an assumed internal velocity field. When global conservation equations are derived using this approximate deformation model, a set of ordinary differential equations is obtained which can be solved numerically using conventional techniques.

The particle is taken to be a rectangular parallelepiped of square planform. It is assumed that for normal impact the particle deforms but that it remains a rectangular parallelepiped. Figure 1 depicts the impact of this particle on a semi-infinite target. The thickness and width of the particle are denoted by ℓ and b, respectively, the mass-center velocity by V_{cm}, the front face velocity by $V_\perp$, and the penetration depth by y. The only external forces acting on the particle are the contact stresses acting at the interface between particle and target. These forces are denoted by the total force F acting on the particle in Figure 1.

With the further assumption that the particle is incompressible, the equations defining conservation of mass, momentum, and energy may be written as follows

$$\ell b^2 = \ell_o b_o^2 \tag{1}$$

$$m_p \frac{dV_{cm}}{dt} = -F \tag{2}$$

$$\frac{dK}{dt} + \frac{dE}{dt} = -FV_\perp \tag{3}$$

where m_p is the particle mass and K and E are the kinetic and internal energy of the particle, respectively. The penetration

*The single cell representation is applicable to small L/D projectiles. A multicell model for long-rod penetrators is presently being developed.

NORMAL IMPACT OF A DEFORMING PARTICLE ON A SEMI-INFINITE TARGET

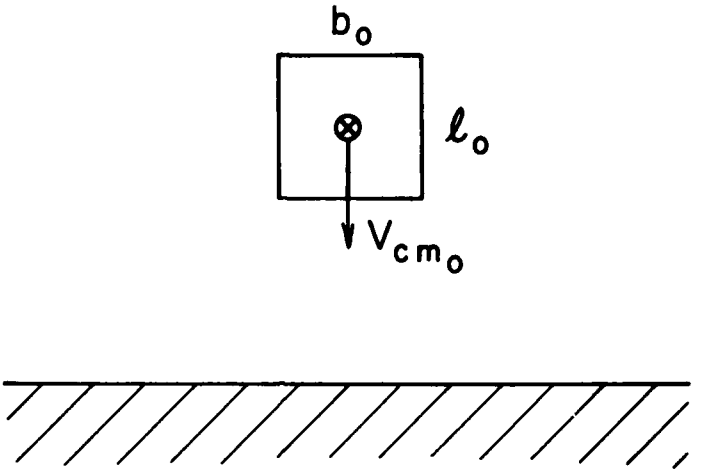

Before impact

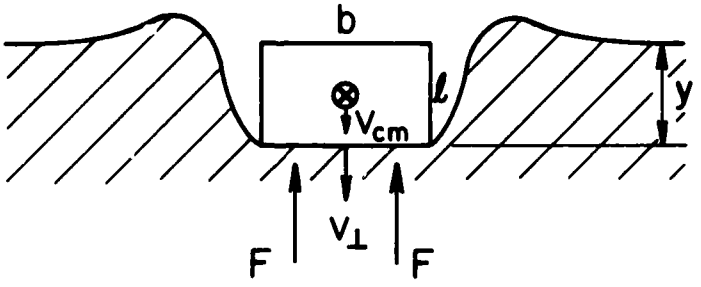

During impact

Figure 1. Normal Impact of a Deforming Particle.

depth, y, is simply obtained as the integral of the front-face velocity

$$V_{\perp} = \frac{dy}{dt} \tag{4}$$

To complete the system of equations, K and E must be related to kinematic variables and the interface force must be defined. For the former, the mode of deformation must be specified. The simplest assumption is that the material velocity varies linearly with position in the particle. If a coordinate system ξ, η, ζ centered instantaneously at the mass center is defined and the components of material velocity are denoted by V_x, V_y, V_z, then the deformation mode may be represented as follows:

$$V_x = \frac{\xi}{b/2} \frac{1}{2} \frac{db}{dt} \tag{5}$$

$$V_y = V_{cm} + \left(\frac{\eta}{\ell/2}\right)(V_{\perp} - V_{cm}) \tag{6}$$

with a distribution similar to V_x for the z direction. The velocity field is illustrated in Figure 2. The kinetic energy in the particle is defined by

$$K = \int_{Vol} \frac{\rho_p}{2} (V_x^2 + V_y^2 + V_z^2) dV \tag{7}$$

and substitution of (5) and (6) into (7) yields

$$K = \frac{1}{2} m_p V_{cm}^2 + \frac{m_p}{6}\left[\frac{1}{2}\left(\frac{db}{dt}\right)^2 + (V_{\perp} - V_{cm})^2\right] \tag{8}$$

The two terms on the right side of (8) represent the kinetic energy associated with the mass center motion and the relative kinetic energy, respectively. This expression can be recast into a more convenient form. Since the particle is homogeneous, the mass center coincides with the geometric center at all times. Therefore, it follows that

$$V_{\perp} - V_{cm} = \frac{1}{2} \frac{d\ell}{dt} \tag{9}$$

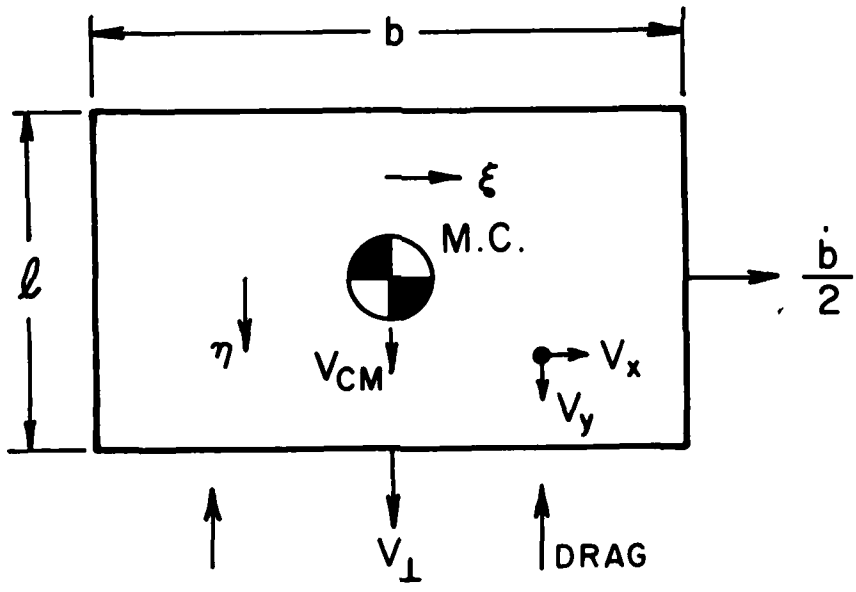

Conservation equations

$$\ell\, b^2 = \text{Constant}$$

$$m_p \frac{dV_{CM}}{dt} = -\text{Drag}$$

$$\frac{dK}{dt} + \frac{dE}{dt} = -\text{Drag} \times V_\perp$$

$$\frac{dy}{dt} = V_\perp$$

Deformation field

$$V_x = (\xi / \frac{b}{2}) \frac{\dot{b}}{2}$$

$$V_y = V_{CM} + (\eta / \frac{\ell}{2})(V_\perp - V_{CM})$$

$$V_z = (\mathcal{L} / \frac{b}{2}) \frac{\dot{b}}{2}$$

$$V_\perp - V_{CM} = \dot{\ell}/2$$

$$K = \int_{Vol} \frac{\rho_p}{2} (V_x^2 + V_y^2 + V_z^2)\, d\mathcal{V}$$

Figure 2. Particle Deformation Field.

Also, (1) may be written in differential form as

$$\frac{db}{dt} = -\frac{1}{2}\left(\frac{b}{\ell}\right)\frac{d\ell}{dt} \tag{10}$$

Substitution of (9) and (10) into (8) yields the following expression for K

$$K = \frac{1}{2} m_p V_{cm}^2 + \frac{1}{2} m_p \left[\frac{1}{2}\left(\frac{b}{\ell}\right)^2 + 1\right] \frac{\left(\frac{1}{2}\frac{d\ell}{dt}\right)^2}{3} \tag{11}$$

Now consider the internal energy. Two modes of energy storage are presently included. The first is an energy density proportional to the mass of material and the other, which is the surface energy, is proportional to the surface area. Since heat transfer is not included in the model, the only source of internal energy is the stress power. Consistent with the kinematic model, the stretching is isochoric; therefore, the dissipation is independent of pressure. Because the shear stress depends only on the stretching at any point within the particle and the stretching is uniform within the particle, the shear stress is uniform within the particle also. If the density term is replaced by the stress power consistent with this model, the internal energy can be written as follows:

$$\frac{dE}{dt} = \frac{3}{2} S\dot{\varepsilon} V + \gamma \frac{dA}{dt} \tag{12}$$

where S and ε are the axial components of the stress and stretching tensors and γ is the surface energy. After expanding the volume and area in terms of the particle dimensions, (12) becomes

$$\frac{dE}{dt} = \frac{3}{2} S \frac{d\ell}{dt} b^2 + 4\gamma\left[(b + \ell)\frac{db}{dt} + b\frac{d\ell}{dt}\right] \tag{13}$$

where the axial component of the stretching tensor was computed from (6) and (9); i.e.,

$$\dot{\varepsilon} = \frac{V_\ell - V_{cm}}{\ell/2} = \frac{1}{\ell}\frac{d\ell}{dt} \tag{14}$$

Finally, the constitutive relations are specified by defining the relations between S and ε. Any model of behavior can be

treated, but, because of their general usefulness, four models have been used:

Hydrodynamic	$S = 0$	(15)
Newtonian Fluid	$S = 2\mu\dot{\varepsilon}$	(16)
Rigid Plastic	$S = \frac{-2}{3}\sigma_y$ for $\dot{\varepsilon} < 0$	(17)
Nondeforming	$\varepsilon = 0$	(18)

where μ denotes fluid viscosity and σ_y denotes material yield strength. The first, third and fourth of these models are used later in this report. The second model has been successfully applied to water drop impact problems.

Ignore for the moment that the force at the interface has not been defined. Then, Eqs. (1)-(4), (9), (11) and (13) form a closed set of ordinary differential equations for the variables b, ℓ y, $V_\perp$, V_{cm}, K, and E. The equations can be integrated numerically to obtain the time history of the velocity field, particle deformation, and the energy partitioning within the particle.

2.2 Target Characterization

Target material properties enter the integral theory through the force term in (2) and (3). The character of this term can be examined by using the following form of the energy equation as applied to the target material

$$\frac{dW_t}{dt} = FV_\perp \tag{19}$$

where W_t represents the work done on the target by the projectile. This energy is absorbed by the target in three different forms. Part of the energy is kinetic (KE_t), and is associated with the acceleration of the target material as it moves around the particle. The other two parts are nonkinetic energy terms; U_p, which is an energy dissipation term primarily associated with plastic deformation of the target, and U_e which is the elastic energy absorbed by the target during elastic deformation. Thus, the energy equation

may be written as

$$\frac{dW_t}{dt} = \frac{d}{dt} KE_t + \frac{d}{dt} U_p + \frac{d}{dt} U_e \tag{20}$$

This equation may also be written as follows

$$\frac{dW_t}{dt} = \rho_t V_\perp \ell^2 \left(\frac{C_D}{2} V_\perp^2 + E_{*p} + E_{*e} \right) \tag{21}$$

In (21), it is assumed that the change in kinetic energy is proportional to the square of the normal velocity at the interface; the constant of proportionality is the drag coefficient C_D . In addition, the change in internal energy is proportional to a quantity E_* which has a plastic, E_{*p} , and an elastic, E_{*e} , component. Equation (21) may be taken as a definition for C_D , E_{*p} , and E_{*e} . Note that with this definition, E_{*p} includes all forms of energy dissipation including plastic deformation, heat of phase change, crack propagation, etc.

Substitution of (21) into (19) yields the final result for the force term

$$F = \rho_t \ell^2 \left(\frac{C_D}{2} V_\perp^2 + E_{*p} + E_{*e} \right) \tag{22}$$

The hydrodynamicist will recognize the kinetic energy term as the Newtonian approximation for the pressure induced on a particle by fluid flowing around it. Newtonian theory, to first approximation, states that the force induced on the surface of the particle is due to the destruction of the normal component of momentum in a thin layer adjacent to the particle. This approximation, which is borrowed from fluid dynamics, may be applied to the penetration of a solid material because the particle shears the target material and causes it to flow in a relatively thin region adjacent to the particle. Using the Newtonian approximation, it can be shown that for a flat disk $C_D \approx 2$ and for a sphere $C_D \approx 1$. In this report and, indeed, in all of our armor work to date, we have used $C_D = 1$ with good success.

Note that the dominant term in the force equation depends on the magnitude of the particle velocity and on the target material properties. For large velocity, the kinetic term dominates and

deceleration is primarily accomplished by target inertia. In this velocity regime, it doesn't pay to buy high E_* protection. However, for low velocity, deceleration is primarily due to energy absorption by the target; in this case, it does pay to buy high E_* protection.

Ordinarily, the deceleration of a projectile includes both velocity regimes. It is therefore possible to combine a dense material to initially decelerate the projectile when the velocity is high with a lighter, high E_* material when the velocity is lower to stop a high velocity projectile. An optimization procedure which shows how to design the most efficient combination of materials is described later in this report.

2.3 Target Material Qualification

All that remains to close the system of equations is evaluation of the two parameters E_{*p} and E_{*e}. These quantities can be obtained experimentally using a qualification procedure which is described below. In addition, a theory has been developed by A.R.A.P. which relates these quantities to more fundamental material properties. The results of the theory are in excellent agreement with the experimental results. A summary of this theory is given at the end of this section.

For purposes of discussion, consider the particle to be non-deforming. Substitution of (22) and (4) into (2) together with $V_\perp = V_{cm}$ for a nondeforming particle yields

$$\rho_p \ell_o^3 \frac{dV_{cm}}{dt} = \rho_p \ell_o^3 V_{cm} \frac{dV_{cm}}{dy} = -\rho_t \ell_o^2 \left(\frac{C_D}{2} V_{cm}^2 + E_{*p} + E_{*e} \right) \qquad (23)$$

Although C_D and E_{*p} are constant, E_{*e} is, in general, a function of the depth of penetration y. As a result, (23) cannot be integrated directly to give a closed form solution. The problem can be circumvented, for illustrative purposes, by integrating (23) in the following manner

$$p = \int_{V_o}^{V_*} V_{cm} dt = -\int_{V_o}^{V_*} \frac{\rho_p \ell_o}{\rho_t} \frac{V_{cm} dV_{cm}}{\left(\frac{C_D}{2} V_{cm}^2 + E_{*p}\right)} \qquad (24)$$

where p represents the final depth of penetration. In (24), the elastic energy term, E_{*e}, has been replaced by a new parameter V_* as a limit of integration. This quantity represents the velocity of the particle at which all its remaining kinetic energy can be absorbed elastically by the target. The integration of (24), for $C_D = 1$, yields

$$\frac{p}{\ell_o} = \frac{\rho_p}{\rho_t} \ell n \frac{V_o^2/2 + E_{*p}}{V_*^2/2 + E_{*p}} \qquad (25)$$

This equation relates the nondimensional penetration depth to the density ratio of particle and target, the impact velocity and the two quantities E_{*p} and V_* (which is related to E_{*e}). Even more importantly, (25) shows that these two parameters can be obtained for a given target material by conducting a series of impact tests using nondeforming cubes over a range of impact velocity, measuring the maximum penetration, and fitting the data using the two parameters.

Such a series of tests has been conducted in the A.R.A.P. Impact Facility under a DARPA contract.* To date, eighteen (18) materials have been qualified. These materials are summarized in Table 1. Typical results are shown in Figures 3-7 for soft metal, armor, brittle, and transparent target materials. All of the tests, except those noted, utilized nondeforming spherical projectiles.† Most of the targets were 1"-thick, 6" diameter disks. To minimize

*Contract No. DAAD05-76-C-0757.

†The penetration equation for the nondeforming sphere is similar to (25) for deep craters ($p/d_o > 0.5$). For shallow craters, the penetration is proportional to the square root of the density ratio. For the sake of brevity, the development of the rigid sphere equations is omitted.

TABLE I. MATERIALS QUALIFIED IN A.R.A.P. IMPACT FACILITY

Target Material	Specific gravity	E_{*p}, Btu/lbm	$E_{*e} = k_1 (P/d_o)^{-N}$	
			k_1	N
Acrylic (Plexiglas)	1.19	110	190	1.5
Aluminum (1100-F plate)	2.73	84	0	—
Aluminum (5083)	2.74	245	15.1	.75
Aluminum oxide (Coor's)	3.40	325	0	—
Boron carbide	2.52	500	148	1.5
Cadmium (Pure, cast)	8.81	29	0	—
Copper (ETP)	9.01	38	0	—
Glass (Corning-Pyrex)	2.18	105	0	—
Iron (Class 40 gray)	7.13	121	7	.75
Kevlar	1.23	171	24.9	1.5
Lead (Pure, cast)	11.3	3.5	0	—
Polycarbonate (G.E. Lexan)	1.21	101	106	1.1
Salt (NaCl)	1.99	86	0	—
Silicon	2.00	~184	—	—
Steel (1020 - HR)	7.86	141	8.9	.75
Steel (R.H.A.)	7.83	203	19	.75
Titanium (Ti-6 Al-4 v)	4.48	328	7.1	.75
Zinc (Pure, cast)	7.19	62	0	—

Material Qualification has been performed under DARPA Contract no. DAADO-76-C-0757

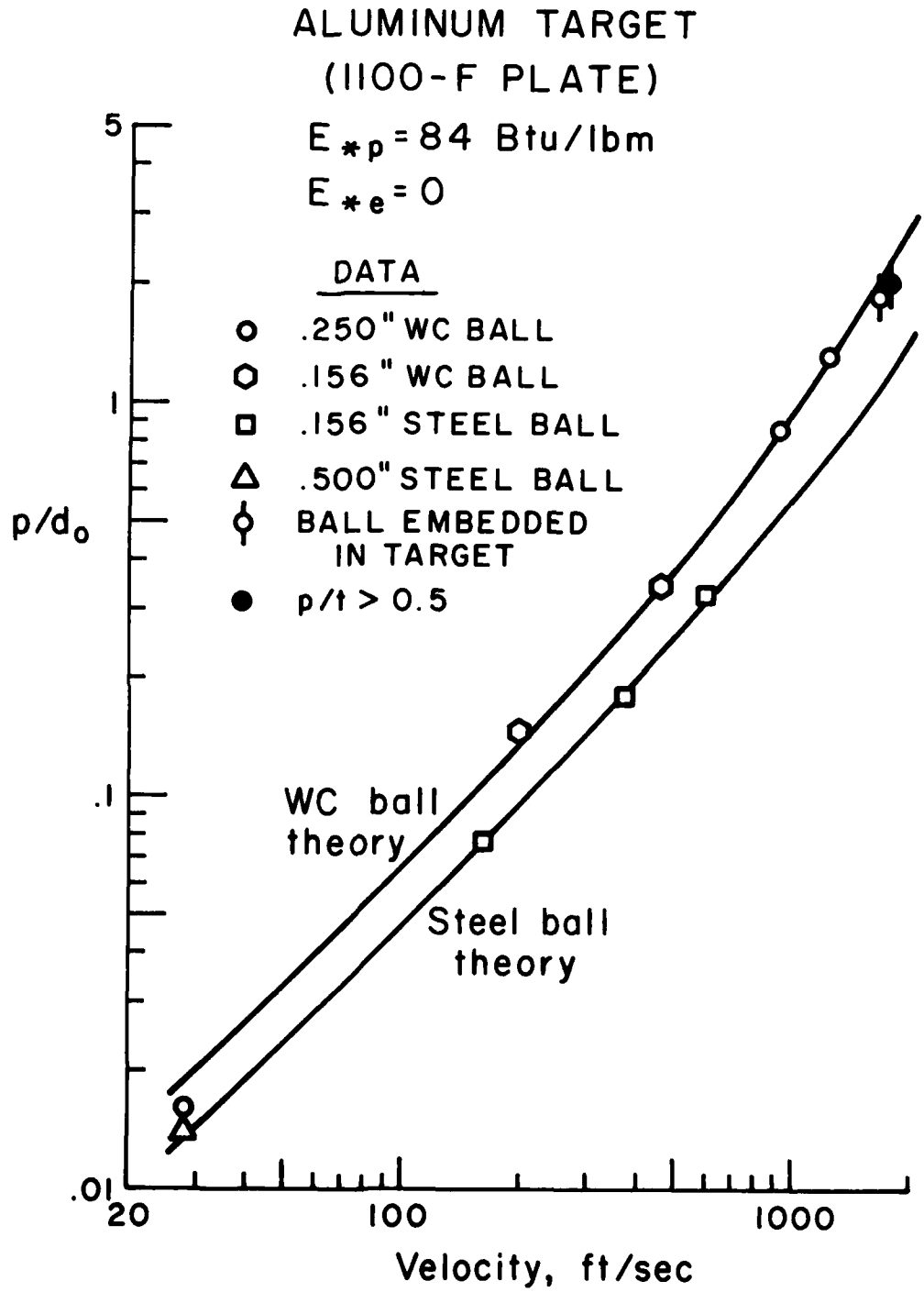

Figure 3. Crater Depth - Aluminum 1100-F Target.

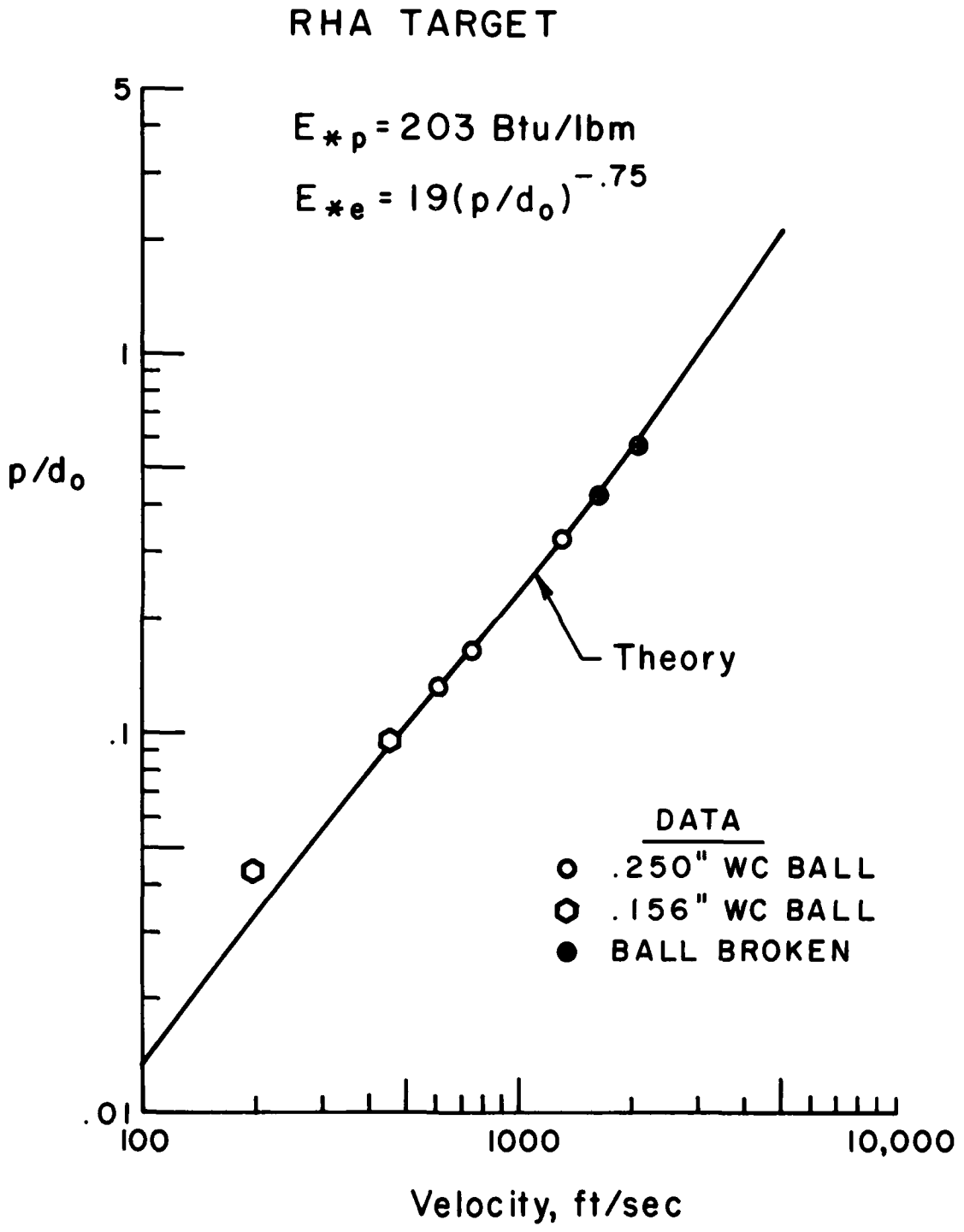

Figure 4. Crater Depth - Rolled Homogeneous Armor Target.

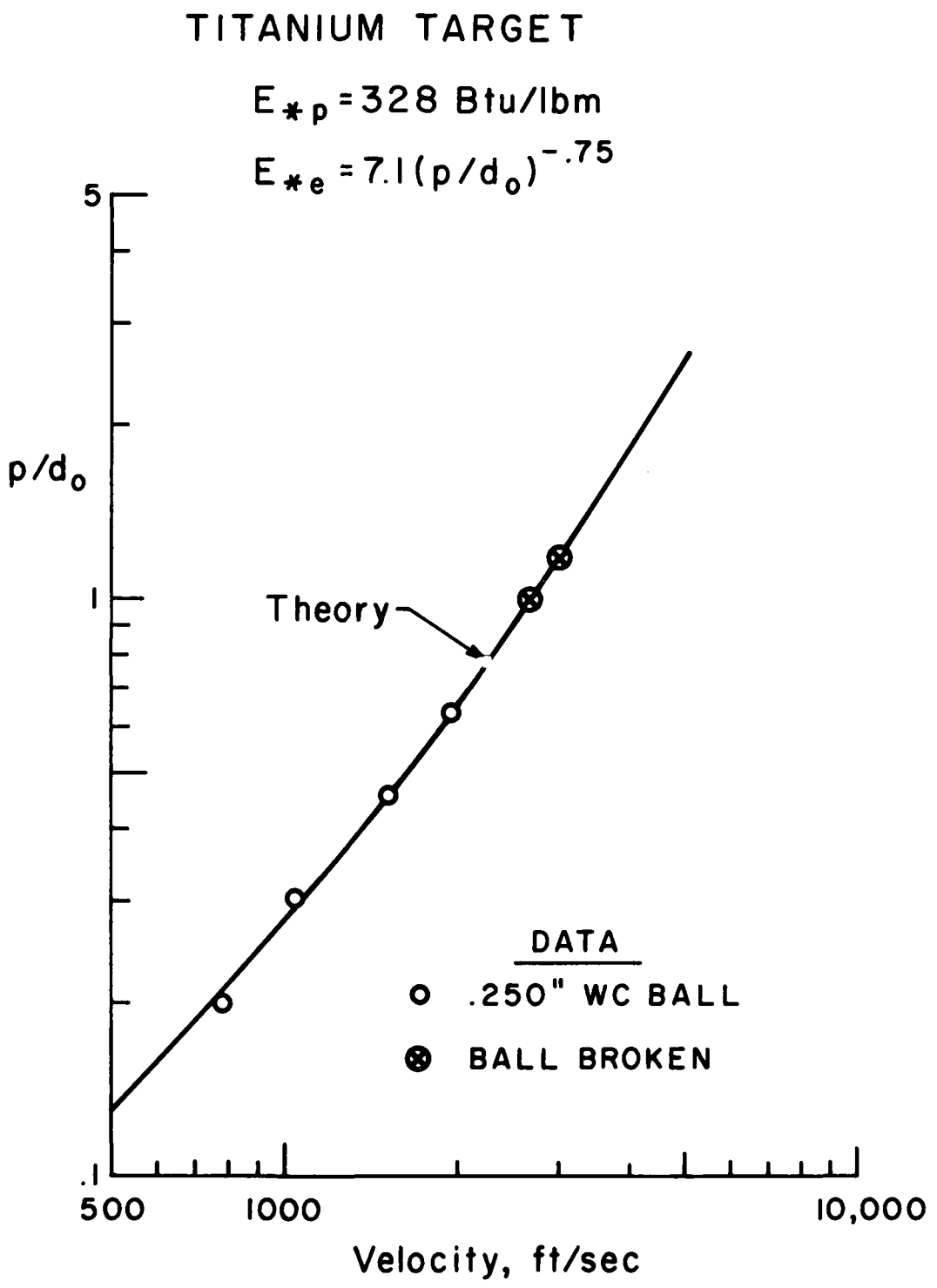

Figure 5. Crater Depth - Titanium Target.

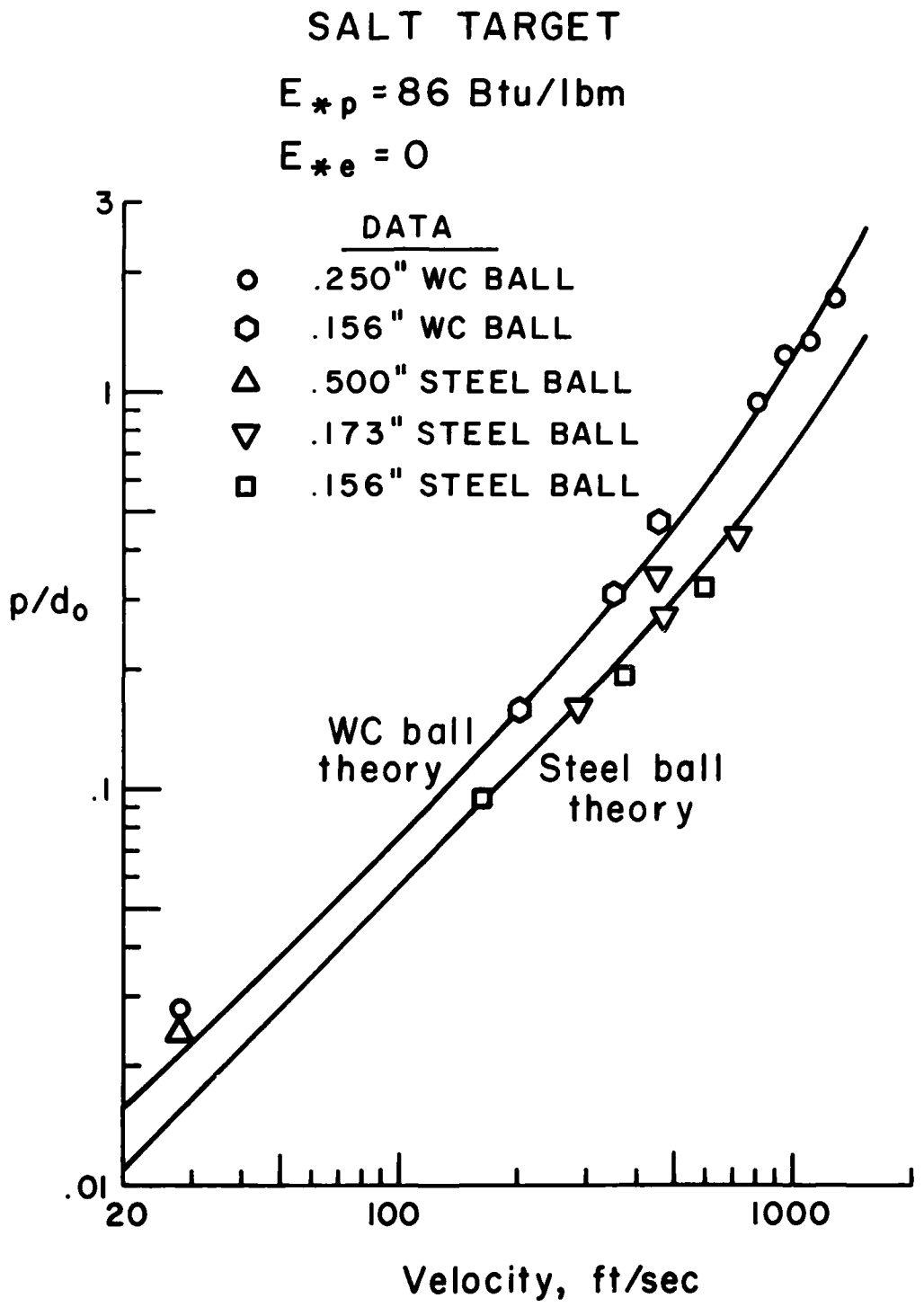

Figure 6. Crater Depth - Salt Target.

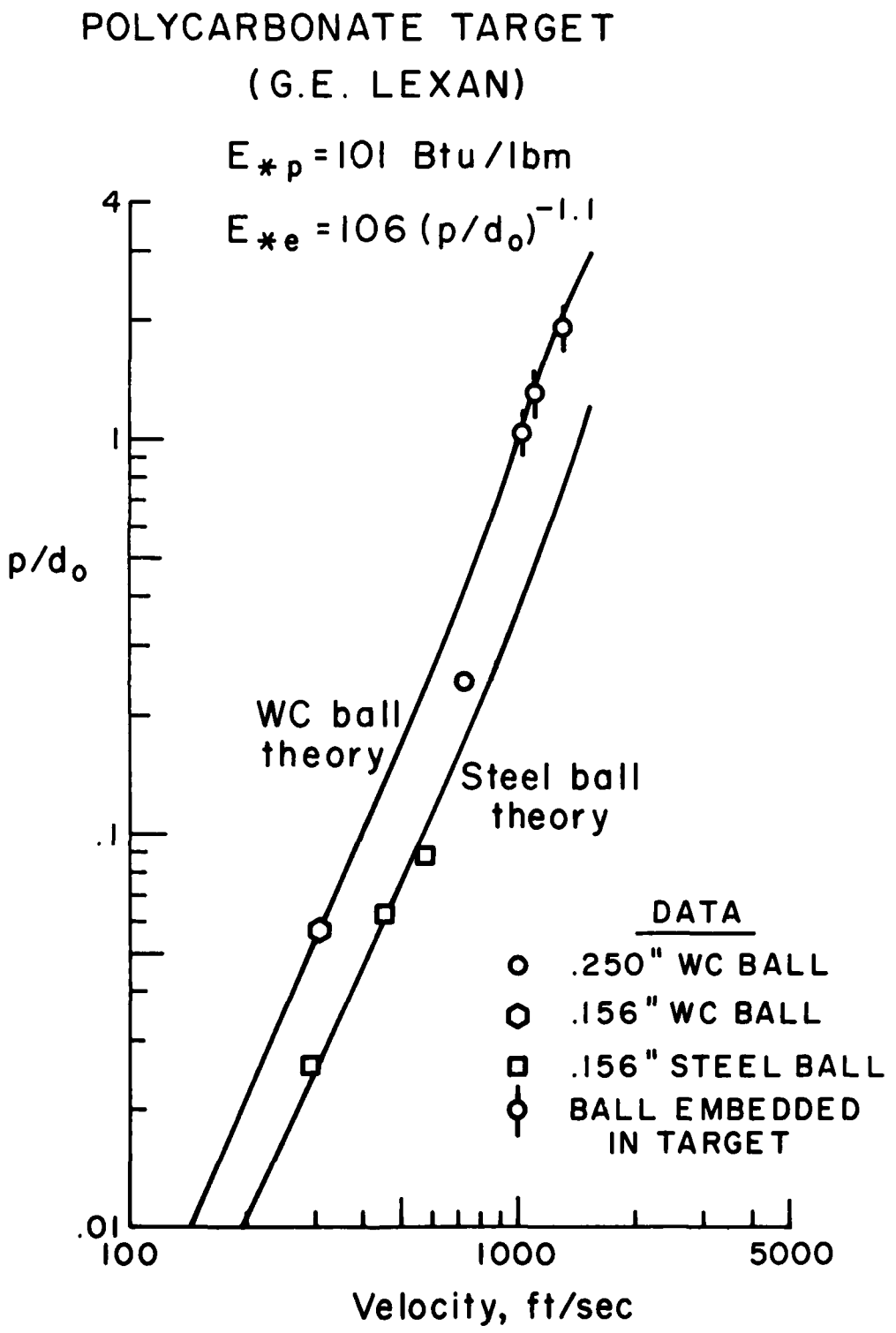

Figure 7. Crater Depth - Polycarbonate Target.

backface effects, crater depths were limited to half the target thickness.

In these figures, the maximum crater depth normalized by projectile diameter is plotted as a function of the impact velocity. Note that both projectile diameter and density are varied. The solid lines represent theoretical calculations using the integral theory and the indicated values of E_{*p} and E_{*e}. Note that the value of E_{*p} increases by a factor of nearly four between soft aluminum and titanium. For the metals, E_{*e} is less than 10% of E_{*p} when $p/d_o \geq 1$. However, for the polycarbonate target, the elastic contribution is larger than the plastic contribution. Also note the accuracy of the correlation for the brittle salt (NaCℓ) target. In general, it can be seen that the theory has the correct velocity, density and particle size dependence.

Coincident with this program of dynamic qualification of target materials, A.R.A.P. has developed a theory which can predict the value of E_{*p} and E_{*e} using more conventional material properties which can be obtained in static test facilities. Without going into the details,* the impact properties may be written as follows:

$$E_{*p} \simeq \frac{1}{3} C_p T_m \ell n\left(1 + \frac{\sigma_F(T,\dot{\varepsilon})}{0.05\rho C_p T_m}\right) \tag{26}$$

and

$$E_{*e} \simeq 1.09 \times 10^{-3} \frac{B^2\gamma}{\rho E} (\rho/d_o)^{-0.75} \tag{27}$$

where C_p is specific heat, T_m is melting temperature, B is Brinell hardness, E is modulus of elasticity, σ_F is the flow stress at the temperature (T) and strain rate ($\dot{\varepsilon}$) of interest, and γ is a strain rate parameter which varies between one and ten depending on the type of material. These equations have been remarkably successful in predicting E_{*e} and E_{*p}. In general, for the metals and soft plastics, an accuracy of about 15% has been achieved; for the brittle ceramics, the accuracy is within

*The development of Eqs. (26) and (27) is discussed in detail in A.R.A.P. Report No. 295.

a factor of two. These equations, therefore, can be used as a tool for the preliminary screening of candidate materials and to predict the properties of those materials which may not be available for testing.

2.4 Layered Targets

It was postulated at the outset of this program, that the response of layered targets could be predicted using the integral theory. Simply, the approach is to compute the penetration through each layer as though that layer is a semi-infinite target using the equations described above and the target material properties (E_* and ρ) of the layer. The computation, however, is terminated at the depth of penetration equivalent to the thickness of the layer. The state of the particle at that instant, i.e., its instantaneous shape, velocity field and energy partition, are then used as initial conditions for the impact of the next layer which has its own set of material properties. This procedure is continued until either the target is perforated or the velocity of the particle is low enough such that all of its remaining kinetic energy can be absorbed elastically by the materials in its path. In the latter case, a crater is produced whose depth is given by the total penetration at the instant that the elastic energy limit is reached.

Before the integral theory can be used for the design of armor systems, it is necessary to prove the validity of three crucial assumptions. First, the theory can be used to predict the response of a given target material using the two parameters E_{*p} and E_{*e}. This assumption has been proven both experimentally and theoretically in the DARPA-sponsored program described earlier. Second, the simple model for a deforming projectile can be used to predict the response of previously qualified target materials. Third, the layered target model can be used to predict the response of layered targets. Verification of the second and third assumptions is the object of the experimental portion of the present program. The results are discussed in the next section.

3. EXPERIMENTAL PROGRAM

This section describes the A.R.A.P. Impact Facility, summarizes the test program, and presents the data obtained. These data are compared to computations using the integral theory which was described in the previous section.

3.1 A.R.A.P. Impact Facility

Figure 8 schematically depicts the A.R.A.P. Impact Facility. This facility consists of a mounted weapon, enclosed test tube and test chamber, and velocity measurement instrumentation. The weapon used for this test program is a Winchester 270 caliber, smooth bore rifle. The rifle is permanently mounted to a rigid support, bore-sighted on the target and fired remotely. Cartridges are hand loaded using Hercules 2400 gunpowder. The velocity range of this weapon for projectile materials of interest is 700-6600 feet per second.*

The projectiles are spherical balls with a maximum diameter of approximately 0.25 inches. Three projectile materials are considered: tungsten carbide, aluminum (1100-F) and lead. The balls are mounted at the end of the cartridge using a bore-fitting Lexan sabot. The sabot is manufactured in four sections which separate aerodynamically upon leaving the muzzle and hit the stripper plate located at the downstream end of the test tube. Only the projectile enters the test chamber and impacts the target.

Targets are mounted in a permanent holder attached to the downstream end of the test chamber. The nominal size of the targets is 4-3/8" by 4-3/8" and the thickness varies from 0.05" to 2.0" depending on the test objective. Two target materials are used: aluminum 1100-F plate and steel 1020-hot rolled. For the crater depth tests, the targets are mounted between an annular steel ring and a semi-infinite plywood disk. For the target perforation tests, the targets are mounted between annular rings.

*The facility also includes a Power Line 880 Air Gun for low velocity testing.

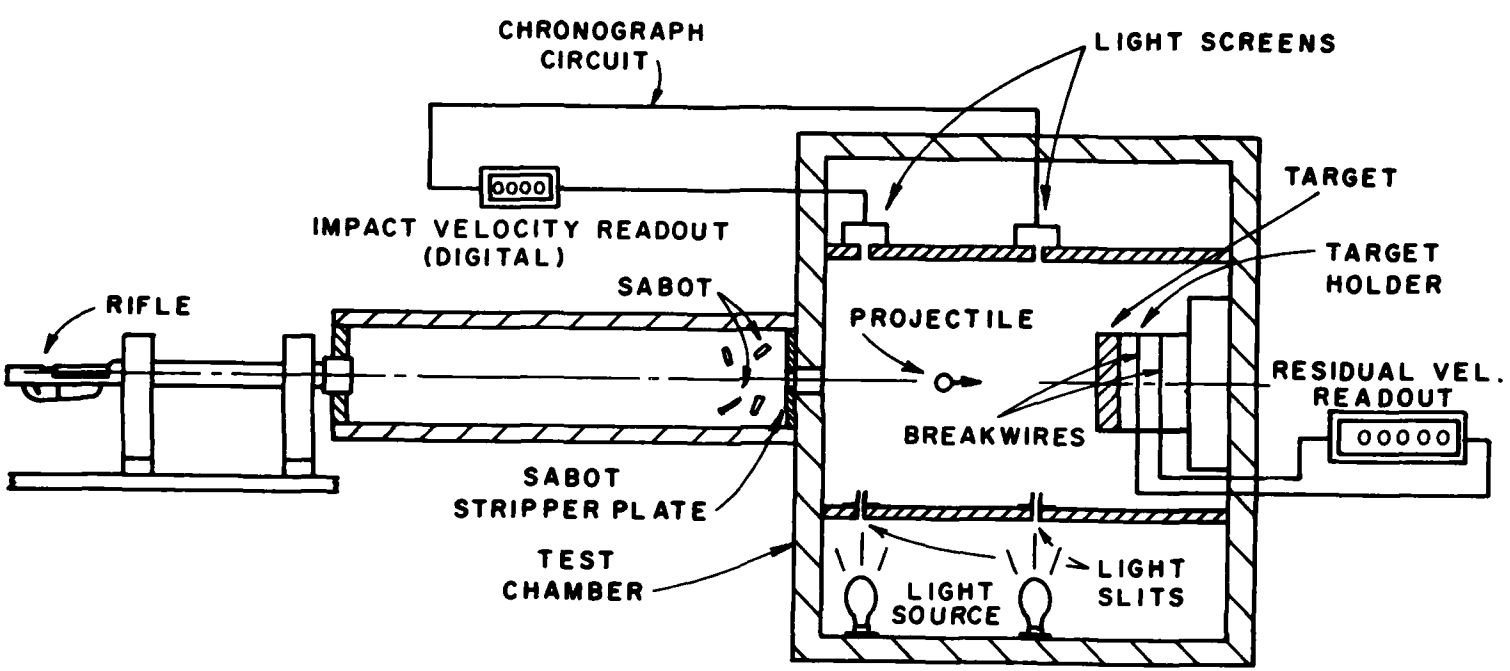

Gun	Projectile	Velocity range
Winchester 270 Smooth bore rifle	Dia. ≤ .25" WC, Aℓ Pb, Glass, Steel	700-6600 fps
Power Line 880 Air gun	Dia. ≤ .172" WC, Steel	160-740 fps

Figure 8. A.R.A.P. Impact Facility.

Projectile velocity is measured using a Schmidt-Weston Standard Chronograph. Light screens are used to measure impact velocity. The screens are two feet apart and sense projectile passage using a photo-resistor element. Breakwires are used to measure residual velocity. The wires are located at two stations 3 inches and 9 inches behind the target. At each station, the wire is continuously wound in three rows with 0.25" separation between rows. The wires are stretched in orthogonol directions at the two stations. The region of overlap is a 0.5" square centered on the axis of the rifle. A witness plate behind the wires is used to determine the shape and impact location of the projectile and debris reaching that plane. No special precaution is taken to suppress spall from the backface of the target. Hence, in those cases where there is considerable debris there is greater uncertainty in the data. These data are noted. Also, no attempt is made to recover the particle intact. Instead the particle is suddenly stopped (and broken) by a steel disk located behind the witness plate. A separate digital readout of the velocity is provided on the display board of both the light screen and the breakwire system.

3.2 Test Matrix

Approximately 125 impact tests were conducted in the A.R.A.P. Impact Facility. A summary of the projectile-target combinations is given in Table 2. Three projectile materials were fired into various one-layer, two-layer, and multilayer targets of aluminum and steel. The two-layer and multilayer targets were pressed together between annular rings; no mechanical fasteners or bonding between adjacent layers was employed.

Approximately one-half of the tests utilized relatively thick targets in which the objective was to stop the projectile prior to perforation of the backface. The bulk of these tests utilized the soft projectiles. The data consisted of crater depth measurements.

The other half of the testing utilized relatively thin targets in which perforation of the target was desired. Residual velocity data were obtained from these tests. Some difficulty was encountered using the breakwire system for tests in which the ball

TABLE 2. LAYERED TARGET TEST PROGRAM

PROJECTILE MATERIAL *	TARGET DESCRIPTION	VELOCITY	NO. OF TESTS	
			CRATER DEPTH	RESIDUAL VELOCITY
LEAD	.05" - 2" ALUMINUM	400 - 6000	12	9
LEAD	.07" - 1" STEEL	2100 - 6000	5	5
ALUMINUM	.05" - 1" ALUMINUM	1300 - 5500	8	4
ALUMINUM	1" STEEL	1600 - 6600	5	—
TUNG. CARBIDE	.05" - 1" ALUMINUM	600 - 4500	—	17
TUNG. CARBIDE	.07" STEEL	1100 - 3500	—	4
TUNG. CARBIDE	.25" ALUM + 1" STEEL	1500 - 5100	7	—
TUNG. CARBIDE	.07" / .25" STEEL + .05" / 1" ALUM	1500 - 3400	5	10
LEAD	.25" ALUM 1" STEEL	1800 - 5900	5	—
LEAD	.07" STEEL + 1" ALUM	2800 - 6000	5	—
TUNG. CARBIDE	16 TO 24 ALTERNATE LAYERS OF .05" ALUM & .07" STEEL	1200 - 4400	7	7
LEAD		200 - 6100	9	—
			68	56

* Spherical projectiles, nominal diameter = .25"

was pulverized during impact and/or significant spallation on the back of the target was encountered. As a result, most of the useful data from these tests are for the tungsten carbide projectile prior to projectile breakup.

In the next two subsections, the data are presented and compared to the results of computations using the Integral Theory of Impact.

3.3 Crater Depth Tests

The data in this section are divided into three groupings: First, the impact of soft projectiles on thick, single-layer targets; second, two-layer targets impacted by both rigid and deforming projectiles; third, multilayer targets impacted by rigid and deforming projectiles.

3.3.1 Deforming Projectiles into Semi-Infinite Metal Targets

Figure 9 presents the crater depth data for the impact of lead spheres into steel targets. In this figure and in the subsequent similar figures, the maximum depth of the crater, p, is normalized by the initial diameter of the sphere and this ratio is plotted as a function of the measured impact velocity. In each of these tests, the projectile was destroyed during impact.

The solid curves in Figure 9 represent the computed crater depth using the theory for a deforming particle which was described in Chapter 2. The band which is shown for the theory represents a 10% uncertainty in the value of E_{*p} for steel; for the upper curve E_{*p} = 141 Btu/lbm and for the lower curve E_{*p} = 155 Btu/lbm. The former value was deduced during the DARPA-sponsored qualification program which was summarized in Table 1. Particle deformation is based on the hydrodynamic constitutive model. In general, the agreement between theory and data is very good.

Figure 10 contains photographs of three of these targets. The photograph at the upper left shows one of the targets prior to impact. The other photographs show progressively larger amounts of damage. The white surface is a thin film of paint sprayed on the targets prior to testing.

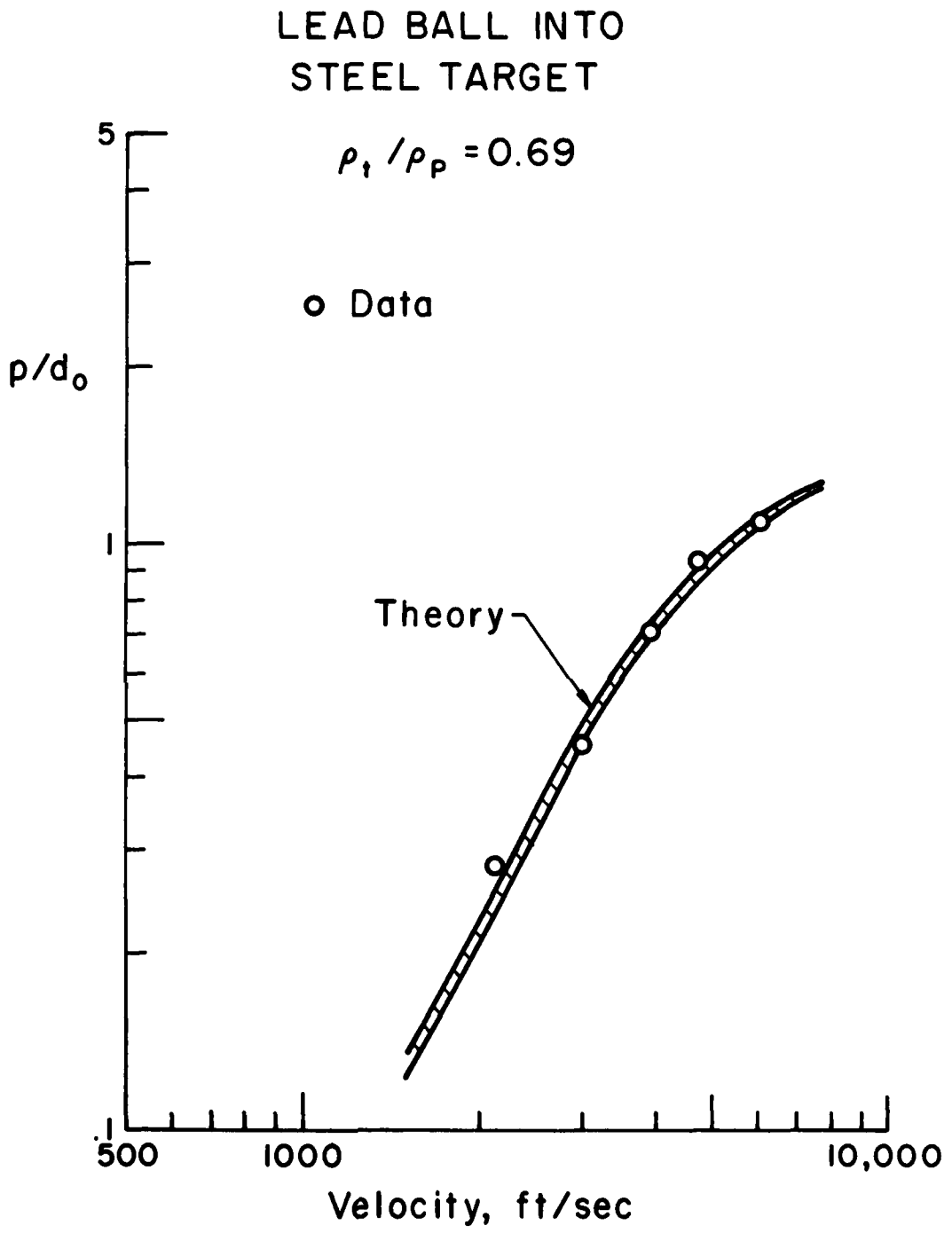

Figure 9. Crater Depth - Lead Ball into Steel Target.

TARGET MATERIAL - STEEL
PROJECTILE MATERIAL - LEAD

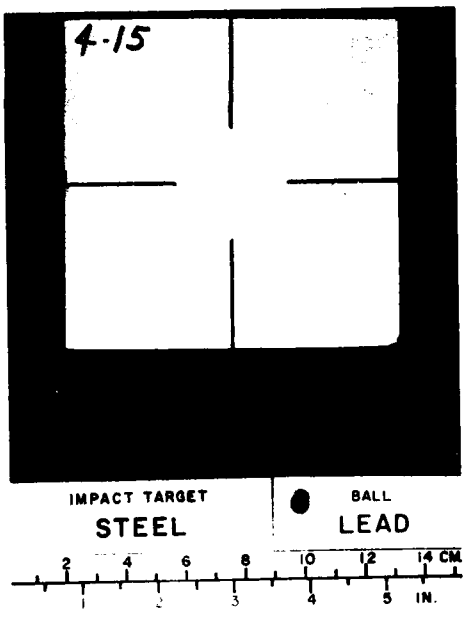

PRE-TEST

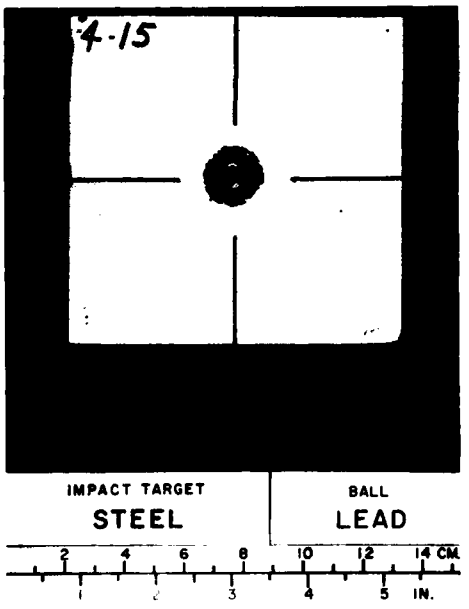

V = 2138 ft/sec
P/d_o = .28

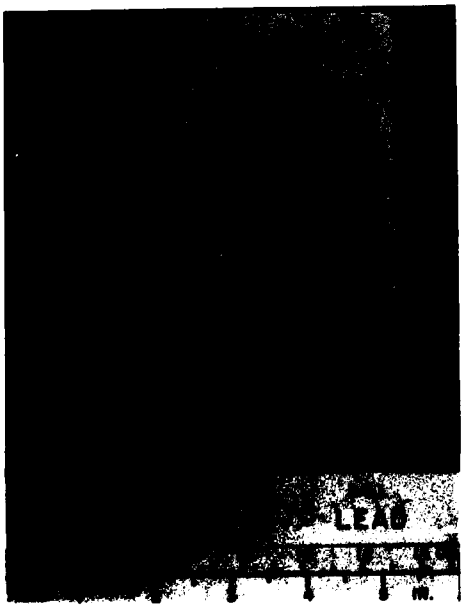

V = 3927 ft/sec
P/d_o = .71

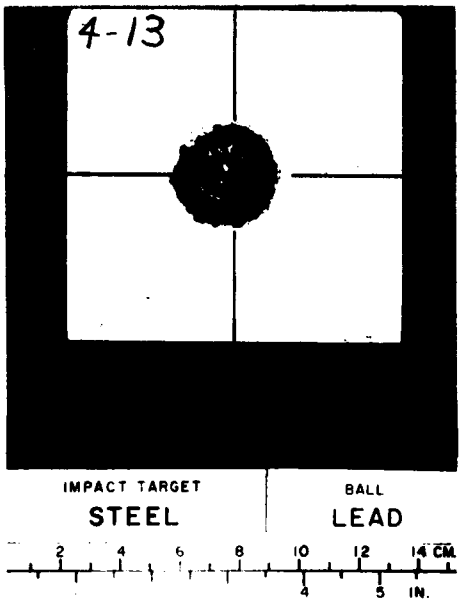

V = 4701 ft/sec
P/d_o = .94

Figure 10. Photographs - Lead Ball into Steel Target.

Figure 11 shows the results for the impact of lead spheres into aluminum targets. The circular symbols are for one-inch thick targets. There was significant plastic deformation of the backface for the test at 5,400 fps. To reduce this backface effect, two tests were conducted using two-inch thick targets. The results for these two tests are shown by the square symbols. For velocities below 5,000 fps, the projectile was deformed but remained intact; for the higher velocities, the projectile was destroyed.

The theory is again presented as a band; for the upper curve E_{*p} = 75 Btu/lbm and for the lower curve E_{*p} = 84 Btu/lbm. The agreement between theory and data is within approximately 20%. For relatively deep penetration, the theory tends to underpredict the crater depth. This discrepancy is due to the simplicity of the particle deformation model. Recall that the particle is modeled as a deforming rectangular parallelepiped; curvature of the front-face of the particle is not considered. As a result, for deep penetration of grossly deformed particles, the contact area and hence the inertial drag will be overpredicted which results in an underprediction for the penetration.

Figure 12 shows photographs of the damage done to four of the targets. The recovered projectiles are also included where possible.

Figure 13 contains the results for the impact of aluminum spheres into aluminum targets and Figure 14 contains post-test photographs of four of the targets. The projectiles remained intact, but deformed, for impact velocities below 5,000 fps. The aluminum projectile is not quite as soft as the lead projectile. To compute particle deformation, the constitutive law defined by (17) with a yield stress of 13,000 psi was used.

Figures 15 and 16 show the results for the impact of aluminum spheres into steel targets. Note that the ordinate in Figure 15 is an order of magnitude smaller than for the previous penetration figures. For crater depths in excess of 0.1 times the ball diameter, the agreement between theory and data is very good. For

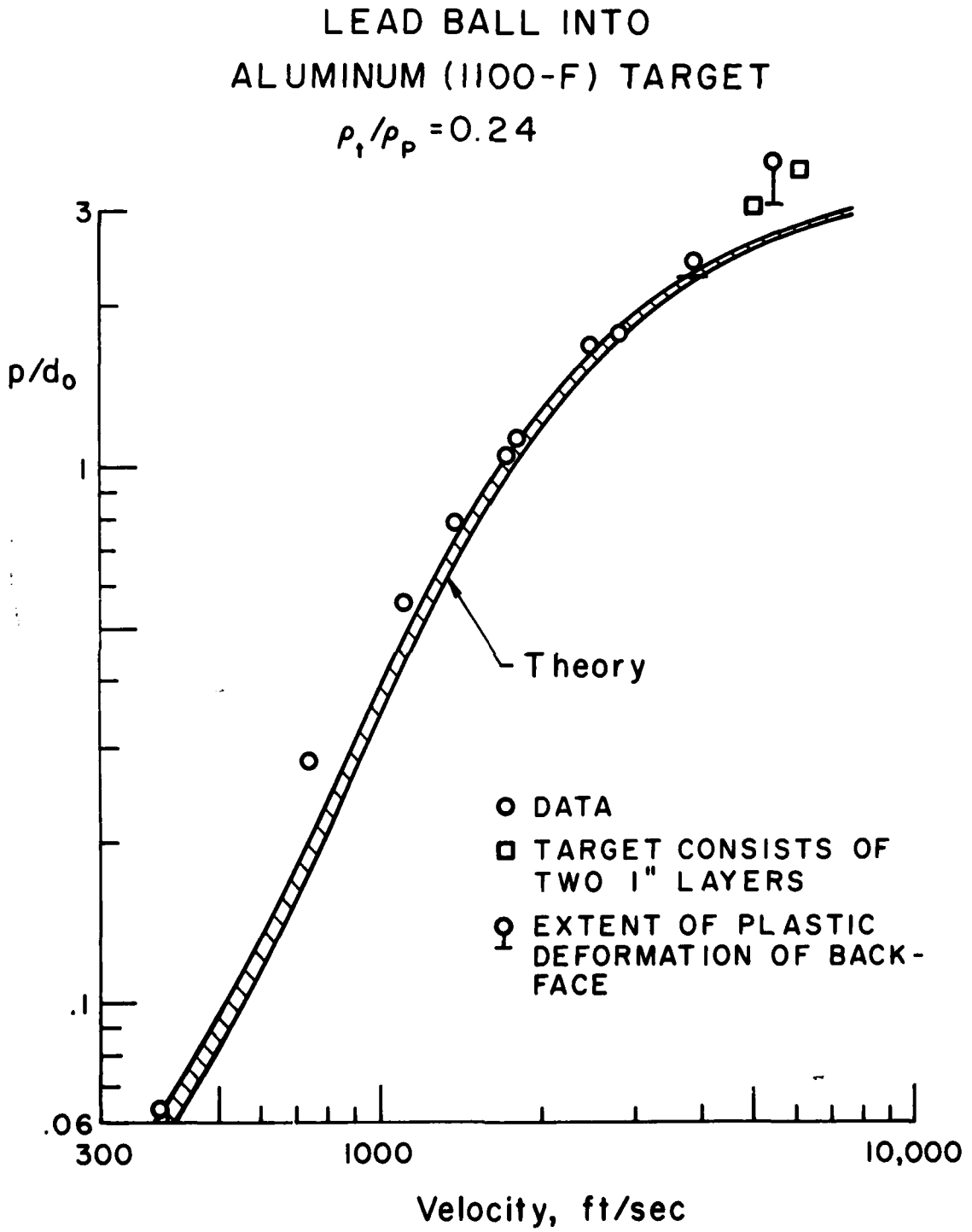

Figure 11. Crater Depth - Lead Ball into Aluminum Target.

TARGET MATERIAL - ALUMINUM

PROJECTILE MATERIAL - LEAD

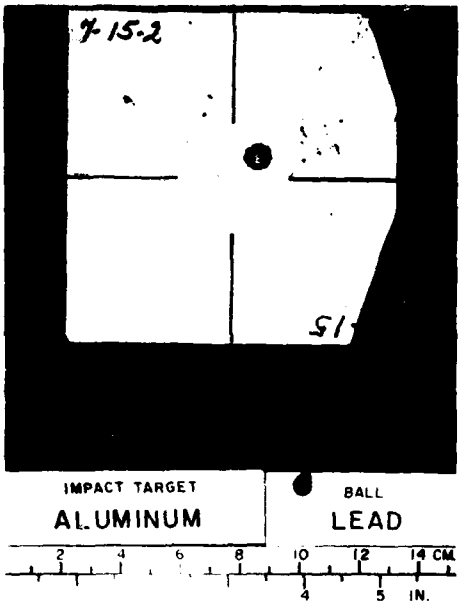

V = 757 ft/sec

$P/d_o = .29$

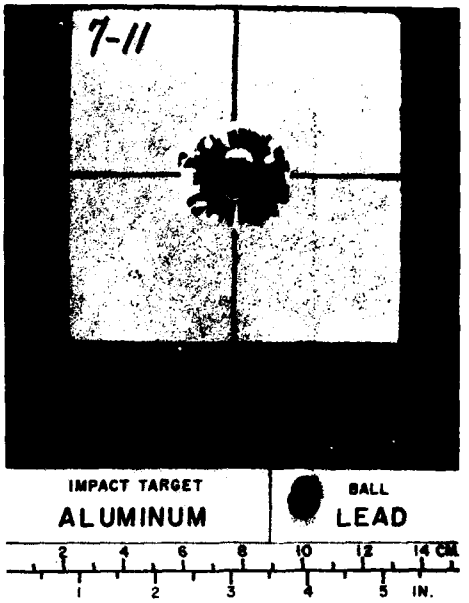

V = 2824 ft/sec

$P/d_o = 1.73$

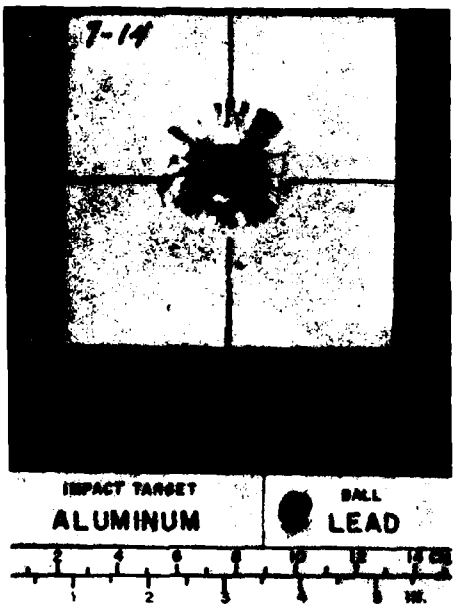

V = 3865 ft/sec

$P/d_o = 2.42$

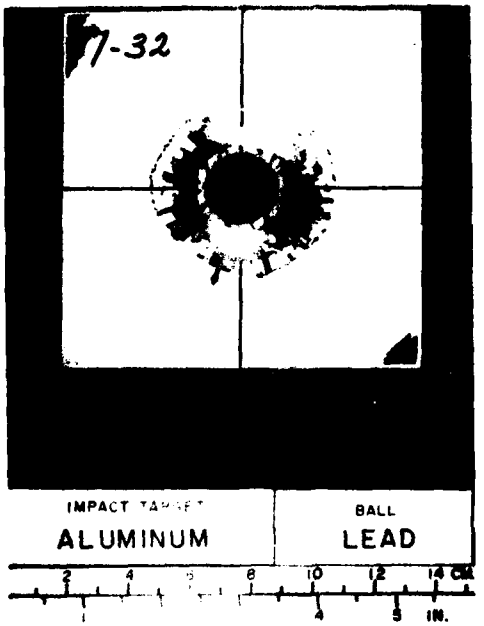

V = 6024 ft/sec

$P/d_o = 3.43$

Figure 12. Photographs - Lead Ball into Aluminum Target.

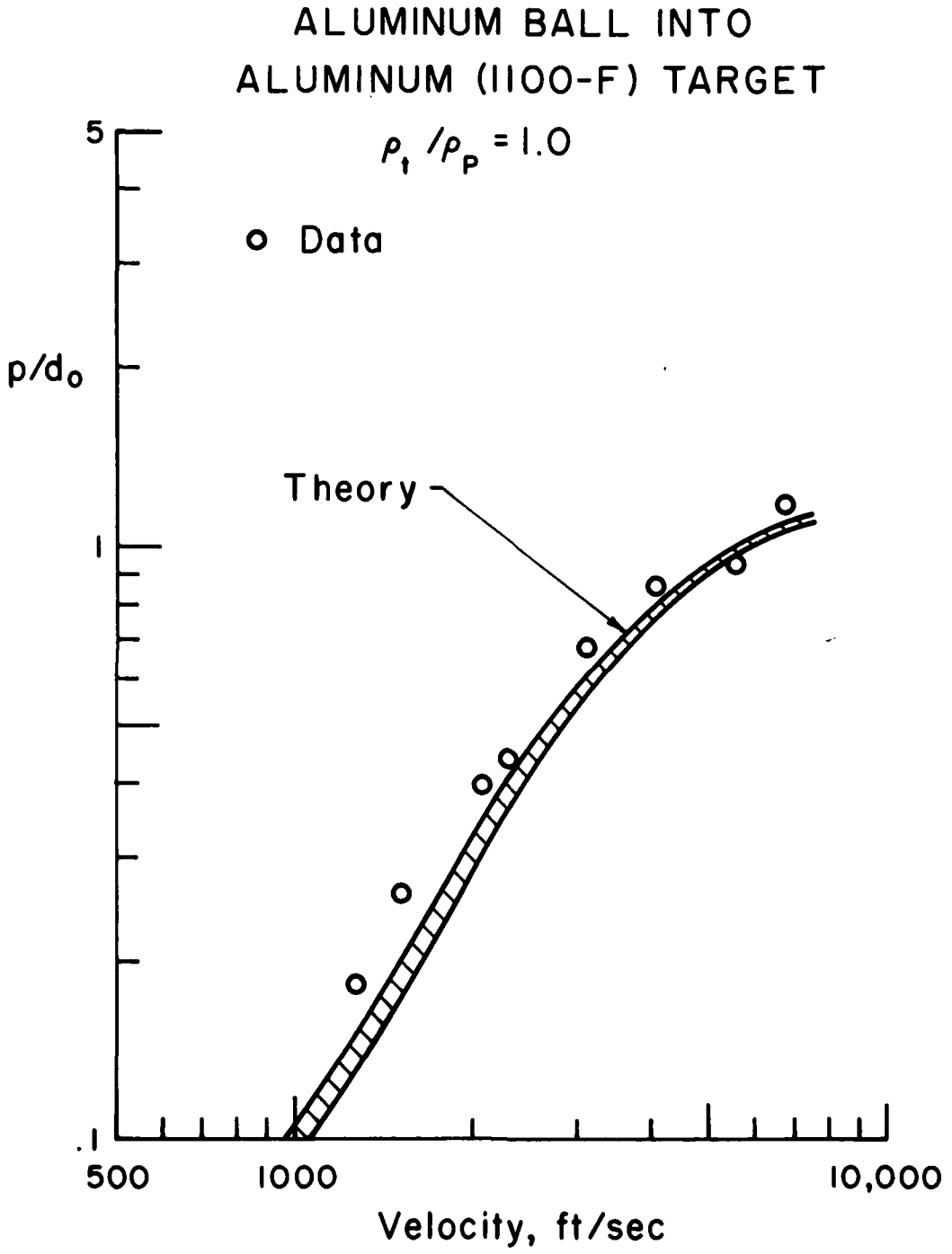

Figure 13. Crater Depth - Aluminum Ball into Aluminum Target.

TARGET MATERIAL - ALUMINUM

PROJECTILE MATERIAL - ALUMINUM

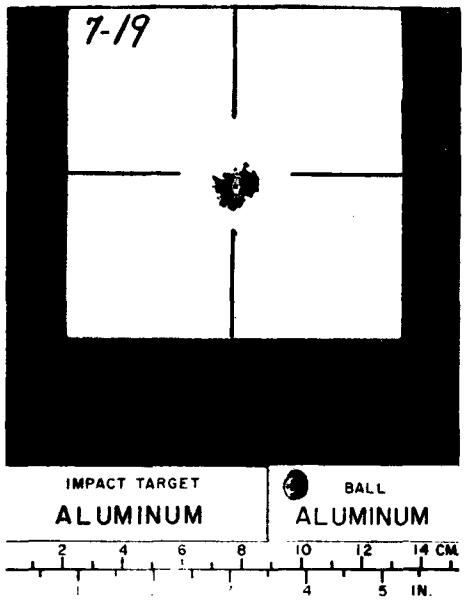

V = 1271 ft/sec

P/d_o = .18

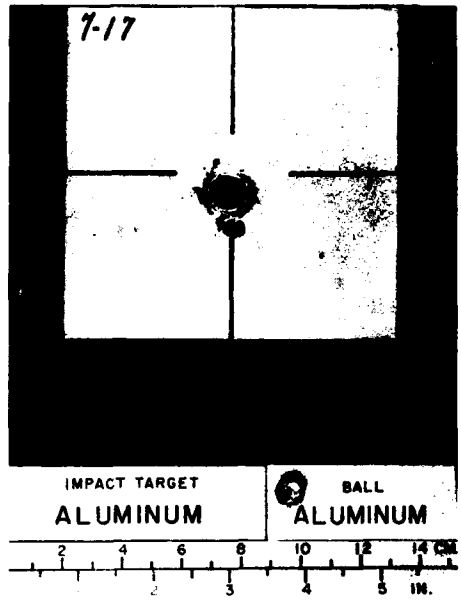

V = 3111 ft/sec

P/d_o = .68

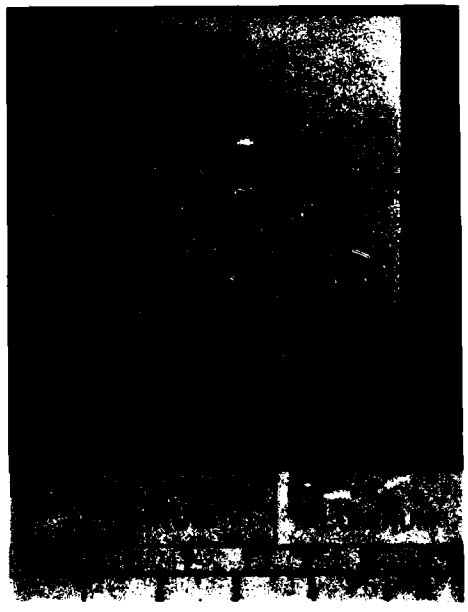

V = 4070 ft/sec

P/d_o = .86

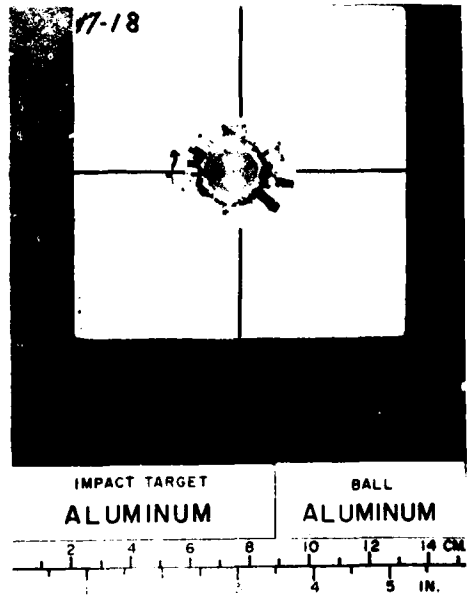

V = 5521 ft/sec

P/d_o = .93

Figure 14. Photographs - Aluminum Ball into Aluminum Target.

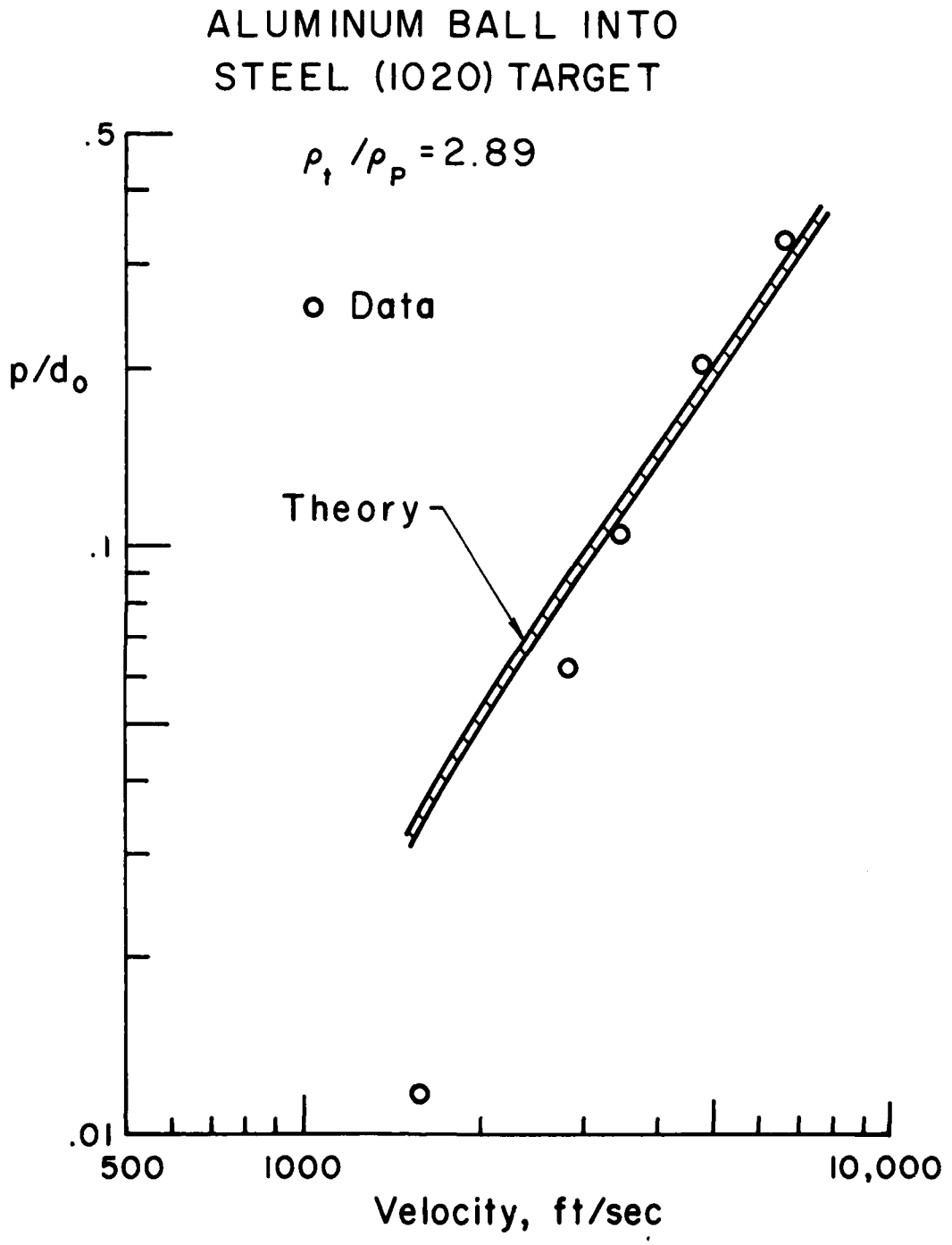

Figure 15. Crater Depth - Aluminum Ball into Steel Target.

TARGET MATERIAL - STEEL

PROJECTILE MATERIAL - ALUMINUM

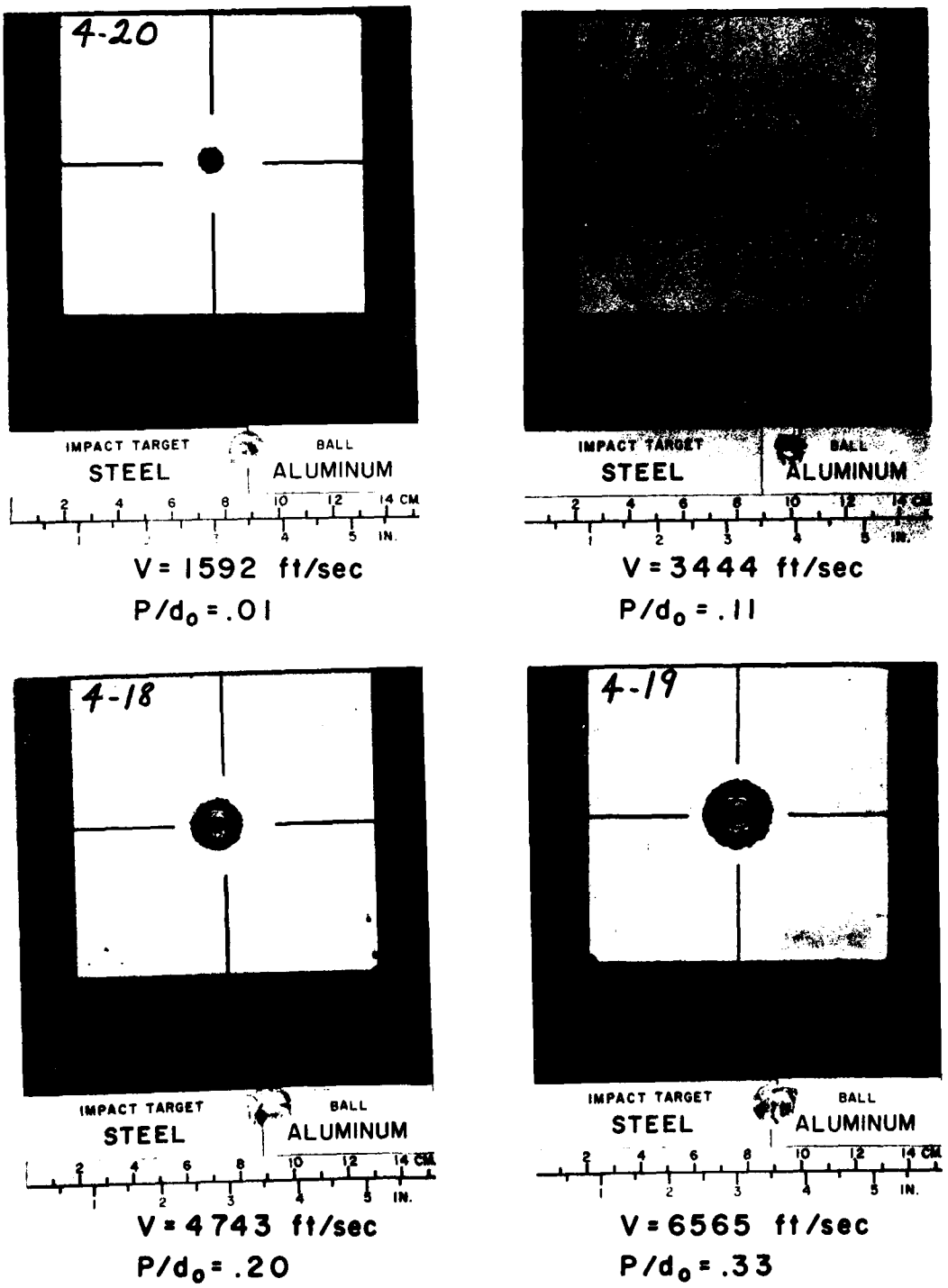

Figure 16. Photographs - Aluminum Ball into Steel Target.

the very shallow craters, the percentage error is large but the absolute error is less than 0.005 inches. It is interesting to note the gross deformation of the projectile which is shown in Figure 16.

3.3.2 Two-Layer Targets

The next series of data is for semi-infinite targets composed of two layers of steel and aluminum. Figure 17 shows the results for the impact of a tungsten carbide sphere into an aluminum/steel target and Figure 18 shows photographs of the post-test targets and projectiles. For these tests, the ball remained intact below 2,000 fps. Approximately 15% of the ball was removed as a result of brittle fracture at 3,000 fps. The ball was broken in half at 4,300 fps and was completely pulverized at 5,000 fps.

Theoretical predictions using the rigid sphere model are shown by the solid curve in Figure 17. Note that the interface is simply taken to be a mathematical discontinuity. The agreement between theory and data is very good in the region where the rigid sphere model is applicable, i.e., for impact velocities below 5,000 fps. Although the ball is broken at 3,000 fps, the rigid model is still applicable at higher velocities because the contact surface remains spherical. Above 5,000 fps, the ball is pulverized at impact. Hence, the crater depth is considerably less than the prediction based on a spherical contact surface.

Figures 19 and 20 show the results for the impact of tungsten carbide spheres into steel/aluminum targets. For velocities below 3,000 fps, the projectile remained intact and embedded in the target. Above this velocity, the ball was broken during impact.

The theoretical computations are again based on a rigid sphere model. Agreement between theory and the rigid ball data is good. The largest relative error occurs for shallow penetration of the second layer and is due to assuming a discontinuity in the value of E_* at the interface. Recall that in the simple model for layered targets, the value of E_* is constant across the thickness of each layer. This constant value is deduced from impact tests of

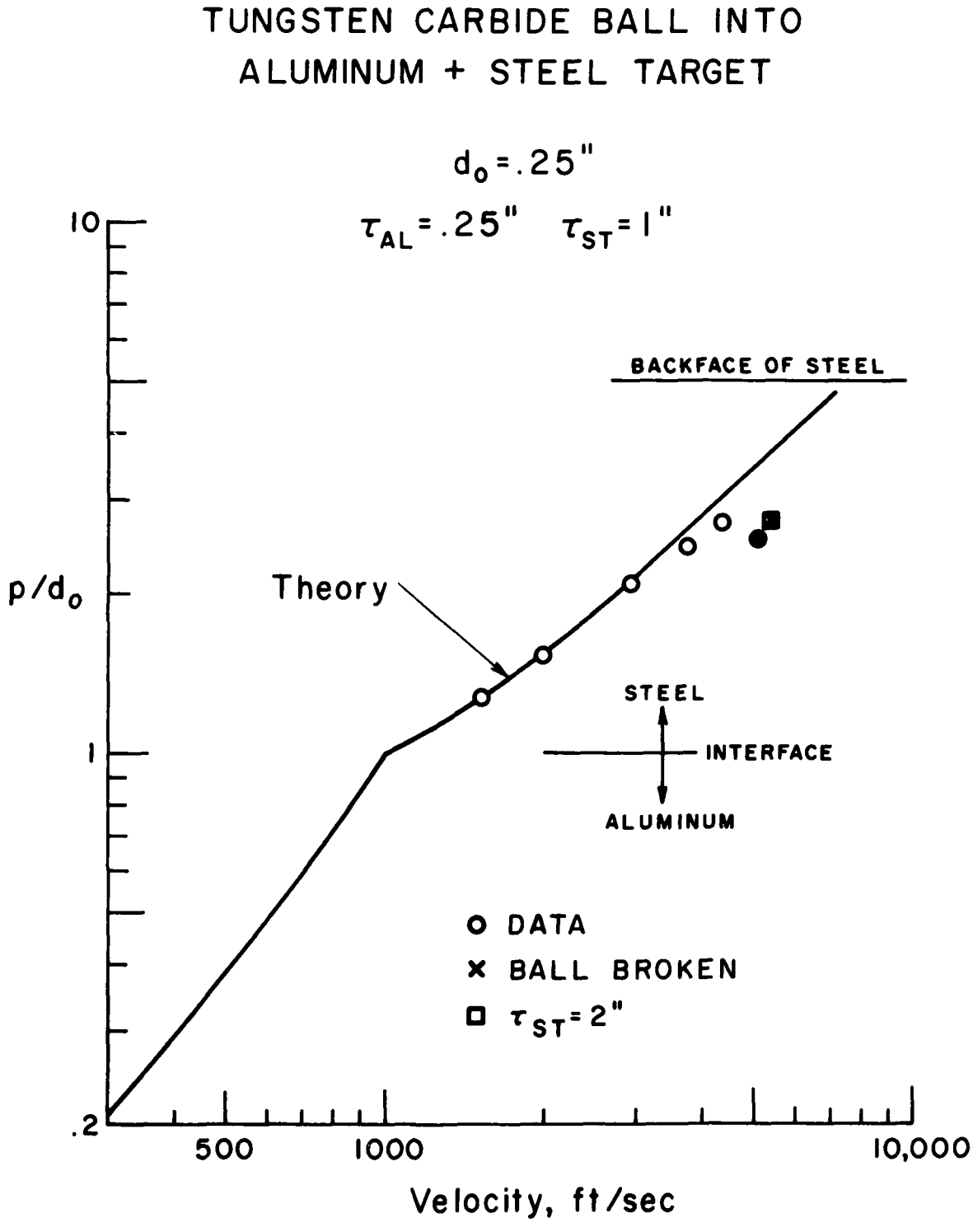

Figure 17. Crater Depth - Tungsten Carbide into Alum/Steel Target.

TARGET MATERIAL - ALUMINUM/STEEL

PROJECTILE MATERIAL - TUNGSTEN CARBIDE

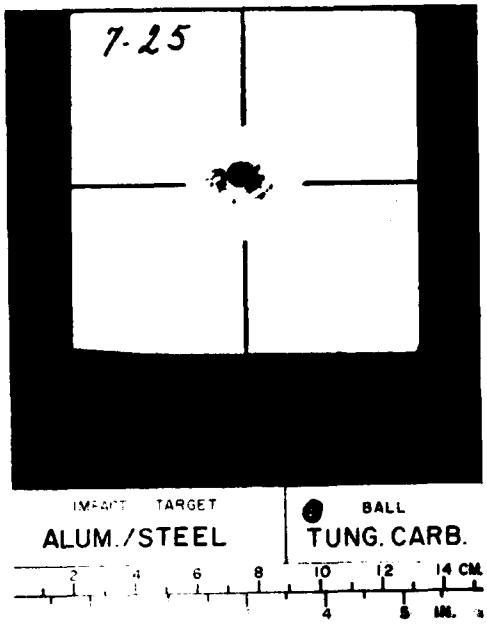

V = 1522 ft/sec

P/d_o = 1.27

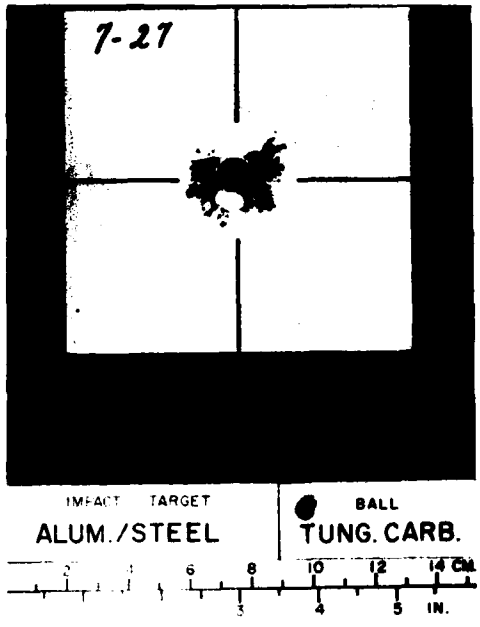

V = 2925 ft/sec

P/d_o = 2.07

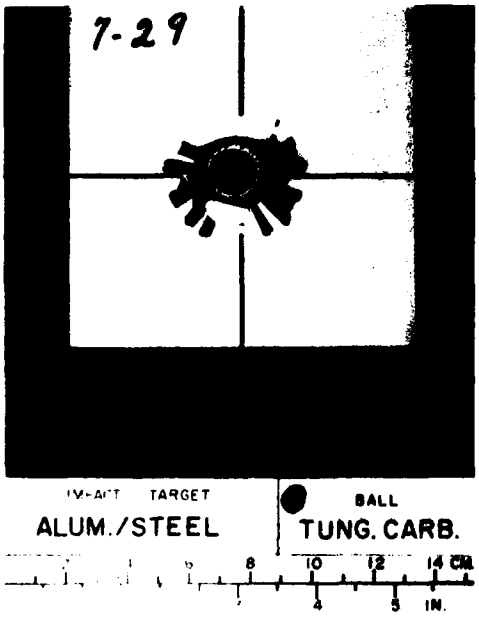

V = 4345 ft/sec

P/d_o = 2.68

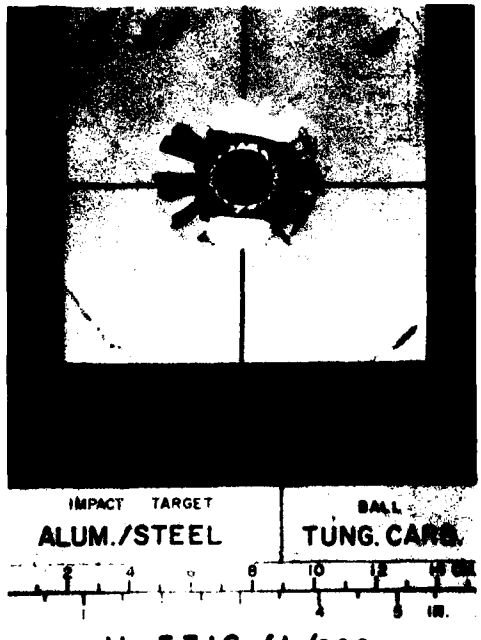

V = 5316 ft/sec

P/d_o = 2.74

Figure 18. Photographs - Tungsten Carbide into Alum/Steel Target.

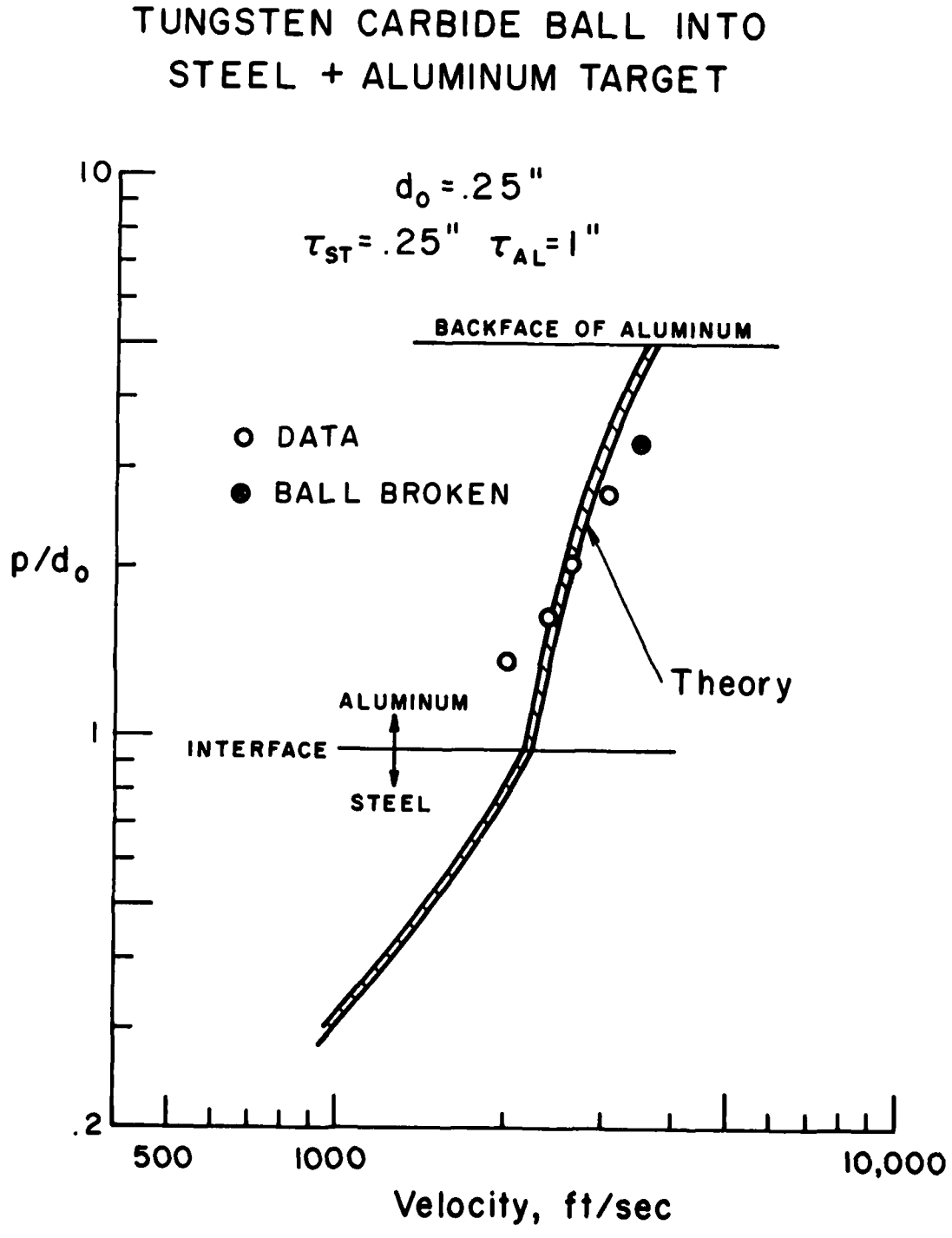

Figure 19. Crater Depth - Tungsten Carbide Ball into Steel/Alum Target.

TARGET MATERIAL - STEEL/ALUMINUM

PROJECTILE MATERIAL - TUNGSTEN CARBIDE

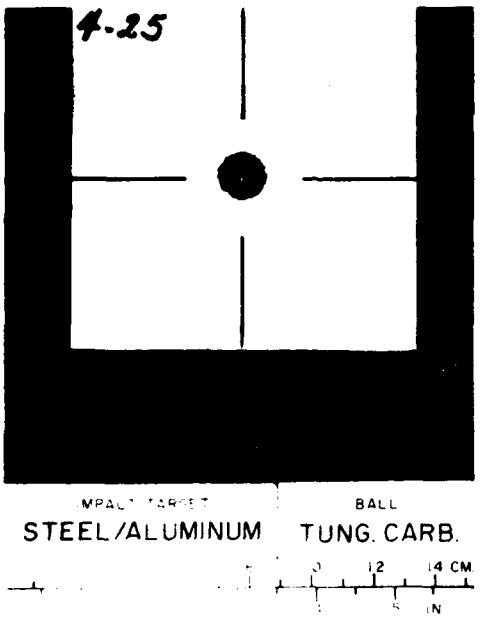

V = 2013 ft/sec

$P/d_0 = 1.37$

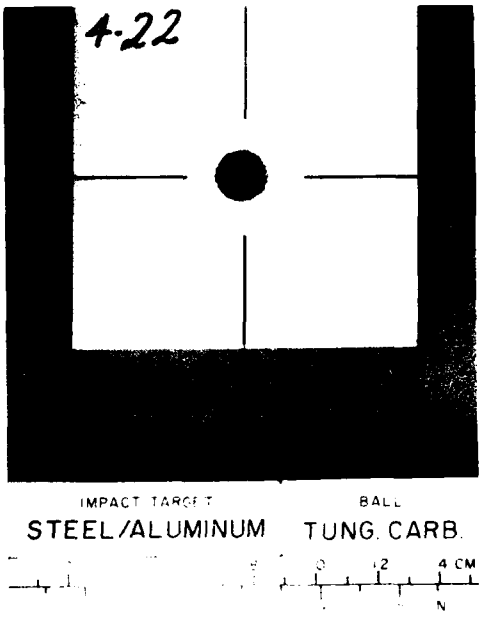

V = 2579 ft/sec

$P/d_0 = 2.05$

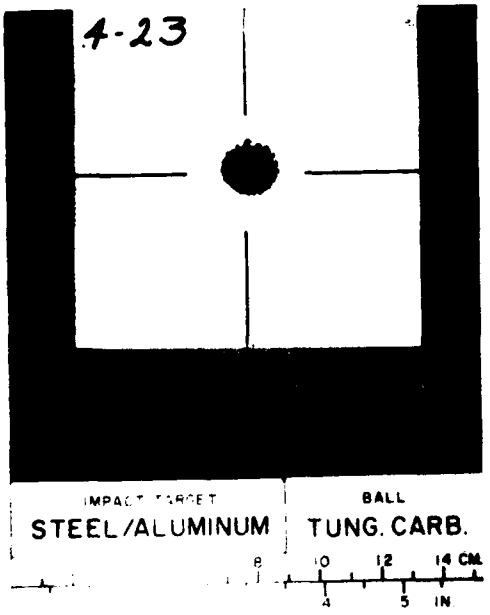

V = 3023 ft/sec

$P/d_0 = 2.66$

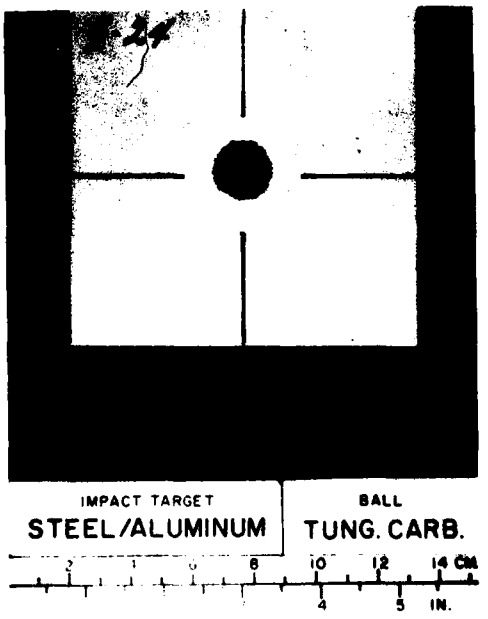

V = 3429 ft/sec

$P/d_0 = 3.32$

Figure 20. Photographs - Tungsten Carbide Ball into Steel/Alum Target.

semi-infinite targets. The results of some recent experimentation, done under a previously mentioned DARPA contract, suggest that for finite thickness layers there is a coupling effect between adjacent layers; i.e., the effective E_* near the backface of the first layer is dependent on the E_* of the material in the second layer. This effect produces a smoother transition between layers for the predicted target response than is shown in Figure 19.

Figures 21 and 22 show the results for the impact of lead projectiles into aluminum/steel targets. Except for the low velocity test, all of the projectiles were destroyed during impact. Computations are based on a constant mass, hydrodynamic model for the lead ball. The agreement between theory and data is within approximately 20% with the bulk of the discrepancy attributed to the assumed mathematical discontinuity at the interface.

Figures 23 and 24 show results for lead impacting steel/aluminum targets. Note that the steel layer is much thinner than for the previous two-layer targets. For velocities below 5,000 fps, the projectile was grossly deformed but remained intact. For higher velocities, the ball was destroyed. The craters for this target were deeper than any of the preceding two-layer targets. In some cases, there was significant plastic deformation of the backface; the extent of deformation is noted by the bar beneath the appropriate data symbols. The bottom of the bar denotes the depth which is obtained by subtracting the measured thickness of target material in the plastically deformed region from the initial thickness of the target.

The theory tends to underpredict by approximately 25% the depth of the craters produced by grossly deformed projectiles. As was noted earlier, this error is primarily due to neglecting the curvature of the front face of the particle during penetration. This result is not a significant limitation on the applicability of the theory to armor design. From a design viewpoint, the most severe test for an armor is its ability to defeat a nondeforming

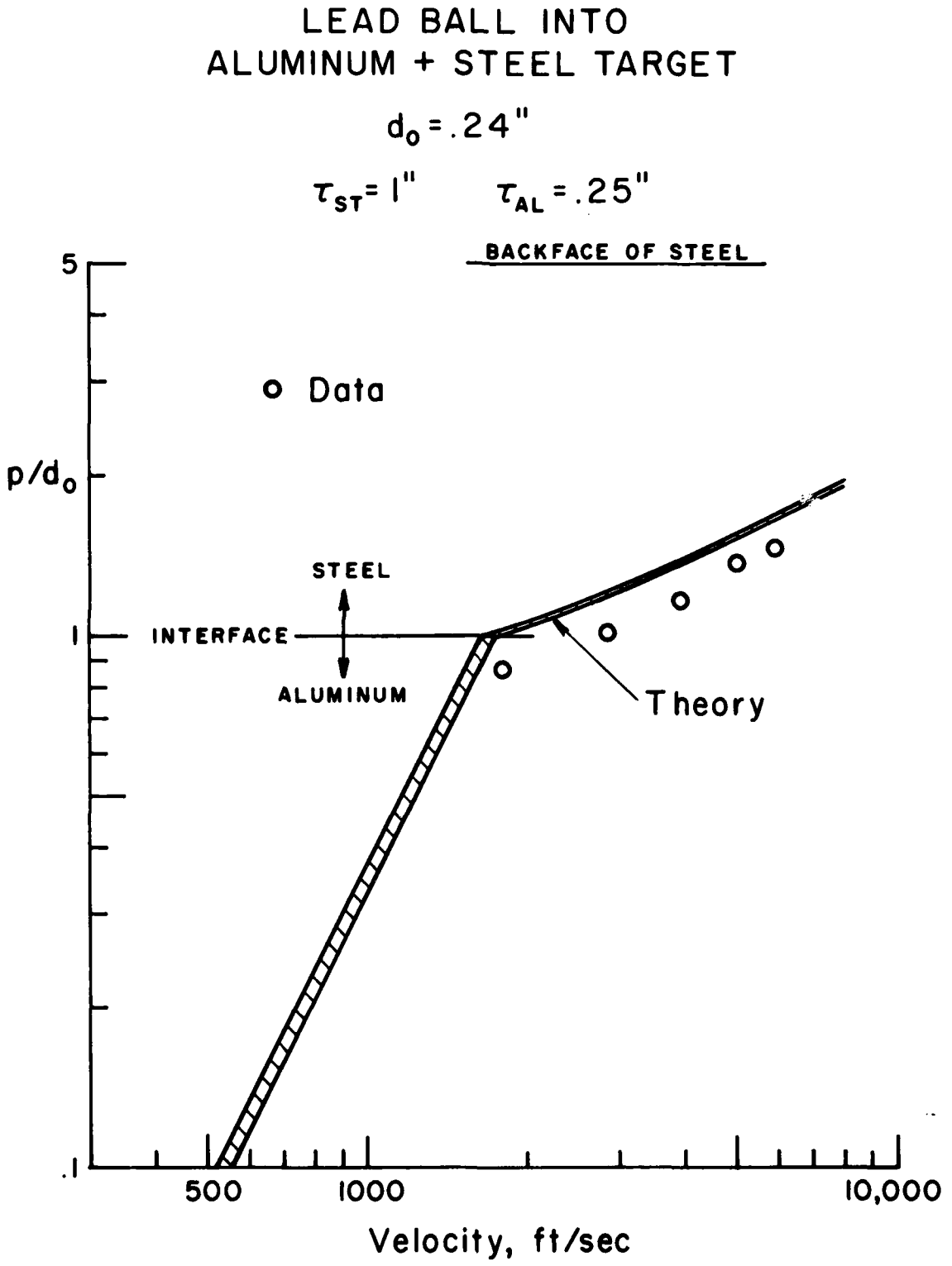

Figure 21. Crater Depth - Lead Ball into Alum/Steel Target.

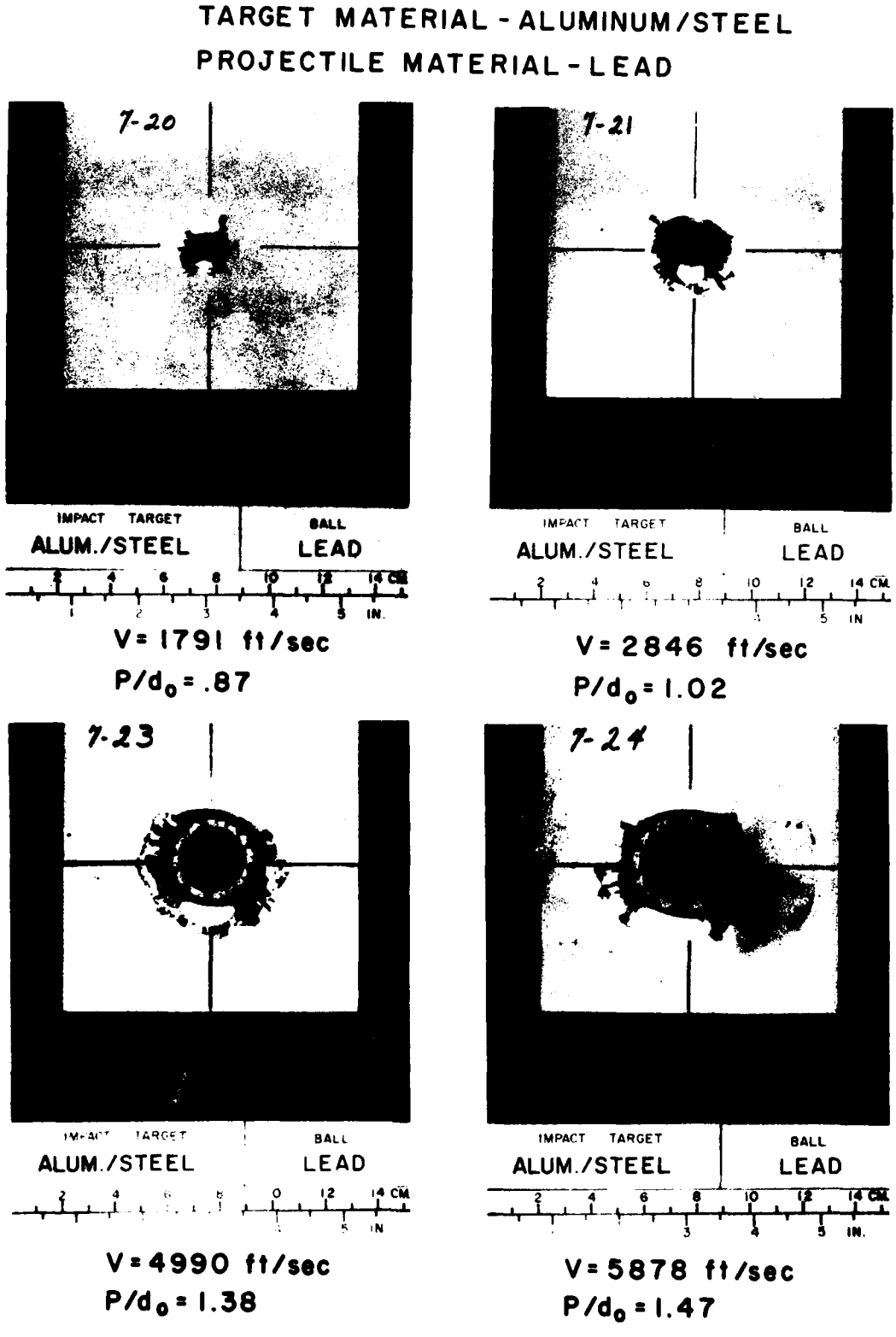

Figure 22. Photographs - Lead Ball into Alum/Steel Target.

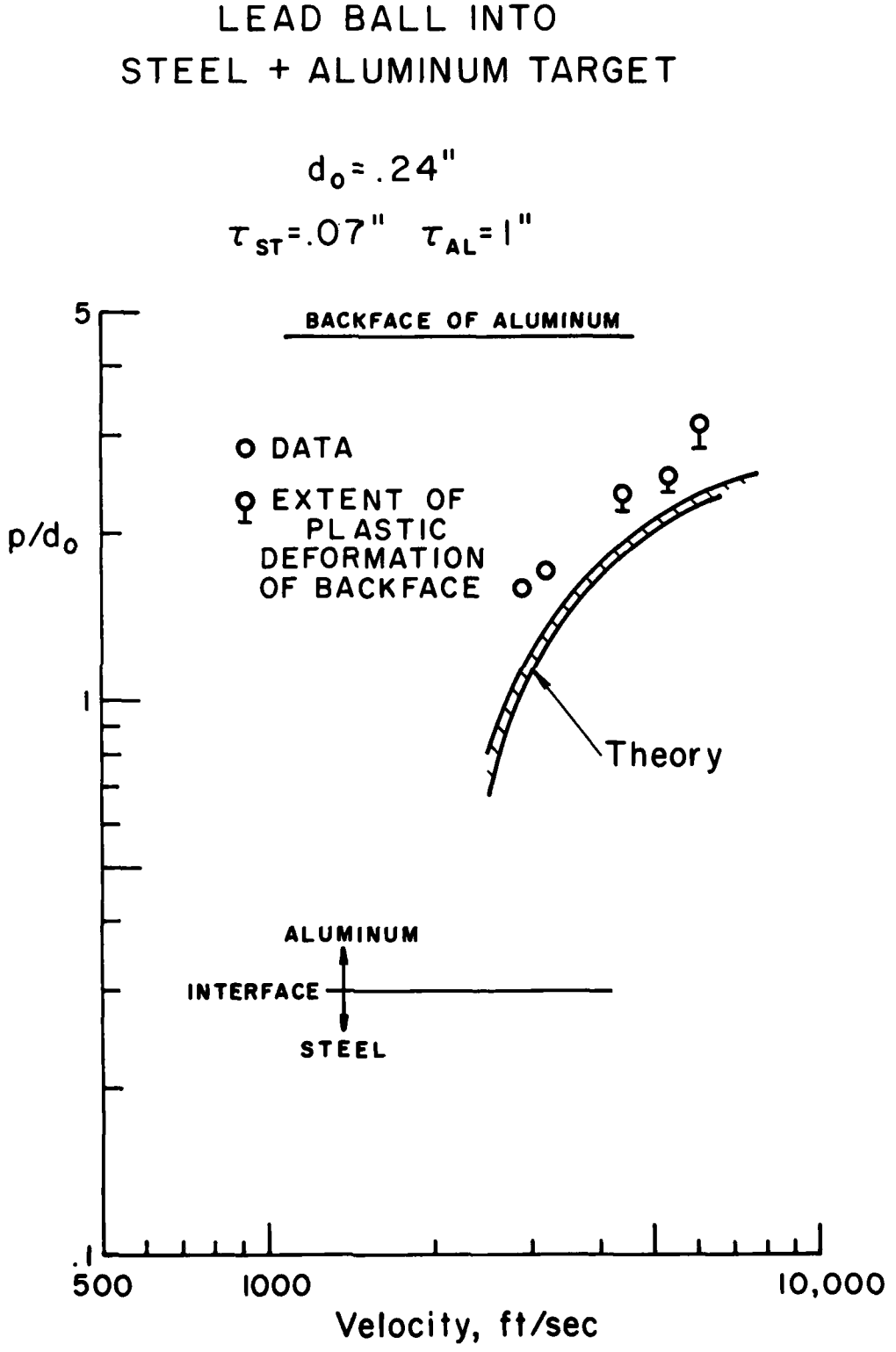

Figure 23. Crater Depth - Lead Ball into Steel/Alum Target.

TARGET MATERIAL - STEEL/ALUMINUM

PROJECTILE MATERIAL - LEAD

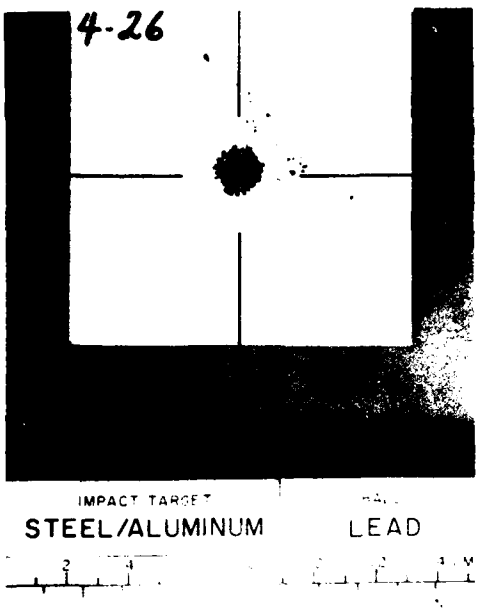

V = 2844 ft/sec

$P/d_0 = 1.6$

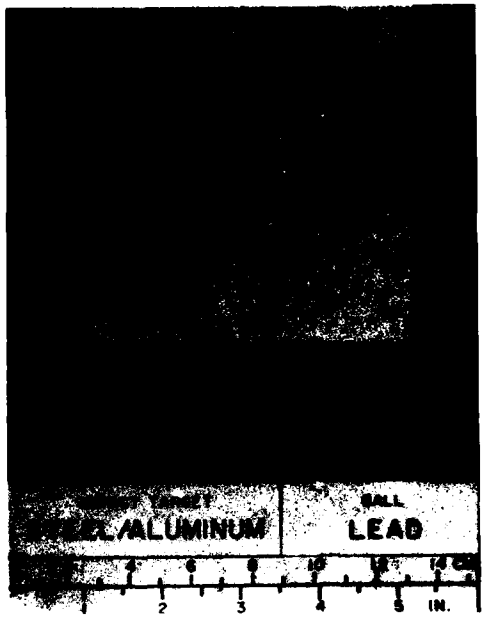

V = 4332 ft/sec

$P/d_0 = 2.37$

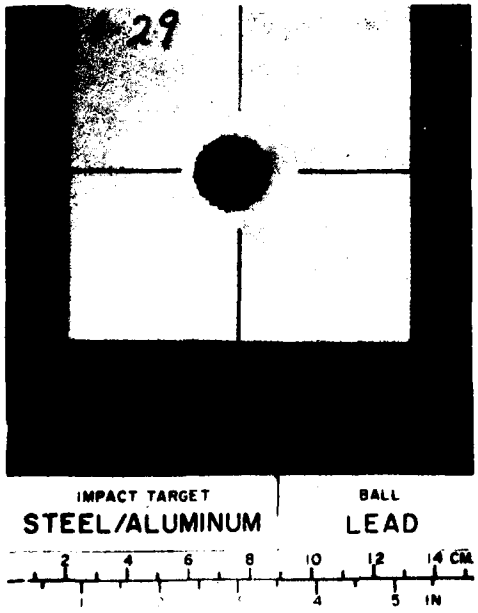

V = 5241 ft/sec

$P/d_0 = 2.53$

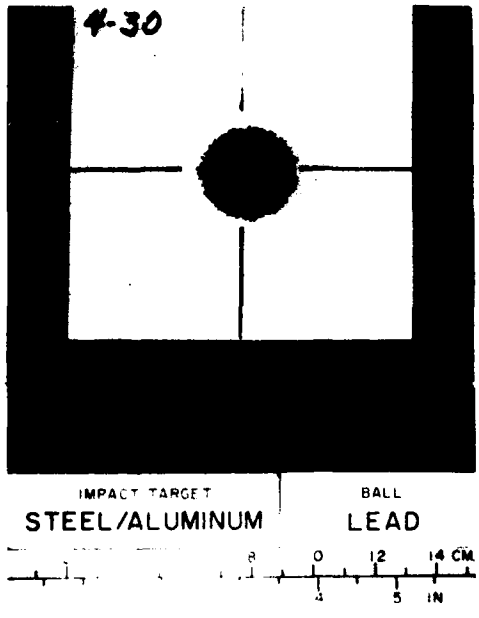

V = 6049 ft/sec

$P/d_0 = 3.28$

Figure 24. Photographs - Lead Ball into Steel/Alum Target.

projectile. The accuracy with which the model predicts target response for rigid particle impacts is illustrated in this section for several layered targets. Deep penetration by soft, grossly deformed projectiles is a less important consideration in the design analysis of an armor. Such tests were chosen for this program because they provide an extreme test for the integral theory. Despite the severity of the test, the model still predicts the data to within 25%.

3.3.3 Multilayer Targets

The next two sets of data are for semi-infinite targets composed of alternate layers of aluminum ($\tau \approx 0.05$ inches) and steel ($\tau \approx 0.07$ inches); the outer layer is aluminum.

Figures 25 and 26 show the results for the impact of these multilayer targets with tungsten carbide projectiles. The horizontal hash marks denote the interface between each of the layers. The circular symbols are for targets composed of 16 layers which results in a target thickness of approximately 1 inch. The triangular symbols are for targets composed of 24 layers backed by a 1-inch thick steel disk which results in a target thickness of approximately 2.5 inches. Significant plastic deformation of the backface was observed for the 16-layer targets for velocities in excess of 2,000 fps. There were no backface effects for the two thicker targets.

The projectile remained intact and embedded in each of the 16-layer targets; it was destroyed during impact at the velocities tested with the two thick targets. Theoretical computations based on the rigid sphere model agree with the data to within approximately 20% for those cases in which the projectile remained spherical.

Figures 27 and 28 show the results for the lead projectiles impacting the multilayer targets. Each of the targets, except one, consisted of 16 layers and was approximately 1-inch thick. The exception had a 1-inch thick steel disk behind the 16 layers. For

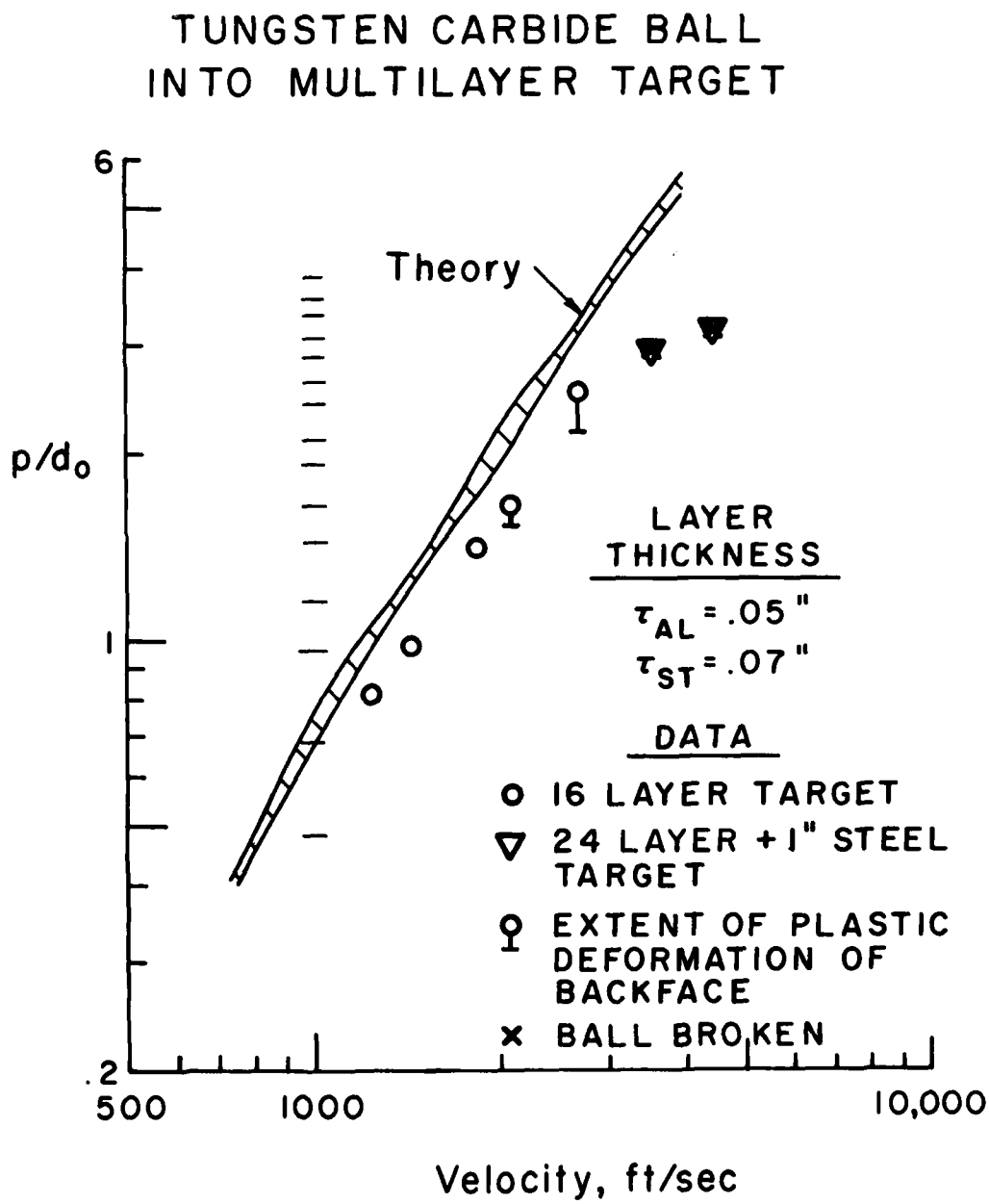

Figure 25. Crater Depth - Tungsten Carbide Ball into Multilayer Target.

TARGET MATERIAL MULTILAYERED
PROJECTILE MATERIAL - TUNGSTEN CARBIDE

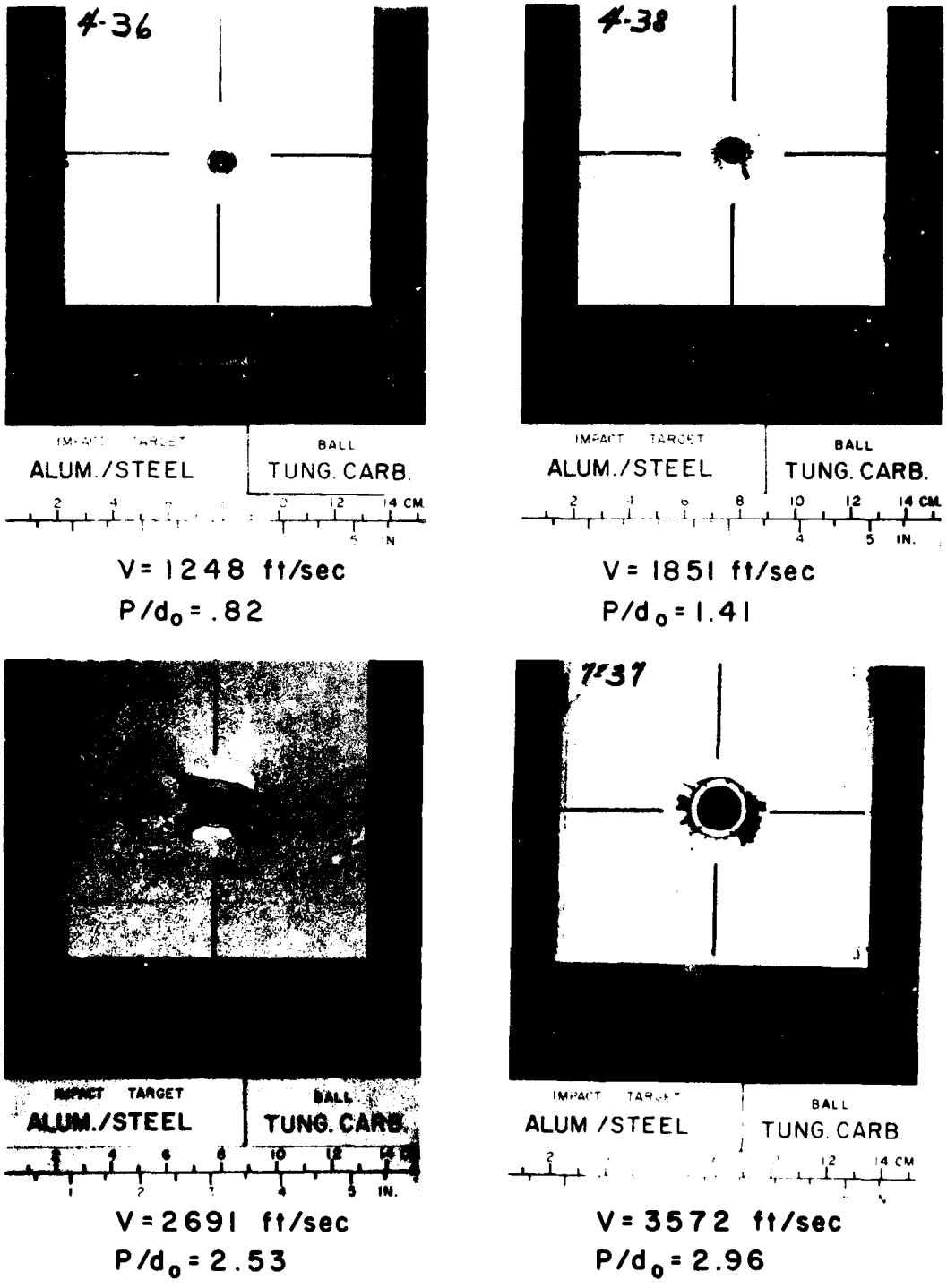

Figure 26. Photographs - Tungsten Carbide Ball into Multilayer Target.

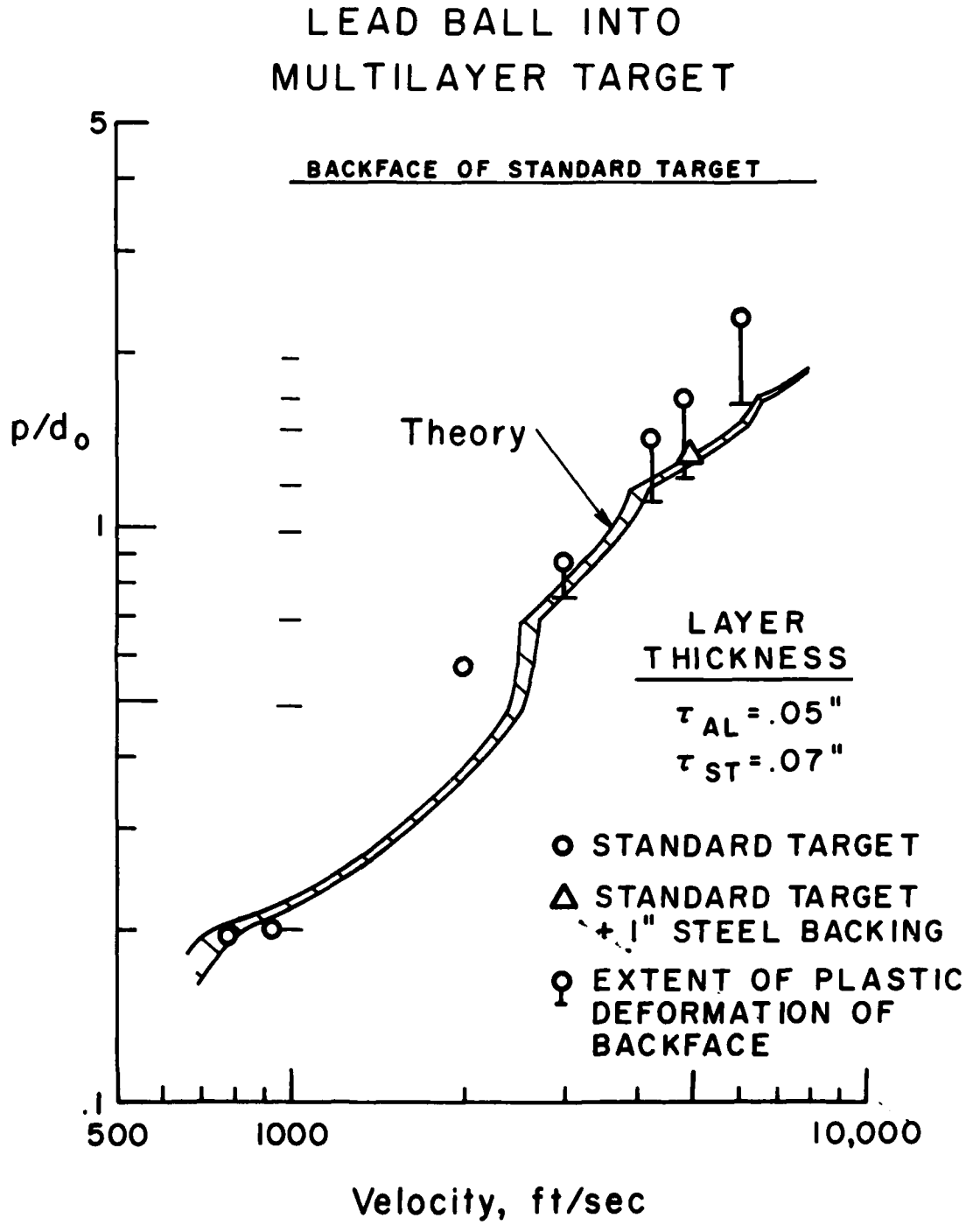

Figure 27. Crater Depth - Lead Ball into Multilayer Target.

TARGET MATERIAL MULTILAYERED

PROJECTILE MATERIAL - LEAD

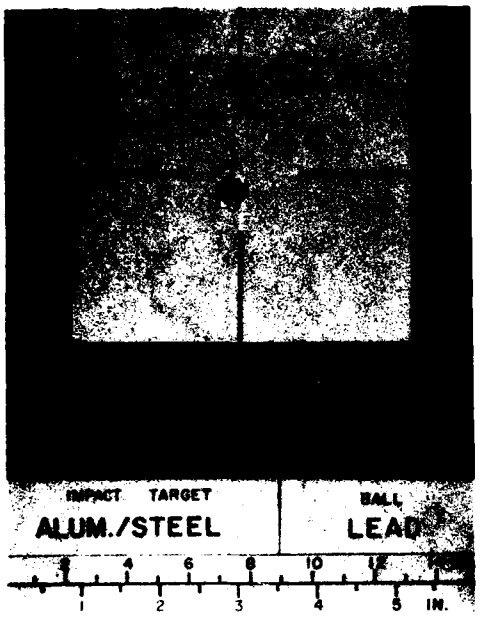

V = 785 ft/sec

$P/d_o = .20$

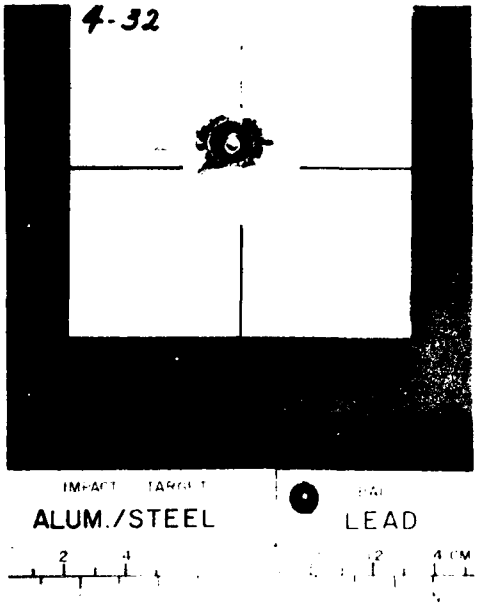

V = 2984 ft/sec

$P/d_o = .87$

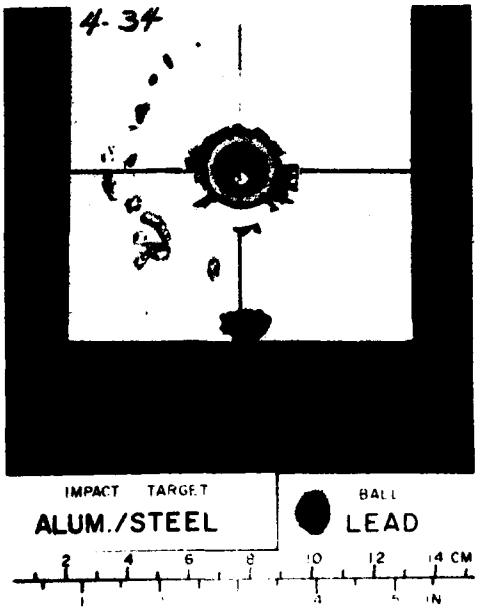

V = 4866 ft/sec

$P/d_o = 1.67$

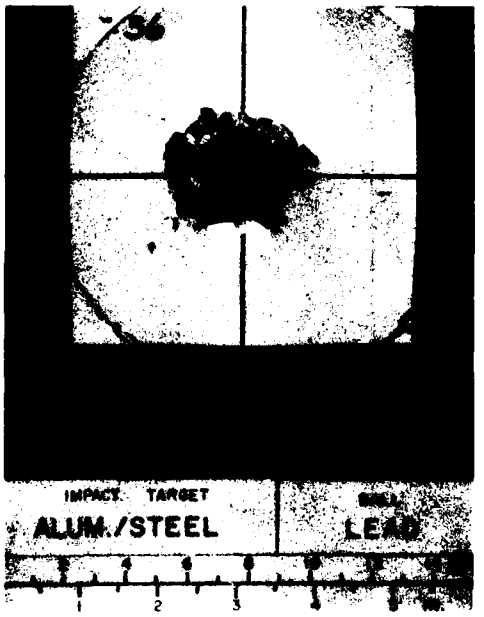

V = 6090 ft/sec

$P/d_o = 2.24$

Figure 28. Photographs - Lead Ball into Multilayer Target.

velocities above 3,000 fps, each of the standard targets had pronounced plastic deformation at the backface. The extent of this deformation is shown by the vertical bar on the data. The target with the steel disk had no backface deformation. Projectiles were recovered for velocities up to 4,970 fps. At this velocity, approximately 70% of the projectile was intact although grossly deformed.

3.4 Residual Velocity Tests

The purpose of the residual velocity tests is to provide additional evaluation of the energy partitioning aspects of the theory.* In order to illustrate the usefulness of the residual velocity data, consider the energy equation for the particle written in the following form:

$$\frac{dK_{cm}}{dt} + \frac{dK_R}{dt} + \frac{dE}{dt} + \frac{dW_t}{dt} = 0 \qquad (28)$$

where K_{cm} and K_R are the kinetic energy associated with the mass center motion and relative to this motion, respectively, E is the energy dissipation in the projectile and W_t is the work done on the target.

If the particle is nondeforming, then $\frac{dK_R}{dt} = \frac{dE}{dt} = 0$. In this case, the change in mass center kinetic energy is equal to the work done on the target. Measurement of both impact and residual velocity is, in effect, a measurement of ΔK_{cm} and, therefore, of the work done on the target. Hence, if the prediction for residual velocity is correct, then the prediction for work done on the target must also be correct.

If the particle is deforming, then $\frac{dK_R}{dt} \neq \frac{dE}{dt} \neq 0$. In this case, a correct prediction for the residual velocity means that each of the terms in (28) is correctly predicted (or errors in one

*Residual velocity data are also useful for application to spaced targets and/or layered targets with large impedance mismatches between layers.

term are compensated by another term). This implies that the projectile deformation as well as the work done on the target are accurately modeled. In the following discussion, both rigid and deforming particles are considered.

3.4.1 Rigid Particles

Figure 29 shows the residual velocity of tungsten carbide projectiles which have impacted aluminum targets of various thickness. The projectile remained intact during perforation of the thin target (τ = 0.05"). Target debris was not observed on the witness plate except for the test at 4,200 fps. Debris was observed at 2,550 fps for the 0.25" target; the projectile again remained intact for all tests. For the 0.5" target, the projectile was apparently broken at 3,600 fps and target debris was deposited on the witness plate at this velocity. The same results were obtained for the 1.0" target; projectile breakup and energetic target debris occurred at 3,500 fps.

Theoretical predictions for the projectile velocity at the exit plane of the target using the rigid sphere model and an E_{*p} = 84 Btu/lbm for aluminum are shown by the solid curves in Figure 29. The agreement between theory and data is excellent for the thin targets and is within 20% even for the thickest targets.

Figure 30 shows the residual velocity of tungsten carbide projectiles impacting thin steel targets. The ball apparently remained intact for these tests. Considerable debris impacted the witness plate for the 3,500 fps impact. Agreement between theory and data is within 10%.

Figure 31 shows the residual velocity of tungsten carbide projectiles impacting two-layer targets. The targets consist of a thin outer layer of steel and an inner layer of aluminum whose thickness varies from 0.05" to 1.0". Projectile breakup occurred at approximately 3,000 fps for all targets except the thinnest. For this target, breakup occurred at 4,100 fps. Considerable debris impacted the witness plate at 3,000 fps for the thin

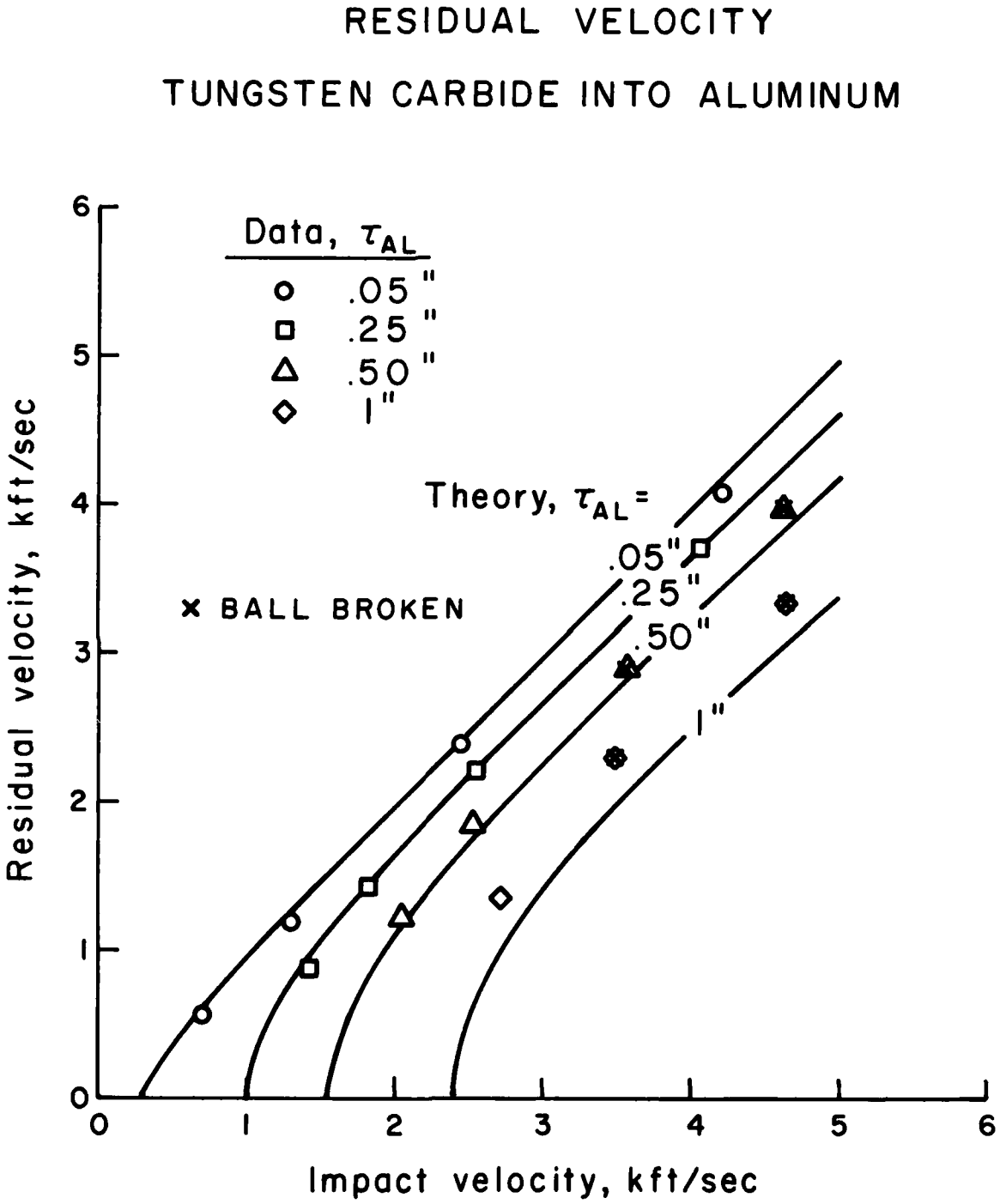

Figure 29. Residual Velocity - Tungsten Carbide Ball into Aluminum Target.

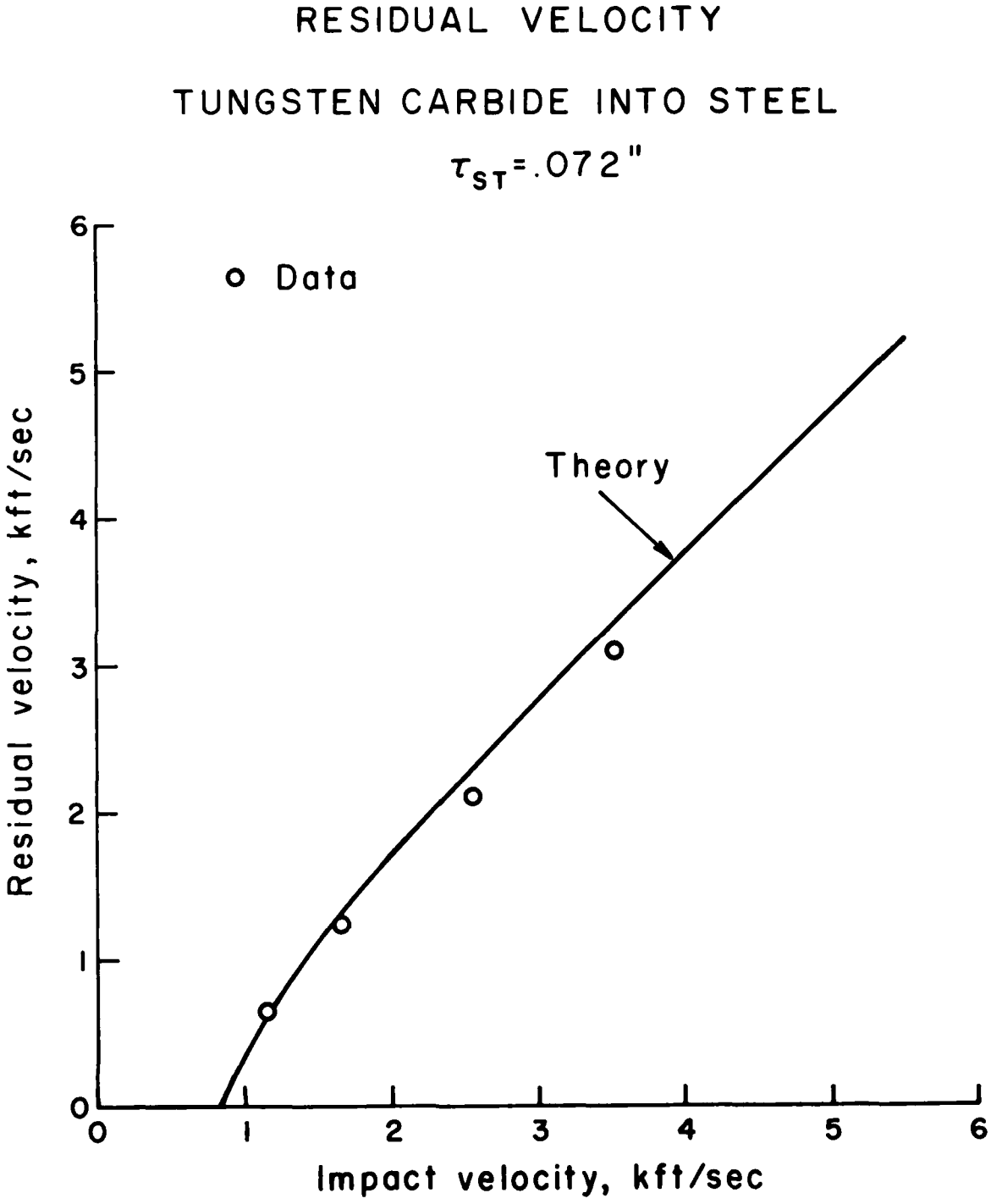

Figure 30. Residual Velocity - Tungsten Carbide Ball into Steel Target.

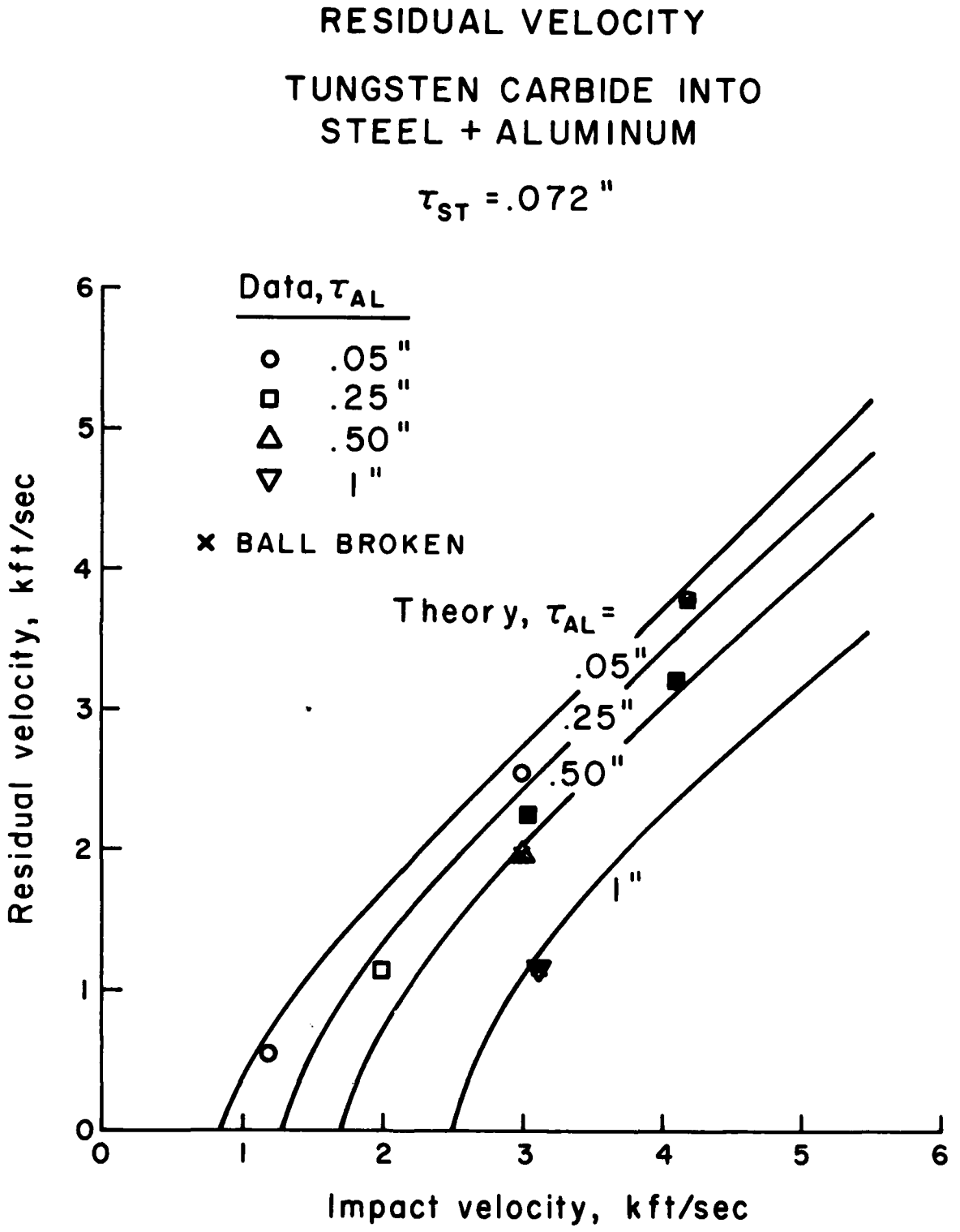

Figure 31. Residual Velocity - Tungsten Carbide Ball into Steel/Alum Target.

target. For the same impact velocity, the amount of debris decreased as the thickness of aluminum increased.

The theoretical predictions are based on the rigid sphere model with the appropriate value of E_{*p} used for each layer. No account is taken of particle breakup. In general, the theory slightly overpredicts the data; the difference, however, is less than 10%.

The residual velocity of tungsten carbide projectiles impacting multilayer targets is shown in Figure 32. Except for the test at 2,600 fps, the projectile was broken during impact for each of the tests. In addition, considerable debris impacted the witness plate. Computations using the rigid sphere model overpredict the residual velocity.

3.4.2 Deforming Particles

The residual velocity of aluminum particles impacting thin aluminum targets is shown in Figure 33. Each projectile was recovered and was plastically deformed. Considerable debris was captured for the two high velocity tests. Predictions for the center of mass velocity at the exit plane of the target based on the deforming cube model are shown by the solid curve. For illustrative purposes, the predicted front-face velocity, V_1, at the exit plane is also included. The theory overpredicts the data primarily because particle deceleration in the 9-inch distance between the target exit plane and the second breakwire station is not inlcuded. This deceleration is significant for a light, blunt shaped particle,* and accounts for much of the difference between the predicted and measured velocity.

The residual velocity of lead projectiles impacting thin steel targets is shown in Figure 34. For these tests, there is considerable uncertainty in the data due to the large amount of projectile and target debris on the witness plate. The projectile

*Particle deceleration for the tungsten carbide spheres is insignificant in this 9-inch distance.

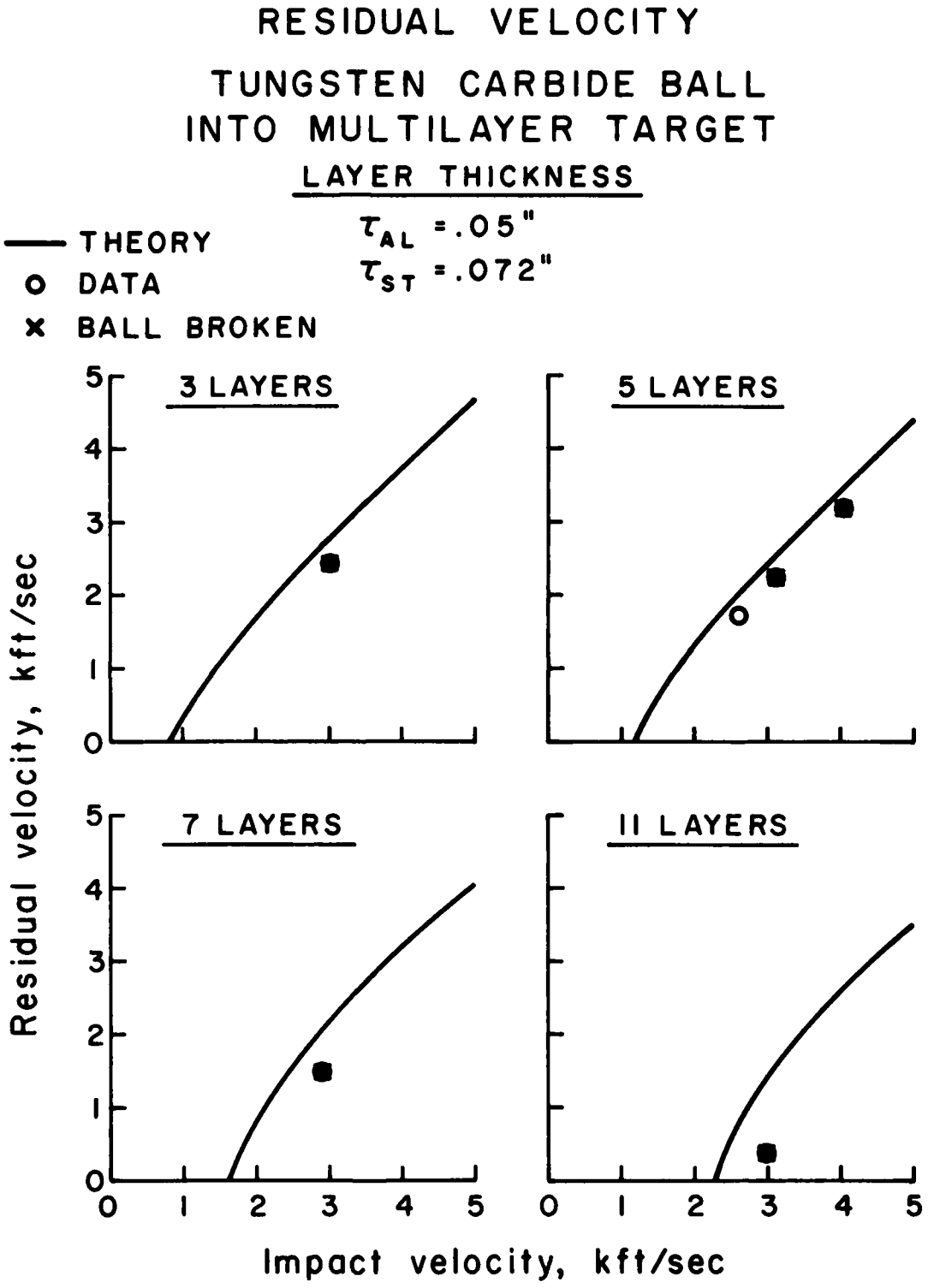

Figure 32. Residual Velocity - Tungsten Carbide Ball into Multilayer Target.

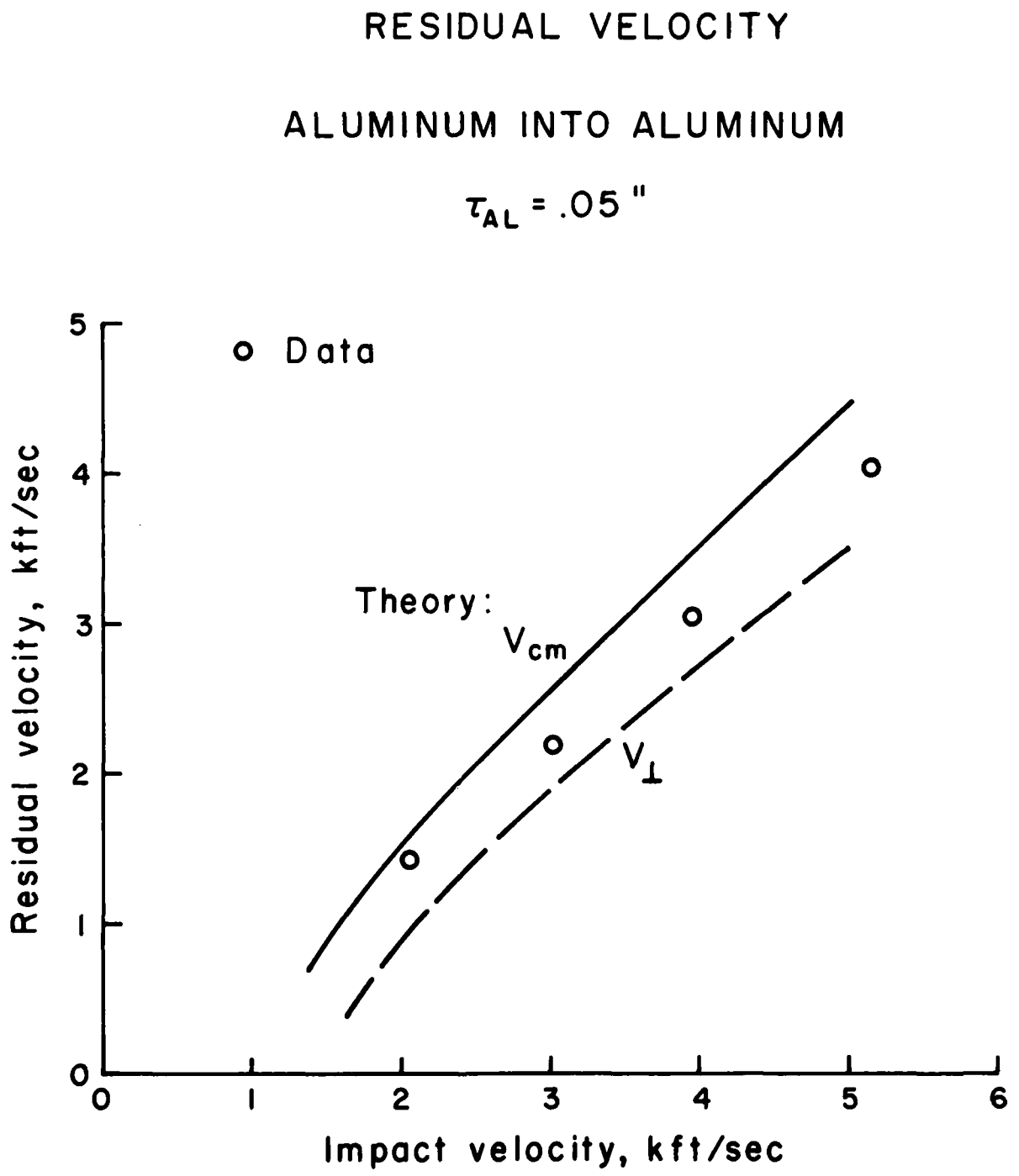

Figure 33. Residual Velocity - Aluminum Ball into Aluminum Target.

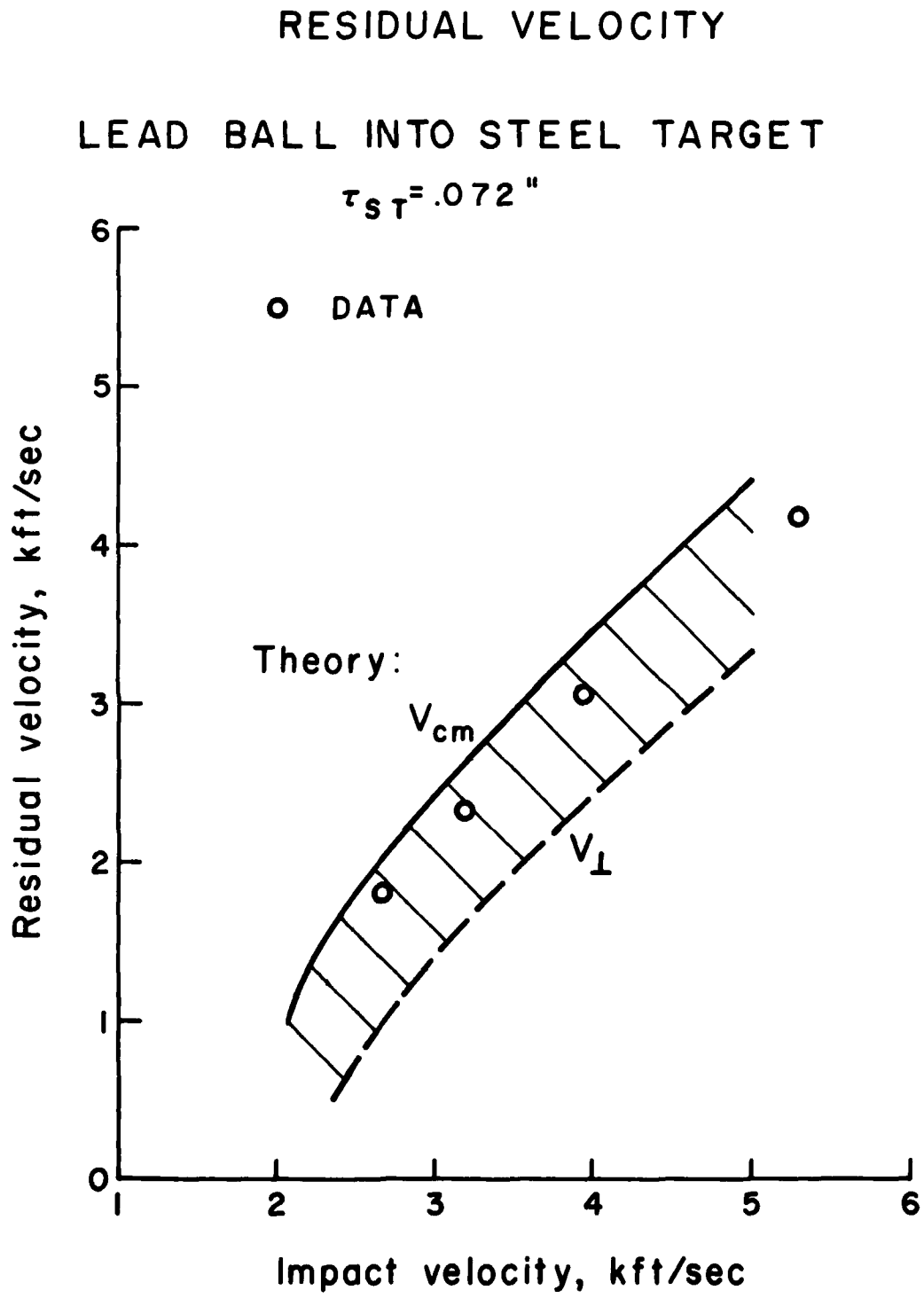

Figure 34. Residual Velocity - Lead Ball into Steel Target.

was recovered intact but grossly deformed for the test at 2,700 fps; the projectile was completely destroyed in the other tests. The predictions are in fair agreement with the data although the only one which is strictly applicable is the prediction at 2,700 fps.

The lead projectiles were also fired into aluminum targets and the results are shown in Figure 35. Below 2,500 fps, the projectiles were recovered intact but deformed; above 3,000 fps, the projectiles were destroyed during impact and the witness plate was covered with lead. These data are questionable.

3.5 Summary

What do all these results show? First, they show that the deforming projectile model can be used to make rational predictions for crater depth or residual velocity. The good agreement between theory and data which was demonstrated could only be achieved if the model for the energy absorption by the target and for the projectile deformation were good approximations for the impact process. There are still some aspects of the model which need improvement. The rectangular approximation for the spherical face does introduce some error for very shallow craters. Also, the assumption of a constant drag coefficient coupled with a rectangular contact area ignores the curvature of the deformed projectile and crater and leads to some error for very deep penetrations by grossly deformed or broken projectiles.

Second, the results show that the simple model for layered targets in which each layer is considered separately and the interfaces are treated as mathematical discontinuities can also be used to make rational predictions. In general, the error introduced by ignoring interface effects is less than 20%.

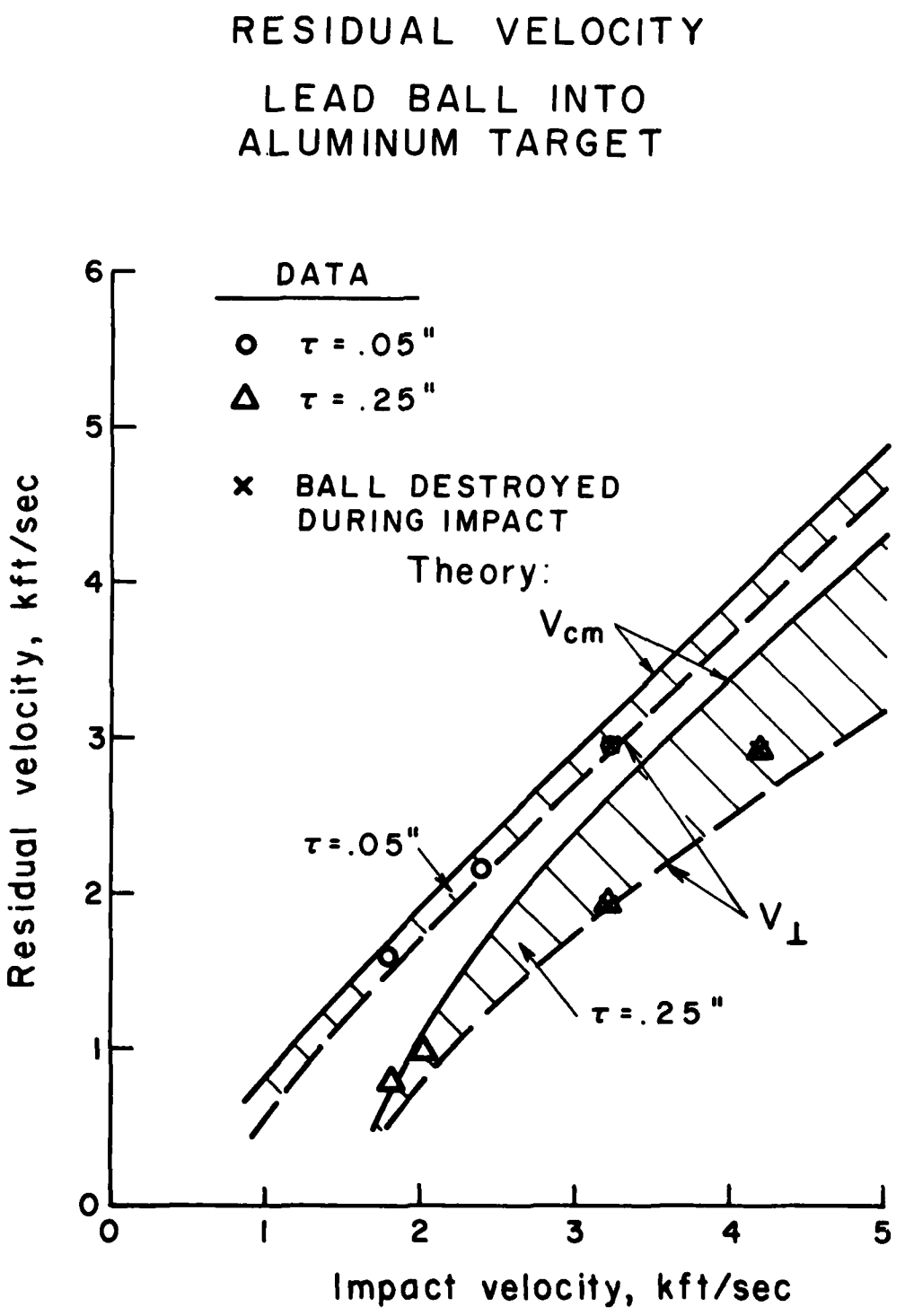

Figure 35. Residual Velocity - Lead Ball into Aluminum Target.

4. ANALYTICAL STUDIES OF LIGHTWEIGHT ARMOR

In this section, the results of some analytical studies in which the Integral Theory of Impact is applied to the design of lightweight armor are presented. These analyses utilize both the deforming projectile and the layered target models which were demonstrated in Section 3. First, the capability of several present-day armor materials, both monolithic and layered, to defeat a typical threat will be compared. Second, certain materials which have attractive impact properties will be identified. Finally, an optimization procedure will be demonstrated which can be used to obtain an improved armor.

4.1 Threat Model

In all of the studies which follow, the threat is taken to be a high velocity steel fragment. The fragment is modeled as a deforming cube. The constitutive behavior of the steel under impact conditions is taken to be hydrodynamic, i.e., material strength is ignored. The impact is normal and occurs on a flat face of the cube. Impact velocity is 5,000 fps.

4.2 Present-Day Armor Materials

Five present-day armor materials were chosen for preliminary investigation: aluminum (5083), steel, titanium, aluminum oxide, and boron carbide. The density and experimentally deduced values of E_* for each of these materials are listed in Table 1.

The thickness of each material which is required to defeat the threat is shown in Figure 36. The center of mass velocity of the projectile is plotted versus depth of penetration made non-dimensional by the characteristic length of the cube. Any point along each curve represents the material thickness which is required to reduce the projectile velocity to the corresponding value on the ordinate. The abscissa, therefore, represents the thickness required to stop the projectile. Alternatively, this figure can be used to estimate the thickness of a stopper-layer which is required to reduce the velocity to a value which can be easily

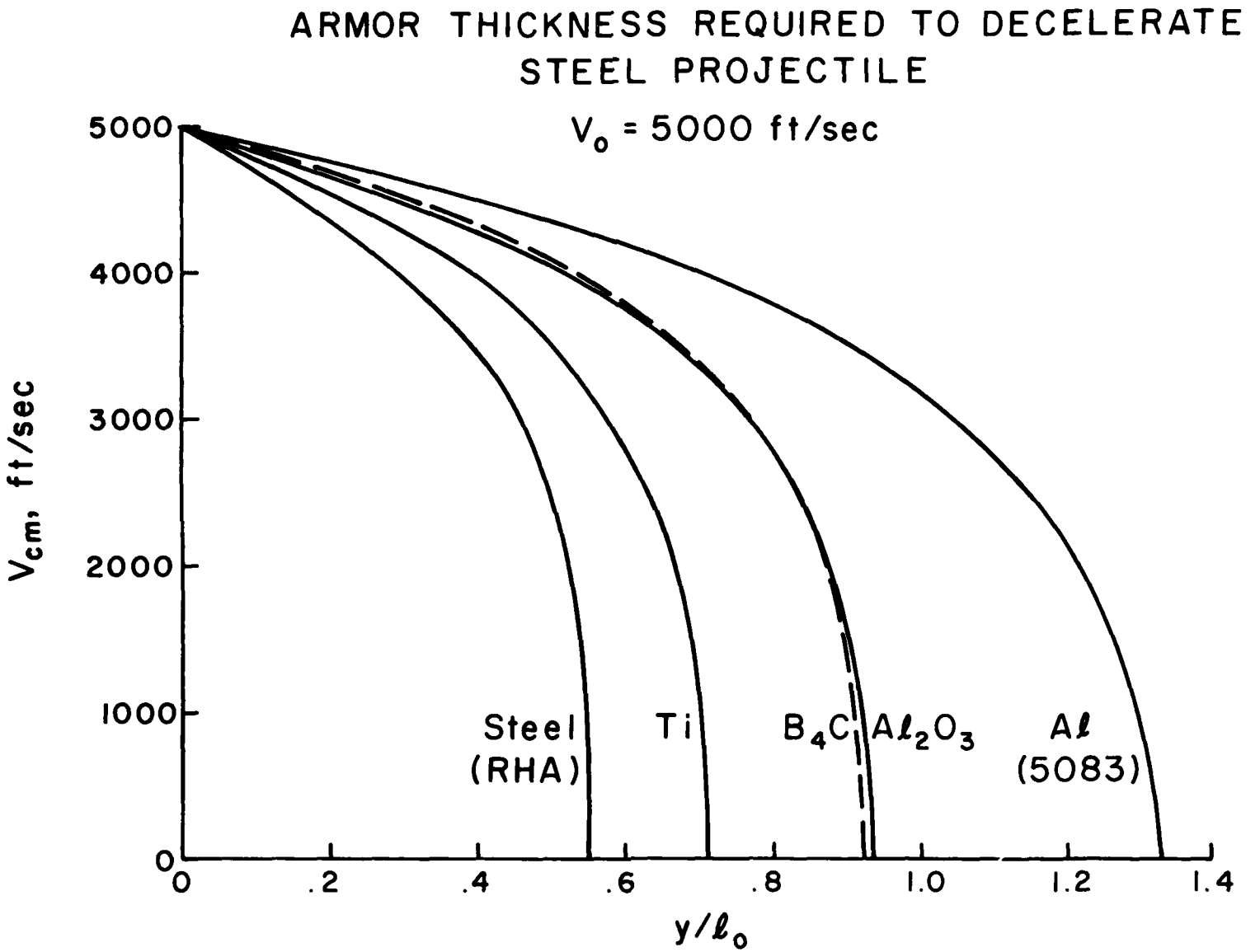

Figure 36. Required Armor Thickness to Decelerate Steel Projectile.

handled by a simple or less costly armor. For these analyses, we consider the threat to be defeated when the velocity is reduced to 1,000 fps. The results, however, are not sensitive to the choice of defeat velocity.

If thickness were the only criterion, then the armor steel would clearly be the best material to defeat this threat. However, thickness is not the only or even primary criterion. For aircraft applications, weight is the primary concern. On a weight basis, the steel does not fare quite as well. Figure 37 shows the required areal density of target material to defeat the same threat. On a weight basis, the ceramics are the lightest and the steel is the heaviest. Note the similarity between titanium and aluminum oxide.

For illustrative purposes, Figure 38 is included and shows the relative deformation of the projectile as a function of the depth of penetration into the target. At the depths corresponding to a velocity of 1,000 fps, the projectile width has increased by a factor of two. A plot such as this can be used to estimate the rate at which the particle is spreading; information which is useful for estimating post-perforation damage potential of a projectile.

Figure 39 summarizes the weight-thickness tradeoffs for four of the materials relative to titanium armor which is taken to be the base case.* The steel, although 25% thinner, is 36% heavier than titanium. In contrast, boron carbide is 30% thicker but is 27% lighter than titanium. Furthermore, if cost is included in the analysis (and it must ultimately be a major factor) then alumina must also be considered. The alumina which was used in the qualification tests was purchased for less than $1.00 per pound; titanium costs roughly $5.00 per pound. More about material costs later.

*These analyses do not consider the base layer material as a variable, although the integral theory can be used to optimize this layer as well as the primary stopper layers. The same base layer is therefore common to all designs considered in this chapter.

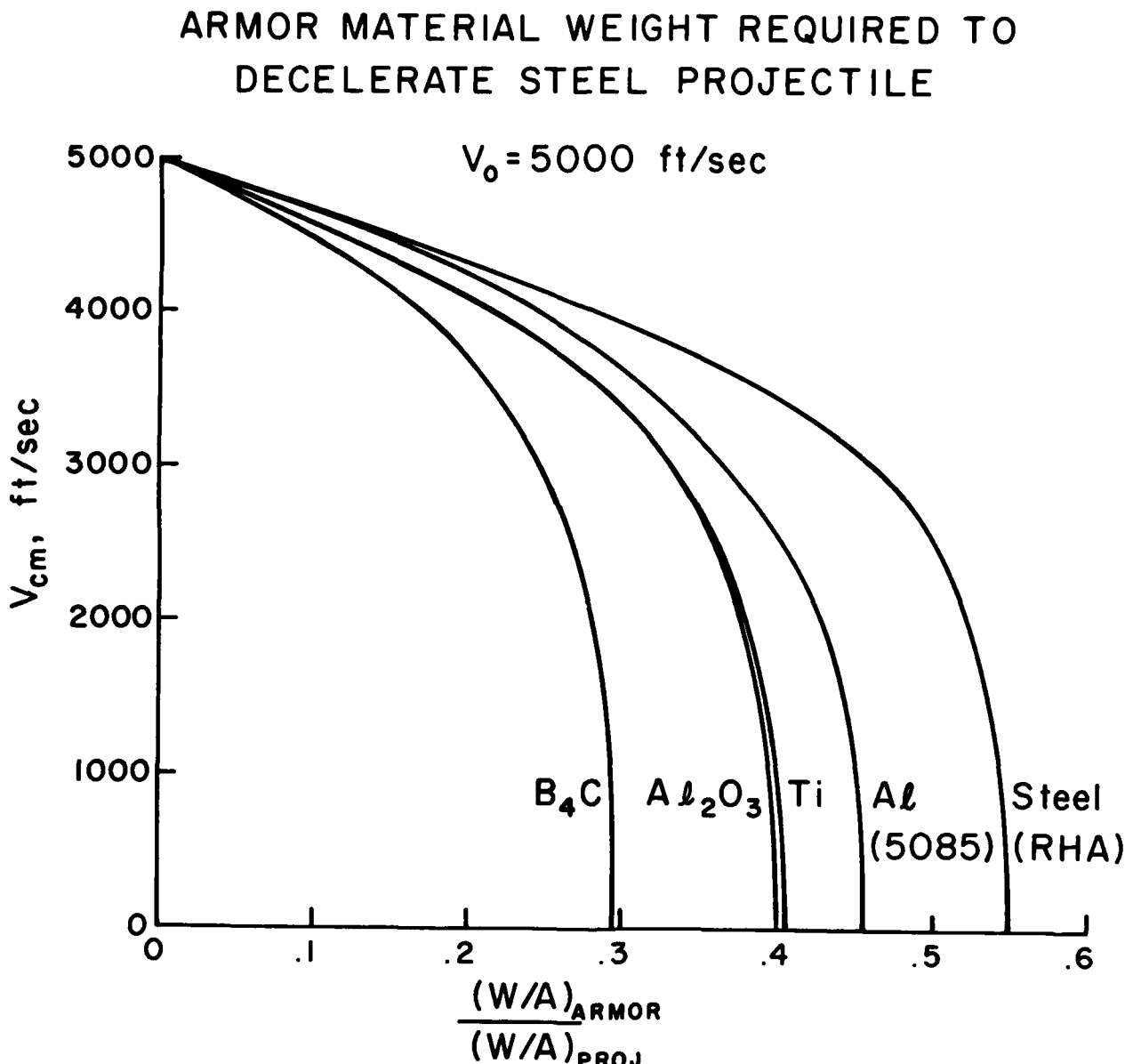

Figure 37. Required Armor Areal Density to Decelerate Steel Projectile.

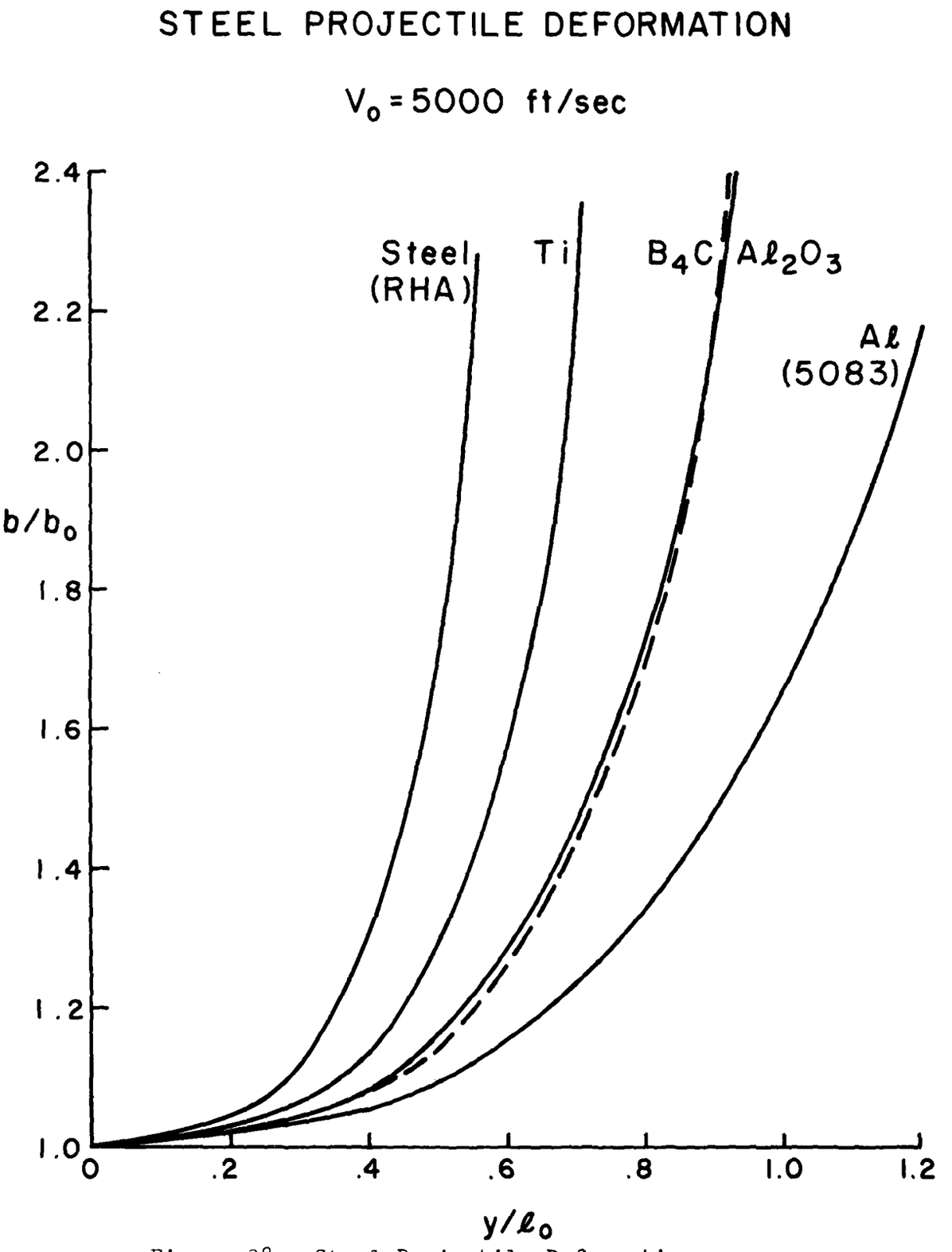

Figure 38. Steel Projectile Deformation.

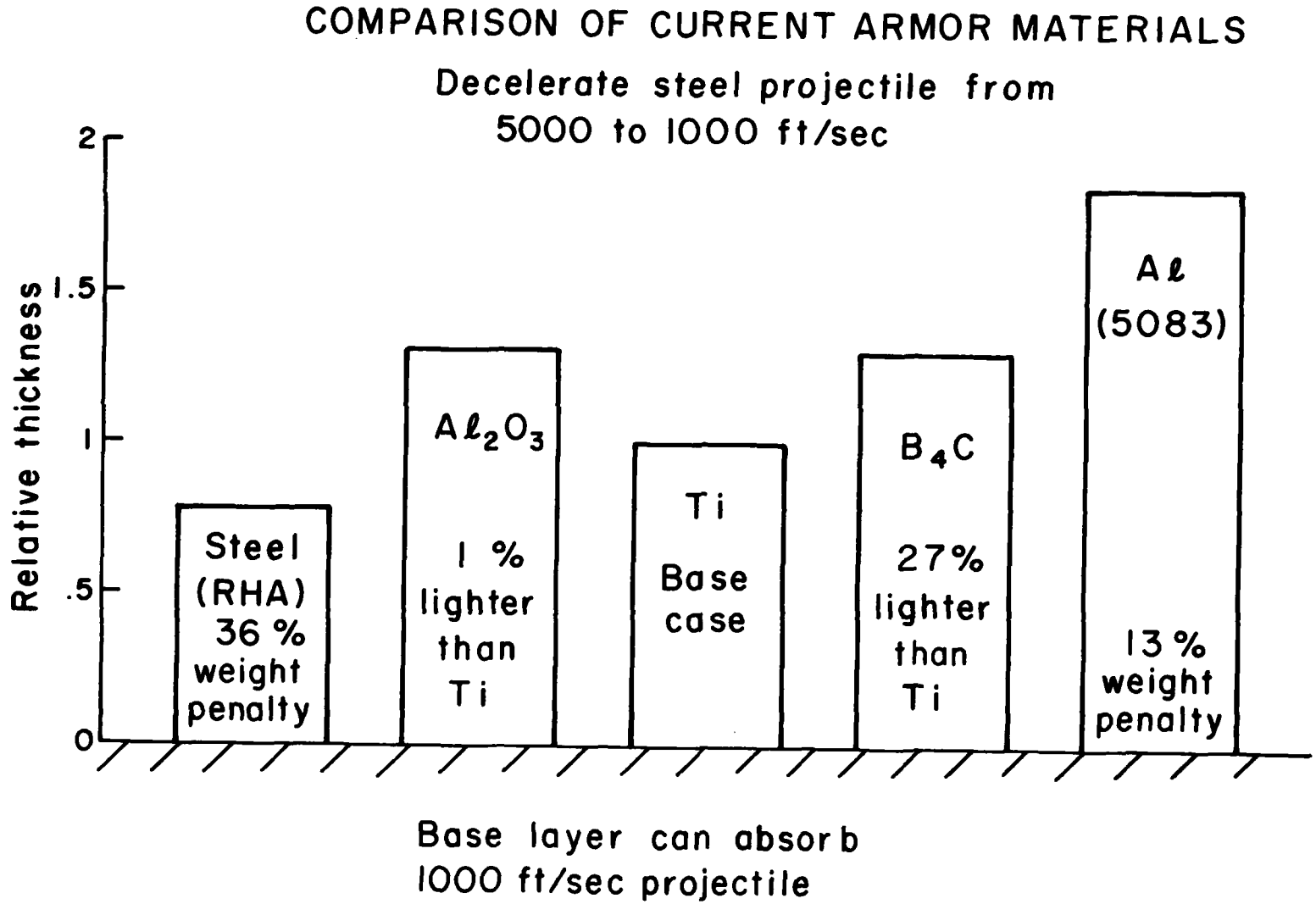

Figure 39. Comparison of Current Armor Materials.

If steel is thinner and boron carbide is lighter than titanium, is it possible to combine the two materials in a layered design and reduce both the weight and thickness of the armor? Figure 40 shows that the answer to this question is no. All possible combinations of steel over boron carbide are shown. The bottom half of the figure shows the relative armor weight and thickness as a function of the amount of steel in the design. At the left, the design is 100% boron carbide; on the right, it is 100% steel. Clearly, as the thickness of the steel layer increases (and that of the boron carbide layer decreases) the layered target becomes thinner but heavier. These results, when placed on the thickness-weight map on the top half of Figure 40, show that there is virtually no payoff using the steel and boron carbide armor in place of titanium armor unless some thickness penalty can be accepted.

4.3 Potential Armor Materials

Before beginning a search for a "better" armor material, it is instructive to consider the required characteristics of such a material. The most important properties are material density and E_* . The thickness-weight map for many possible combinations of these two properties is shown in Figure 41. It is evident that the primary method of reducing thickness is to increase density and the primary method of reducing weight is to increase E_* . If the goal is to get within the dashed rectangle, then moderate density materials with E_* above 400 Btu/lbm are required. If the goal is to reduce weight, albeit with a thickness penalty, then lower density materials can be considered.

As part of the materials qualification program which was conducted for DARPA, we have compiled and tabulated the properties of a vast number of materials and calculated the theoretical E_* based on Eq. (26). This equation has predicted the E_* for every metal which has been tested to within approximately 15% and every ceramic within a factor of two. The properties for ten of the most promising of these materials are summarized in Table 3. Note that the value of E_* which is tabulated is a conservative estimate equal to half the theoretical value. Each of these materials is a ceramic.

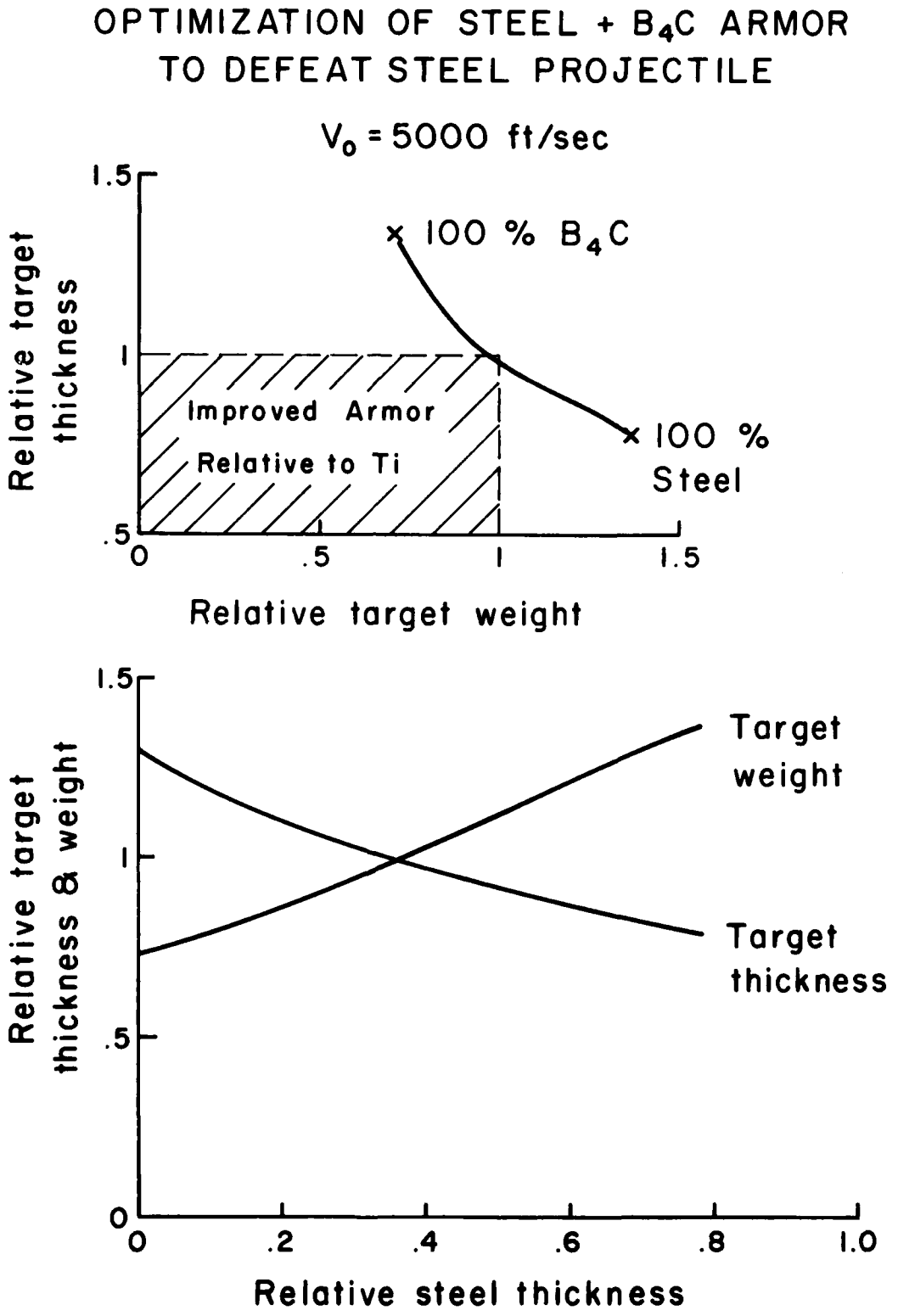

Figure 40. Optimization of Steel/Ceramic Armor.

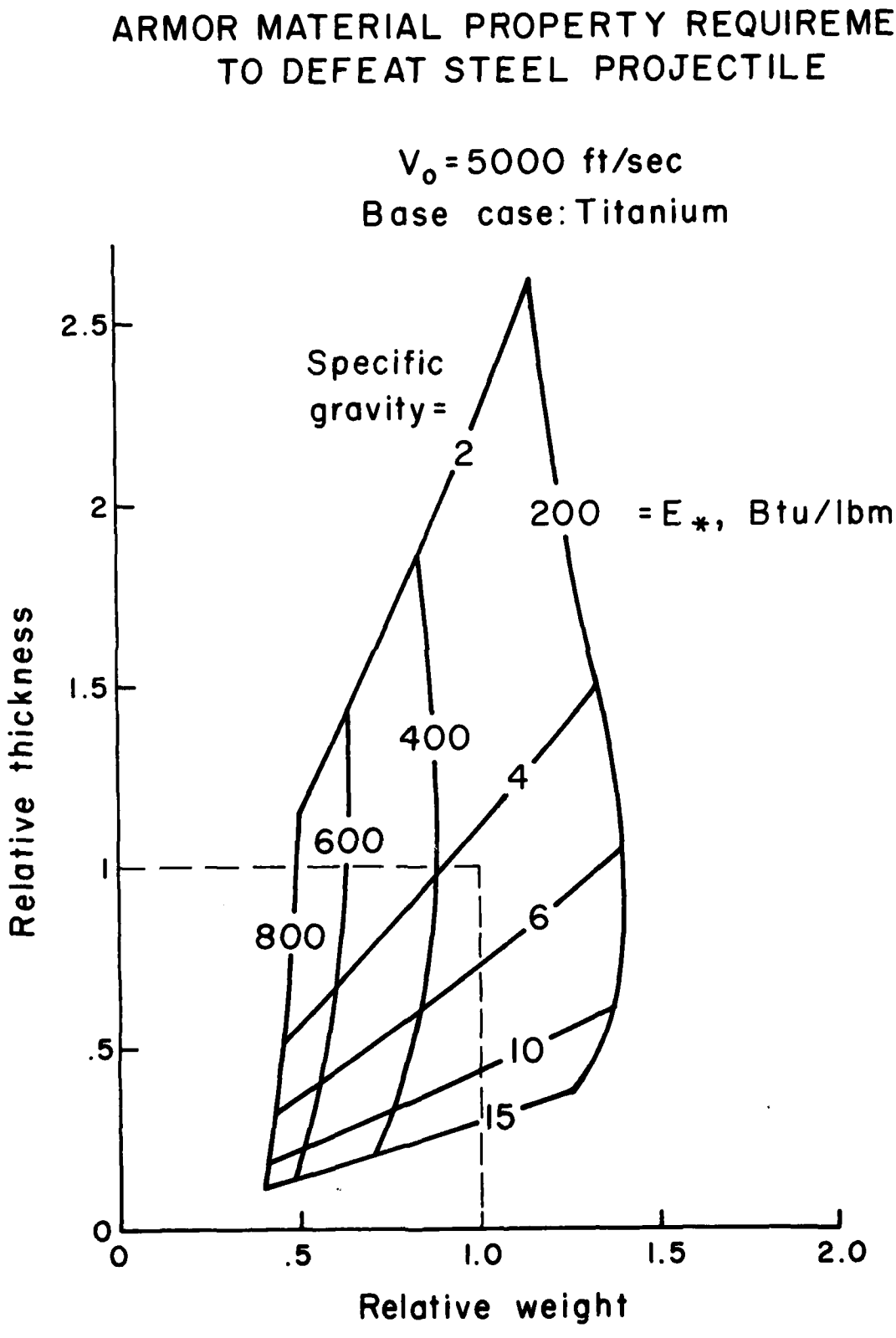

Figure 41. Armor Material Property Requirements.

TABLE 3. CANDIDATE ARMOR MATERIALS

Material	Specific gravity	E_{*eff}, Btu/lbm	ρE_*, psi
BN	3.49	650	7.65×10^5
TiB_2	4.50	490	7.43×10^5
TiN	5.22	420	7.39×10^5
NbC	7.60	280	7.17×10^5
VC	5.77	350	6.81×10^5
TaC	14.0	140	6.61×10^5
VN	6.13	310	6.41×10^5
ZrC	6.90	270	6.28×10^5
Ti	4.48	328	4.95×10^5
Al_2O_3	3.40	325	3.73×10^5
Al(5083)	2.74	245	2.26×10^5
B_4C	2.52	500	4.25×10^5
Steel(RHA)	7.83	203	5.36×10^5

A comparison of these materials on a thickness-weight map is shown in Figure 42. Four of these materials lie within the dashed rectangle and, including the two ceramics already considered, six materials have the potential for reducing target weight relative to titanium. With the exception of alumina, each of these materials is more expensive than titanium, although projected costs for some of these materials are comparable to titanium.

The material cost aspects of armor design have not been emphasized in this analysis because the cost for many of these ceramic materials is highly sensitive to factors which are difficult to estimate. Each of the ceramics which has been identified can be produced by present-day hot pressing technology, except boron nitride which requires a more advanced technology. Although the ceramic powders are relatively inexpensive, the high initial set-up and operating costs tend to highly inflate the cost for small, specialty orders. A higher quantity production run could make some ceramic costs more attractive. Table 4 summarizes the costs for some of these materials. Although some promising ceramics are too expensive at present, there is potential for a considerable cost reduction in the future. Note that one ceramic, Al_2O_3 , whose performance is comparable to titanium is already considerably cheaper than titanium.

Although semi-infinite ceramic targets exhibit high E_{*p} , the value deduced from impact tests is still considerably less than the theoretical limit. This is because a significant amount of material in the path of the projectile fractures off the front face of the target before any plastic work has been done to it. When thinner ceramic targets are used, i.e., when the target thickness is of the order of the projectile diameter, there is also a marked decrease in the effective E_{*p} because of the tendency for target material to fly out of the path of the projectile without absorbing any plastic deformation. In recent tests, A.R.A.P. has found that by confining ceramic targets on the front and back by more ductile materials, the effective E_{*p} for the ceramic can be raised to near its theoretical limit. Thus, by

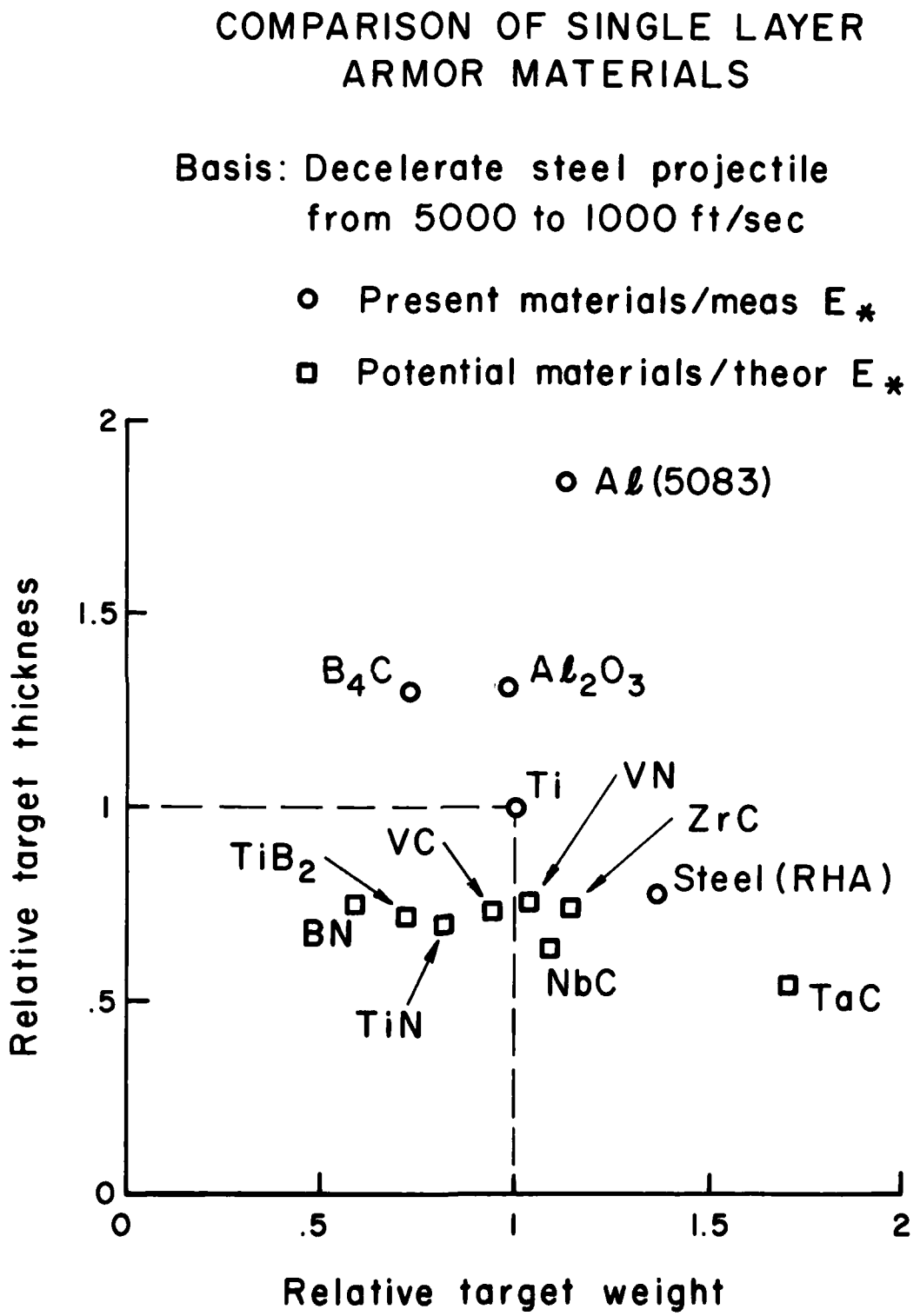

Figure 42. Comparison of Armor Materials.

TABLE 4. ESTIMATED MATERIAL COST

Material	Cost per lb.	
	Present	Future *
Titanium	5.00	
Steel (Armor)	2.00	
Al_2O_3 (Crystal)	370.00	
Al_2O_3 (Coor's)	~1.00	
B_4C	300.00	~3.00
MgO	70.00	~3.00
TiB_2	200.00	
SiC		~2.00
TiC	200.00	
TiN	200.00	
BN (Cubic - powder)	11,000.00	

* Future costs are based on AMMRC studies

inertial restraint, it is possible to achieve the weight-reduction potential of the ceramic.

There is an optimal way of layering an armor which makes best use of E_* and the density of different materials at various stages of penetration. On the outside face of an armor, the velocity of the projectile will be high initially, and the $C_D V^2/2$ drag term will dominate the E_* term in determining the energy deposited in the initial layer. It is desirable in this initial layer to break the projectile or produce rapid deformation to increase its frontal area. This will be done by generating a large decelerating pressure on the front face of the projectile. In the integral theory, this pressure is given by $\rho(C_D V^2/2 + E_*)$. Hence, one wants a material which is strong and dense, such as steel, as the outer layer. In this initial layer, the density of the armor is the most important parameter. This layer should be followed by a layer with the highest possible E_{*p}, to absorb dissipatively the kinetic energy of the projectile and maintain a high frontal pressure. This is the layer in which ceramics offer the most potential. Finally, on the back of the armor, when the projectile has been decelerated to a relatively low velocity (approximately 1,000 fps), there should be a material with a very high E_{*e} to absorb the remaining energy elastically. In what follows, this layered target approach to armor design is considered in more detail.

Consider the force equation, (22), once again and ignore, for the moment, the elastic term E_{*e}. The pressure exerted on the projectile by the target at any instant is composed of two terms, a hydrodynamic term proportional to the square of the velocity and an E_{*p} term independent of velocity. The hydrodynamic term dominates for high velocity; the E_{*p} term dominates for small velocity. The tradeoff between the two terms depends on the relative magnitudes of E_{*p} and the velocity.

As a simple illustration, consider the use of a target material whose $E_{*p} = 500$ Btu/lbm , a relatively high value, in place of titanium. This value of E_{*p} corresponds to a velocity of approximately 5,000 fps. If the impact velocity is much greater than 5,000 fps, then the primary resistance to the projectile is due to inertial drag. It would be foolish to spend money to buy the high E_{*p} material when a high density target material is required. However, as the projectile decelerates, then the E_{*p} term becomes dominant. A point is reached where it no longer pays to increase the thickness of the dense layer; the target becomes too heavy. Instead, it may be beneficial to utilize the high E_* material to further decelerate the projectile. Finally, when the velocity is sufficiently low, the E_{*e} term becomes important. Hence, an elastic layer at the rear of the target is desirable.

Weight-thickness tradeoffs for a number of two-layer targets utilizing a dense outer layer over a ceramic layer are shown in Figure 43. The point common to all curves represents a monolithic steel armor; the other end of each curve is an all-ceramic armor. In between are all combinations of steel and ceramic. Figure 44 shows the layer thicknesses for three of these combinations. The use of this figure can be illustrated by a simple example.

Assume that 1 inch of titanium is required to defeat the postulated fragment threat. Then, 0.75 inches of steel will also defeat the threat, but the steel will be 36% heavier. However, an armor which was only 0.75 inches thick could be made using 0.14" (20% of target thickness) of steel over 0.56" (80% of target thickness) of titanium diboride. The weight of this target would be 80% of the titanium and it would also defeat the threat. The steel-boron carbide armor is also significantly lighter than titanium for some combinations of the two materials but for this armor there is a thickness penalty which must be considered. Presently, the armors which contain boron carbide or titanium diboride would be more expensive than titanium. The steel-boron nitride armor is the most effective of the combinations investigated. Unfortunately, the high cost of boron nitride removes this armor from serious consideration. Another layered armor which is

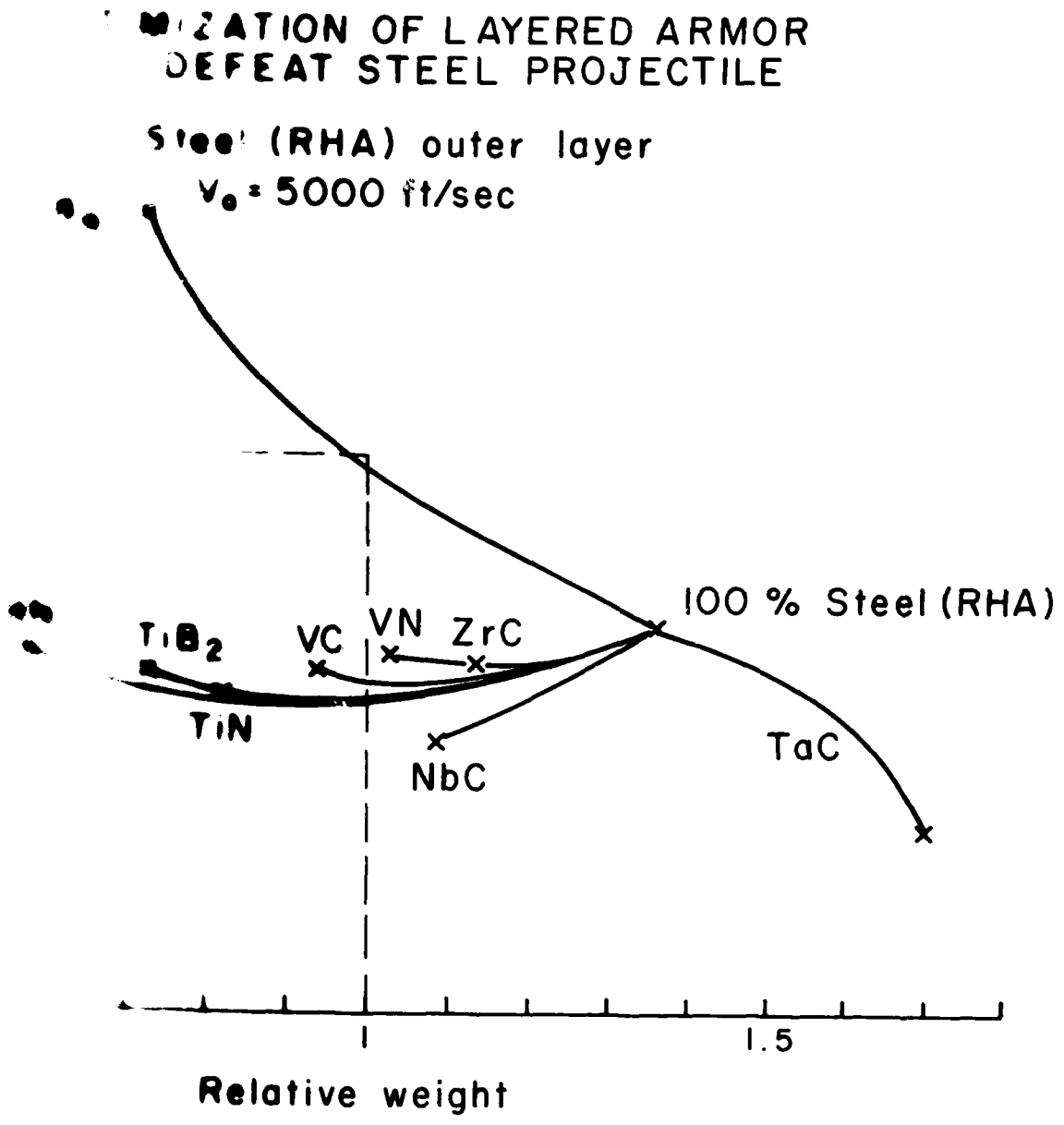

Optimization of Layered Ceramic/Steel Armor.

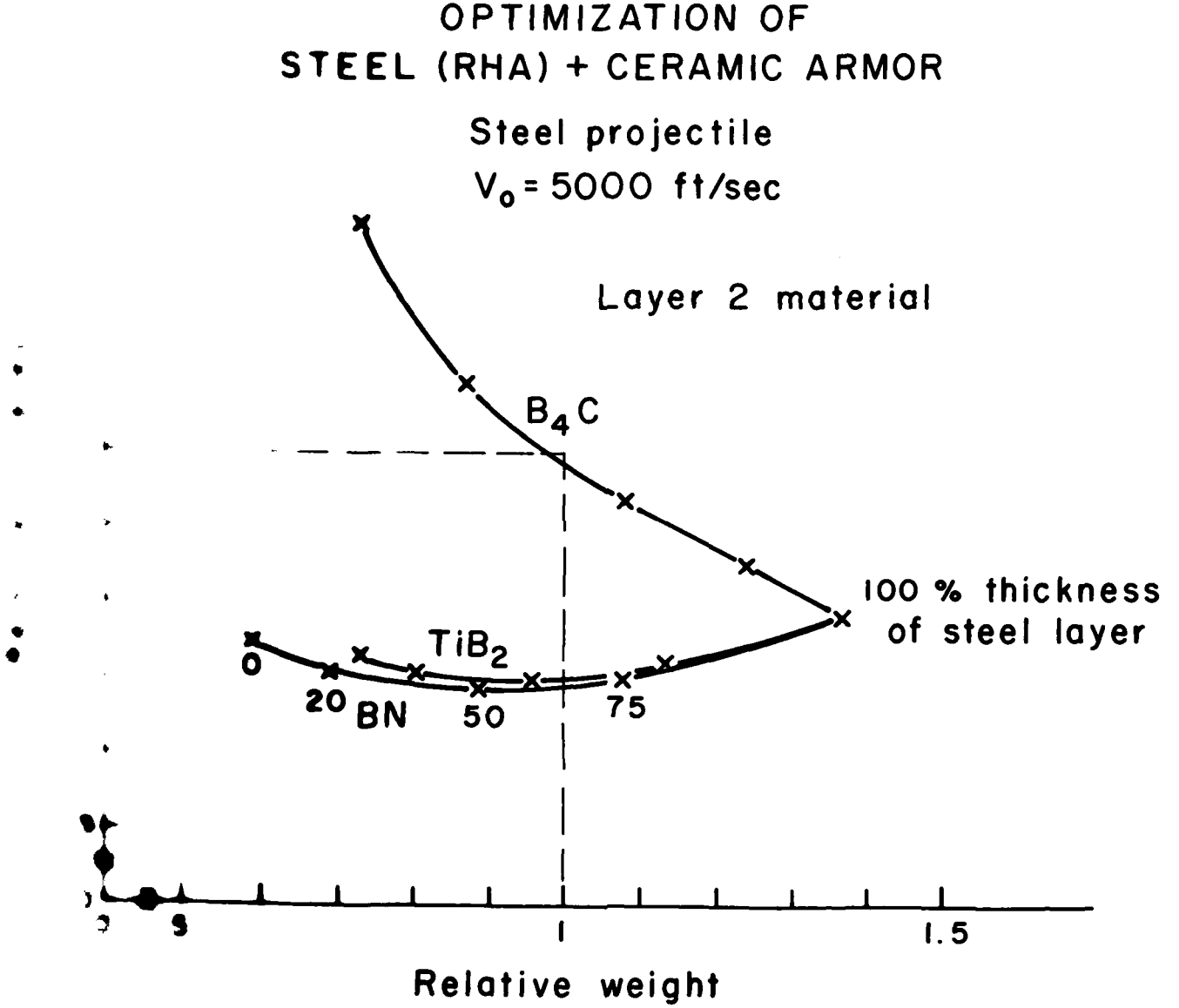

Fig. 44. Optimization of Ceramic/Steel Armor.

not shown is steel over aluminum oxide. This armor is comparable to titanium on a weight basis, has a small thickness penalty, but is considerably cheaper.

It should be noted that all of these analytical designs are based on conservative estimates of E_{*p} for the ceramic materials. Theoretical values are divided by two because the qualification tests for boron carbide and aluminum oxide showed an effect of this magnitude for nonrestrained targets. Recent tests, which have not yet been fully analyzed, suggest that E_{*p} for ceramics is closer to the theoretical value when the ceramic is inertially restrained. If this result is further demonstrated, then the end-points in Figure 44 move to the left;* i.e., the targets will become lighter. In addition, for lower velocity threats, the E_{*p} effects will be even more significant.

All of the designs considered thus far utilize a steel outer layer. Figure 45 shows the effect of using a more dense material in place of steel. In general, a thinner armor is obtained but at the cost of increased weight and price.

These results demonstrate the manner in which the Integral Theory of Impact can be used to optimize an armor design. Only one threat has been considered. Certainly a practical design must be based on the entire anticipated threat spectrum. The theory can be used to investigate this spectrum and show sensitivities to various threat parameters such as velocity, material strength, density or shape. It can identify trends and required tradeoffs [illegible]

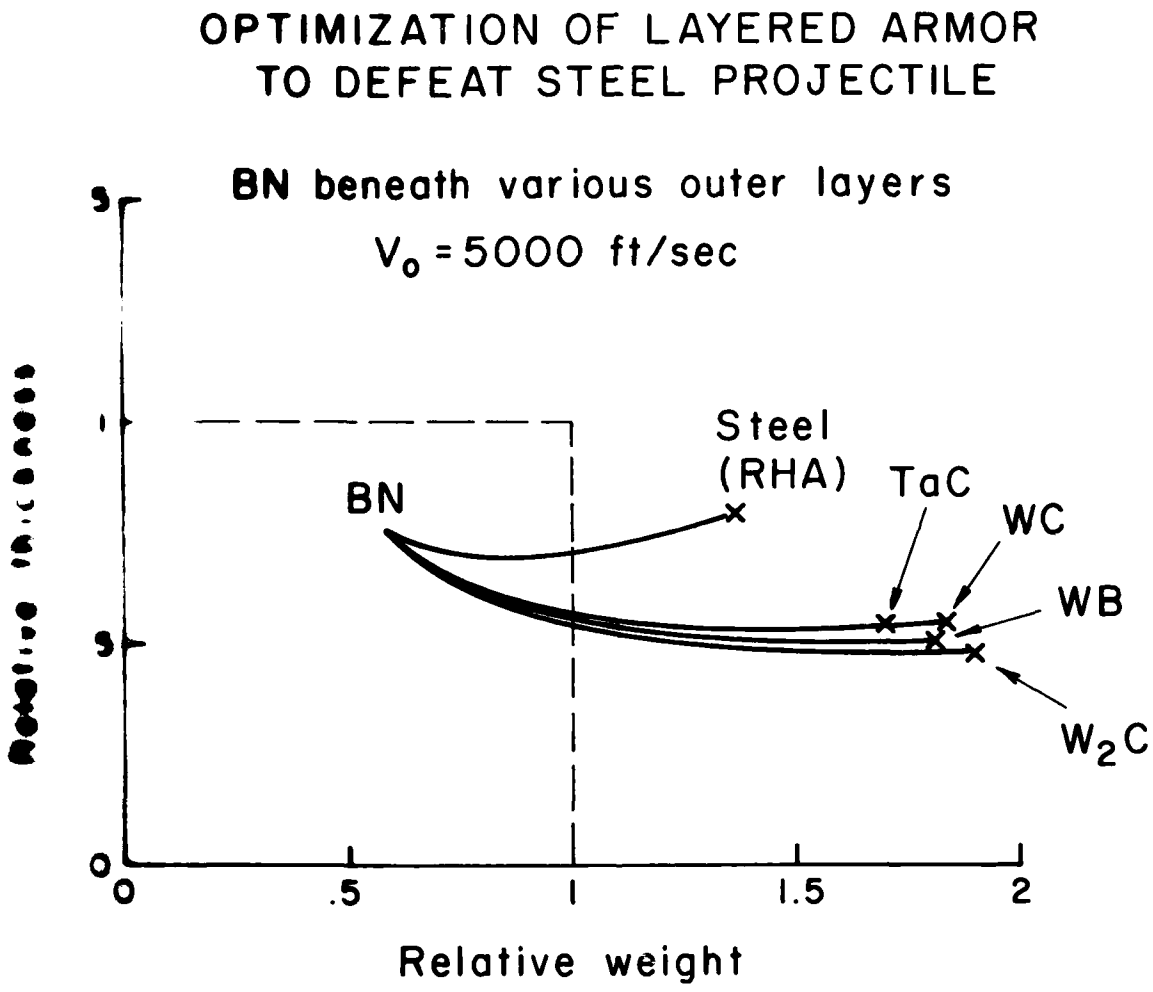

Figure 45. Optimization of Layered Armor.

5. CONCLUSIONS

An analytical and experimental program has been conducted during the past year, the purpose of which was the development and application of the Integral Theory of Impact to the design of lightweight armor systems.

The experimental program consisted of approximately 125 impact tests in the A.R.A.P. Impact Facility. These tests utilized both deforming and nondeforming (low L/D) projectiles impacting both monolithic and layered targets. The test program verified two key aspects of the theory: (1) the simple, single-cell representation for a deforming particle can be used to predict the gross response of a target which is impacted by a relatively soft projectile, i.e., a projectile whose yield strength is considerably less than the stresses generated by the impact; and (2) the theory can be used to predict the gross response of a layered target.

The analytical program consisted of identifying those materials which have the potential to improve lightweight armor systems. In general, these materials are ceramics, the most promising of which are boron carbide, aluminum oxide, and titanium diboride.

An optimization study using these ceramics beneath a steel outer layer which inertially restrains the ceramic was completed. This study demonstrated the weight, thickness, and cost tradeoffs which are required and suggested the potential payoff - either less weight or less cost for the same weight relative to titanium armor. The optimization was based on a steel fragment threat traveling at 5,000 feet per second relative to the target.

6. RECOMMENDATIONS FOR FUTURE WORK

1. The optimum design of an armor system must be based on the entire spectrum of threats which the system must encounter. An inexpensive tool is available, i.e., the Integral Theory of Impact, which can facilitate the optimization procedure by quantifying the required tradeoffs. It is therefore recommended that the sensitivity of armor design to threat design be investigated using this tool. As a minimum, the sensitivity analysis should include the effects of threat velocity, shape, and material strength.

2. The optimization procedure to defeat a given threat has been theoretically demonstrated. It is recommended that the procedure now be demonstrated experimentally.

3. The integral theory of impact can be applied to the design of armor systems other than lightweight systems. It is, in fact, presently being applied to the design of land-based armor. In addition, the principles can be applied to the design of transparent armor systems. However, it is necessary to first obtain the experimental data necessary to qualify candidate transparent materials. It is recommended that an experimental program be conducted to obtain the necessary data for a number of materials. This information can then be used in optimization studies to estimate the potential improvement relative to present transparent systems.

These recommendations have been included in a proposal submitted to AFFDL for continued support.

*U.S.Government Printing Office: 1978 — 757-080/360